THE UNIVERSITY OF MANITOBA

THEORETICAL STUDY OF POSITRON ANNIHILATION WITH CORE ELECTRONS IN SEVERAL METALS

by

ALLIN GOULD

A THESIS

SUBMITTED TO THE FACULTY OF GRADUATE STUDIES

IN PARTIAL FULFILMENT OF THE REQUIREMENTS FOR THE DEGREE

OF DOCTOR OF PHILOSOPHY

DEPARTMENT OF PHYSICS

WINNIPEG, MANITOBA

October, 1972

TABLE OF CONTENTS

LIST OF FIGURES

LIST OF TABLES

PUBLICATIONS

1. Calculations of Angular Distributions from Metals Using Positron Wavefunctions with Proper Crystal Symmetry. A. G. Gould, R. N. West, B. G. Hogg, accepted by Can. J. Phys.

2. Positron Annihilation in Copper Single Crystals. E. M. D. Senicki, E. H. Becker, A. G. Gould, R. N. West and B. G. Hogg, accepted by J. Phys. Chem. Solids.

3. Study of Single Crystals of Magnesium and Zinc by Positron Annihilation. E. H. Becker, E. M. D. Senicki, A. G. Gould and B. G. Hogg, accepted by Can. J. Phys.

4. Angular Correlation of Positron Annihilation Radiation in Copper Single Crystals. E. M. D. Senicki, E. H. Becker, A. G. Gould, B. G. Hogg, submitted to Physics Letters.

ACKNOWLEDGEMENTS

I would like to thank my supervisor, Dr. B. G. Hogg, for the support and encouragement provided during the course of this work.

I would like to especially thank Dr. R. N. West, who first suggested this project, for his guidance and encouragement during the early stages of this work.

I wish to thank Dr. O. E. Mogensen and Dr. D. C. Connors for kindly providing me with their original data on zinc and cadmium respectively. I wish to thank Dr. E. H. Becker and Dr. E. M. D. Senicki, both for their point detector data on copper, gold, zinc and magnesium, and for their helpful advice during the course of this work.

Helpful discussions with Mr. M. Buchheit are also gratefully acknowledged.

Finally the writer wishes to express his appreciation of the financial support given him during the course of this work. The research was supported by a grant from the National Research Council of Canada to Dr. B. G. Hogg. A N.R.C. bursary was held by the author during the academic year 1970-71.

ABSTRACT

A positron wavefunction incorporating the proper crystal symmetry is calculated and applied to the determination of that part of the momentum distributions of annihilation photons arising from the annihilation of core electrons in magnesium, copper, zinc, cadmium and gold. The core electrons are treated in the tight binding approximation.

Angular distributions are calculated using very simple models for the conduction electrons. Results are presented for the point detector geometry for magnesium, copper, zinc and gold, and for the long slit detector geometry for copper, zinc and cadmium.

These results are compared to experimental distributions and to theoretical distributions in which the core contributions are calculated using a Wigner-Seitz positron wavefunction.

CHAPTER I

INTRODUCTION

1.1 Annihilation of Positrons

An electron and a positron in close proximity can annihilate one another. In terms of Dirac theory for a free electron and positron (Dirac 1930), the electron scatters from the positive energy state $m_e c^2$ to the negative energy state $-m_e c^2$, emitting energy $2m_e c^2$. In the absence of external fields two photons must be emitted in order to conserve energy and momentum. In the presence of external fields, energy and momentum may be transferred to the fields and they do not impose any restrictions on the number of photons emitted. However for the fields found inside solid matter the probability of no photon or one photon annihilation is negligible (Wallace, 1960). The probability for three photon annihilation has been calculated by Ore and Powell (1949), and while it is much smaller than the probability for two photon annihilation, it is much larger than the probability for zero or one photon annihilation. The probability for more than the three photon annihilation is again negligible.

The positron and electron are both spin 1/2 particles. In the absence of coupling to external fields the positron electron pair must have total spin angular momentum 0 or 1. Yang (1950) has shown from symmetry arguments that two photon annihilation is forbidden when the system has total angular momentum 1. Since, in a solid, the coupling of the two particles' spin angular momenta to external fields is negligible, if the positron forms a bound state with a single electron this state will have definite spin angular momentum of 0 or 1. In the ground state there will be no orbital angular momentum and so the state having

spin angular momentum of 1 must annihilate by a three photon process. As pointed out in the previous paragraph, this process has a much smaller cross section than two photon annihilation, and so this state has a much longer lifetime. Such a long lived state annihilating by three photon annihilation is indeed observed in non-conducting solids. In metals, however, there is no evidence for such a state. This is a consequence of the moderately high density gas of conduction electrons found in a metal. Arponen and Jauho (1968), Bergersen (1969) and Arponen (1970) have shown that in an electron gas of these densities no meaningful bound state is formed. In metals, therefore, the only important annihilation process is that in which two photons are emitted. Since we are only concerned with metals in this work, the rest of the discussion deals only with two photon annihilation.

1.2 Angular Correlation of the Annihilation Radiation

If the positron-electron pair is at rest in the laboratory frame and if external fields may be neglected, the two photons are emitted at 180 degrees with respect to each other and each will have energy $m_e c^2$. If the positron-electron pair is not at rest, the deviation of the two photons from 180 degrees is proportional to the momentum of the pair measured in the laboratory frame. If the positron has only thermal energy, it will contribute negligible momentum, and the angular distribution of annihilation photons will reveal the momentum distribution of the electrons.

The first measurements of the angular distribution of annihilation radiation were made by Beringer and Montgomery (1942) and Vlassov and Tzirelson (1948). These measurements established that the angular spread of radiation was of the order of magnitude expected from electronic

momenta. The application to the study of electronic properties of solids really began, however, with the work of DeBenedetti, Cowan, Konneker, and Primakoff (1950).

They performed a careful angular correlation measurement on positrons annihilating in gold using a "long slit apparatus". A schematic of a typical long slit apparatus is shown on Figure 1. The counting rate is proportional to the number of positron-electron pairs having one component of momentum equal to $mc\theta$ in the laboratory frame. The curve obtained by DeBenedetti et al displayed the by now familiar bell shape.

Following this work, a large number of metals were investigated by various workers. Green and Stewart (1955), Stewart (1955, 1957) and Lang and DeBenedetti (1957) produced curves which showed that metals could be roughly classified into two groups. The transition metals showed the bell shaped curve like that of gold while the alkali and alkaline earth metals showed a central inverted parabola with a tail at larger angles. Ferrell (1956) showed that free conduction electrons would give an inverted parabolic angular distribution. He interpreted the large angle tails as being due to higher momentum components in the electronic wavefunctions, and the bell shaped curves as being the result of the "excluded volume effect". It was later shown (Berko and Plaskett 1958) that in fact annihilation with core electrons was the most important factor in both cases.

This simple interpretation of the curves led to the idea that positron annihilation could be used to map Fermi surfaces. Beryllium, magnesium, lithium, and sodium were all studied as single crystals and shown to have anisotropies (Berko , 1962, Stewart, 1967). The deter-

FIGURE 1

Schematic Diagram of Angular Correlation Apparatus

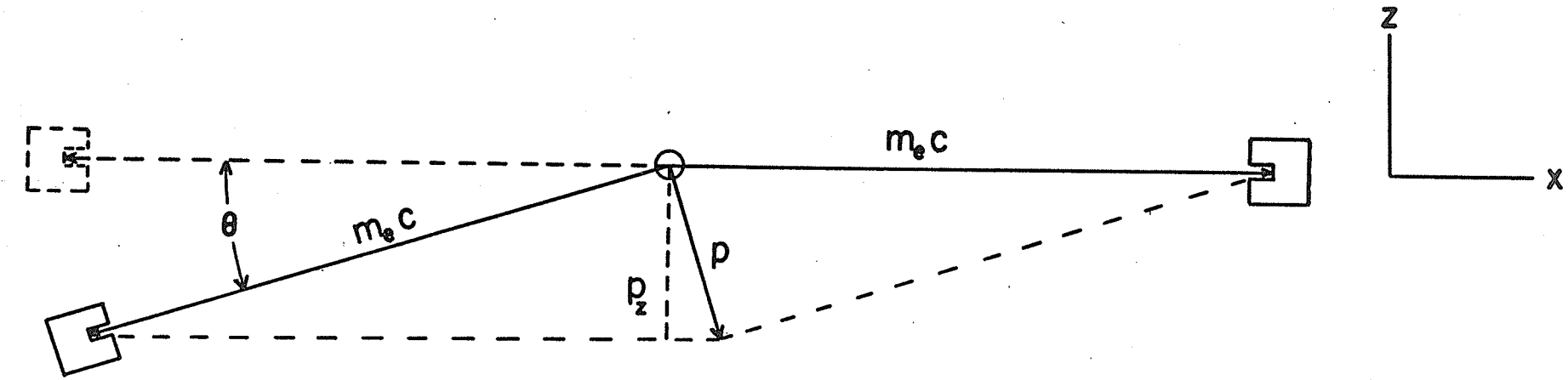

MOVABLE DETECTOR

SAMPLE

FIXED DETECTOR

mination of Fermi surfaces from the angular distributions, however, proved difficult (Stewart, 1967). A model for the Fermi surface had to be postulated, the resulting angular distribution calculated and then compared to experiment.

In an attempt to simplify the interpretation and reduce the ambiguity Colombino, Fiscella and Trossi (1963,1964) introduced the point detector geometry in which the counting rate of the apparatus is proportional to the number of positron-electron pairs having two specified components of momentum. This geometry has been used by Colombino et al to study silicon, aluminum and germanium and by Williams, Becker, Petijevich, and Jones (1968) to study the Fermi surface of copper.

Fujiwara and Sueoka (1966) have used a crossed slit geometry in which the second component of momentum is only restricted to be smaller than the Fermi momentum. This reduces the number of counts corresponding to higher momentum components in the electronic wavefunctions, but allows a higher counting rate than the point detector apparatus.

These latter two methods show promise in determining the Fermi surfaces of alloys. The conventional methods of determining Fermi surfaces depend either on the splitting of the conduction band into discrete levels (Landau levels) upon application of a strong magnetic field or on a long mean free path for conduction electrons. In disordered alloys neither of these conditions obtains. Williams and Becker (1971), Akahane et al (1971), and Thompson et al (1971) have all worked with such materials.

1.3 Theoretical Treatment of Angular Correlation

The probability of a positron annihilating an electron and yielding two photons of total momentum $\underline{p}$ may be calculated from covariant perturbation theory. As shown in Ferrell (1956), the part of the second order Hamiltonian operator that produces a two photon final state of momentum $\underline{p} = h\underline{k}$ is proportional to

$$\sum_{\underline{k}_1} \sum_{\underline{k}_2} A_{\underline{k}_1} b_{\underline{k}_2} \delta_{\underline{k}_1+\underline{k}_2,\underline{k}}$$

where $A_{\underline{k}_1}$ and $b_{\underline{k}_2}$ are the plane wave annihilation operators for the electron and positron respectively. In terms of the point annihilation operators $\alpha(\underline{r})$ and $\beta(\underline{r})$, this may be expressed as

$$\int d\underline{r}\ e^{-i\underline{k}\cdot\underline{r}}\ \alpha(\underline{r})\ \beta(\underline{r}) \qquad [1]$$

Since, in most angular correlation measurements there is never more than one positron in the sample at any one time, the initial state of the system is taken to consist of n electrons and one positron. If we assume that this state can be represented by the product of a single particle positron wavefunction and an n dimensional Slater determinant, and if we further assume that the n-1 non-annihilating electrons remain in their original states until annihilation is complete (Chang Lee 1958), then taking the matrix element of [1] between the initial and final states, squaring the absolute value and summing over final states yields n terms of the form

$$\left|\int d\underline{r}\ e^{-i\underline{k}\cdot\underline{r}}\ \phi(\underline{r})\ \psi(\underline{r})\right|^2 \qquad [2]$$

where $\phi(\underline{r})$ is a one particle electron wavefunction and $\psi(\underline{r})$ is a one particle positron wavefunction. Since the most general n electron wave-

function may be written as a linear combination of Slater determinants, the annihilation probability is a linear combination of terms of the form [2].

In the independent particle model, the one electron and one positron wavefunctions are taken to be independent of one another. The simplest independent particle model treats the positron and the conduction electrons as plane waves. This yields the inverted parabola characteristic of metals, however it ignores the core electrons entirely and it underestimates the conduction electron annihilation rates.

A more sophisticated independent particle model treats the positron as propagating in the Hartree-Fock field of the nuclei and all the electrons with the annihilating electron propagating in the Hartree-Fock field of the nuclei and n-1 other electrons. Although the exchange interaction between electrons is accounted for, the electron-electron and positron-electron Coulomb interactions are taken into account only in an average and trivial way. However, as pointed out by DeBenedetti et al (1950), the Coulomb attraction between the electron and positron would be expected to have no first order effect on the momentum distribution, although it would greatly affect the annihilation rate. In fact this model does give good results for the shape of both core and conduction momentum distributions.

The positron wavefunction for such a model was generally calculated in the Wigner-Seitz approximation (Daniel 1957, Donovan and March 1958). Conduction electrons have been treated in the nearly free electron approximation (Erskine and McGervey 1966), the orthogonal plane wave approximation (Melngailis and DeBenedetti 1966), and the augmented plane wave approximation (Loucks 1966). Berko and Plaskett obtained a

reasonably good fit to the angular distribution of copper using a Wigner-Seitz positron wavefunction, tight binding functions for the core electrons, and nearly free electron wavefunctions for the conduction electrons. They showed that the large tail in the copper distribution is due to annihilation with core electrons, the principal contribution coming from the 3d shell. Rockmore and Stewart (1967) used a Wigner-Seitz positron wavefunction to calculate core electron distributions for a number of other metals. The agreement with experiment was not, in general, very good.

Stroud and Ehrenreich (1968) expanded the positron wavefunction in a Fourier series in terms of reciprocal lattice vectors. They demonstrated that the positron wavefunction could be well represented by a reasonable number of plane waves and showed how to obtain angular distributions using such a positron wavefunction.

1.4 Thermalization of Positrons in a Metal

In both the Wigner-Seitz and Fourier expansion methods for calculating the positron wavefunction, it is assumed that the positron is at the bottom of the lowest band available to it in the solid. Bethe (1935) first suggested that a positron entering a solid would quickly lose almost all of its initial energy. DeBenedetti et al (1950), in an appendix to their paper on positrons annihilating in gold, showed that due to collisions with ions at lattice sites alone the positron would drop to thermal energies in about 3×10^{-10} seconds. This is slightly longer than the lifetime of about 2×10^{-10} sec. in a typical metal. However, Garwin (1953) pointed out that collisions with conduction electrons are much more important than those with ion sites.

Lee-Whiting (1954) included electron-positron collisions using perturbation theory with an exponentially screened Coulomb interaction between the positron and electrons. He obtained a thermalization time of 3×10^{-12} seconds. Carbotte and Arora (1967) noted that the thermalization time computed by this method was quite sensitive to the choice of screening parameter. Using the many body Green's function technique in the random phase approximation they obtained the thermalization time as a function of electron density for different temperatures. The thermalization times they obtained for room temperature, while longer than those of Lee-Whiting were still substantially less than the positron lifetimes.

Carbotte and Woll (1967) showed that electron-positron collisions led to a Maxwell-Boltzmann distribution for the positron at equilibrium. Mikeska (1970) showed that the effect of phonon-positron interactions was to speed up thermalization but also to broaden the equilibrium distribution. The broadening effect appears to be small, however, and so the positron is reduced to an energy of the order of .025 e.v. in a time short compared to its lifetime. Since the bandwidth of the lowest band for the positron is of the order of 5 e.v., the assumption that the positron is at the bottom of the band is justified.

1.5 Many Body Effects

The lifetime calculations based on the independent particle model fall well below experimental values. Ferrell (1956) using the perturbation theory approach of Bohm and Pines (1953) for an interacting electron gas calculated enhancement rates. His values for the lifetimes in metals while much closer than those of the independent particle model, were still lower than the experimental values. Kahana (1960)

pointed out that the Bohm-Pines theory is not very satisfactory for the positron case since the short range interaction is not small. He used instead a Bethe-Goldstone (1957) equation. This approach overestimated the annihilation rates because it failed to take the screening of the interaction into account properly.

Kahana (1963) used the many body Green's function technique in the ladder approximation to recalculate the enhancement factors. He took for the interaction potential the screened Coulomb potential obtained from the random phase approximation in the high density limit. To extend the method to electron densities in the range found in real metals, he replaced the dynamic potential by the zero frequency limit. This method gave enhancement factors in reasonable agreement with experiment. In addition the enhancement factors were only weakly momentum dependent.

Carbotte and Kahana (1965) checked the validity of the ladder approximation by investigating some of the terms ignored in this approximation. They found that due to cancellation effects, the ladder approximation using the zero frequency limit to the dynamic potential was equivalent to including self energy corrections with the correct dynamic potential. The calculation has been redone by a number of workers (Zuchelli and Hickman 1964, Crowell et al 1966, Arponen and Jauho 1968) for different effective interactions and by Kanazawa et al (1965) for a more general subset of diagrams. Their results were all very similar to those of Kahana and Carbotte. A good review of the reasons for the success of the ladder approximation at high and intermediate densities is given by Bergersen (1969).

Carbotte (1965) and Carbotte and Salvadori (1967) applied the ladder approximation to core annihilation in sodium. They obtained en-

hancement factors considerably less than those found for conduction electrons but again largely momentum independent.

1.6 Motivation of Present Work

Thus we see that although the prediction of correct lifetimes of positrons in metals requires a many body calculation, such a calculation is not necessary to determine the angular distribution of annihilation photons.

Recent studies of positrons annihilating in metals (MacKenzie et al 1967, Hautojarvi et al 1970) have demonstrated a strong dependence of the commonly measured annihilation parameters on the purity and structural state of the metal. This has led to intensive studies of defect properties in metals (Connors et al 1971, Dave et al 1971). To understand these defect experiments, it is necessary to be able to separate the distributions into valence and core contributions. West et al (1967) and Arias-Limonta and Varlashkin (1970) have shown convincingly by means of experimental studies of melting and of materials having similar ion cores that the broad part of the distributions is indeed due to annihilation with core electrons.

It is the purpose of the present work to calculate core annihilation distributions using an independent particle model. In view of the statement at the beginning of this section and the relative simplicity of constructing independent one-particle wavefunctions compared to the calculations of Schrader (1970) or Fujiwara (1970) it is felt that such an independent particle model is the best approach.

Long slit angular distributions are calculated for polycrystalline copper, cadmium, and zinc. Point detector distributions are calculated for various single crystal orientations of copper, magnesium, zinc and gold.

CHAPTER II

METHOD OF CALCULATION

2.1 Introduction

Berko and Plaskett (1958) made the first quantitative calculation of the core contribution to angular correlation distributions for crystalline solids having closed shell core structures. They used the Wigner-Seitz approximation to calculate the positron wavefunction. In this approximation the polyhedral primitive cell in the solid is replaced by a sphere having the same volume and the Schrodinger equation for the positron is solved numerically inside this sphere, subject to the boundary condition that the slope of the wavefunction be zero on the surface of the sphere. The potential inside the sphere is taken to be the spherically symmetric potential created by the nucleus and core electrons of the atom at the center of the sphere together with a uniform density of conduction electrons distributed throughout the sphere. This ignores the potential due to other atomic sites. The solid is then assumed to be composed of N such spheres, where N is the number of atoms in the crystal. A more detailed description of the Wigner-Seitz method is given in appendix I.

Berko and Plaskett (1958) then calculated the overlap of this positron wavefunction with the core electron wavefunctions. For the core electrons in copper they used the atomic wavefunctions calculated by Hartree (1933) and by Hartree and Hartree (1936).

Stroud and Ehrenreich (1968) took into account the periodic nature of the potential "seen" by the positron. They expanded the positron wavefunction in a Fourier series in terms of reciprocal lattice vectors and solved for the coefficients. The secular equation

they derived for the Fourier coefficients of the positron wavefunction involved the Fourier coefficients of the crystal potential. They obtained these from X-ray scattering data.

The present calculation makes use of their method of expanding the positron wavefunction in a Fourier series, but obtains the Fourier coefficients of the crystal potential in a different manner.

The charge distribution about each atom is calculated using the Hartree-Fock-Slater free atom wavefunctions for the core electrons and distributing the valence electrons uniformly over the Wigner-Seitz sphere. If we denote by σ_{core} the radial charge density of core electrons, we have

$$\sigma_{core}(r) = - \sum_{n,\ell} 2(2\ell+1) \, |P_{n\ell}(r)|^2$$

where $P_{n\ell}(r)$ is r times the radial part of the core electron wavefunction.

The total electronic radial charge density is then

$$\sigma_{tot}(r) = \begin{cases} \sigma_{core} - \dfrac{3n_v r^2}{r_s^3} & \text{for } r < r_s \\ \sigma_{core} & \text{for } r > r_s \end{cases}$$

where n_v is the number of valence electrons per atom and r_s is the radius of the Wigner-Seitz sphere.

The potential is then calculated from electrostatics as

$$U(r) = \frac{2z}{r} + \frac{2}{r}\int_0^r \sigma_{tot}(r')dr' + 2\int_r^\infty \frac{\sigma_{tot}(r')}{r'}\, dr' \qquad [3]$$

where z is the charge on the nucleus. The crystal potential is then taken to be a superposition of these spherically symmetric potentials and the Fourier coefficients are calculated by numerical methods as explained in the following section.

In equation [3] the energy is expressed in Rydbergs, length and charge are in atomic units. In atomic units $e = \hbar = m_e = 1$, $c = \frac{1}{\alpha} = 137$, the unit of time is $\frac{\hbar^3}{m_e c^4} \approx 2.42 \times 10^{-17}$ sec., and the unit of length is the radius of the first Bohr orbit of the hydrogen atom, $\frac{\hbar^2}{m_e c^2} \approx .529 \times 10^{-8}$ cm. In the remainder of this work atomic units will be used, with the exception that energies will be expressed in Rydbergs. One Rydberg = 13.6 e.v. = $\frac{1}{2}$ atomic unit of energy (Hartree unit).

The Hartree-Fock-Slater free atom orbitals used both for the calculation of the crystal potential and later for the construction of the tight binding functions for the core electrons are those of Herman and Skillman (1963). It is believed that these wavefunctions are slightly better than those of the earlier calculations by Hartree (1933) and Hartree and Hartree (1936) used by Berko and Plaskett (1958).

The method of Fourier expansion of the positron wavefunction has been applied to the metals mentioned at the end of the last chapter. These metals fall into two distinct symmetry groups. Gold and copper have face centered cubic structure with space group O_h^5, while magnesium, zinc and cadmium have hexagonal close packed structure with space group D_{6h}^4. The solution of the positron wavefunction for these two symmetries is presented in section 2.2

The calculation of the distribution in momentum space of annihilating pairs from these positron wavefunctions and tight binding core electron wavefunctions is presented in section 2.3. The calculation of angular distributions from these distributions in momentum space is the subject of section 2.4.

2.2 Positron Wavefunction

A. General

The positron is taken to be in the ground state ($\underline{k} = 0$). The wavefunction is then periodic by Bloch's theorem and we may expand it as a Fourier series in terms of reciprocal lattice vectors.

$$\psi_+(r) = \sum_{\underline{K}} A_{\underline{K}} e^{i\underline{K}\cdot\underline{r}} \qquad [4]$$

Substituting this into the Schrodinger equation

$$-\nabla^2 \psi_+(\underline{r}) + V(\underline{r}) \psi_+(\underline{r}) = E\psi_+(\underline{r}) \qquad [5]$$

we obtain

$$\sum_{\underline{K}} (|\underline{K}|^2 A_{\underline{K}} e^{i\underline{K}\cdot\underline{r}} + V(\underline{r}) A_{\underline{K}} e^{i\underline{K}\cdot\underline{r}} - EA_{\underline{K}} e^{i\underline{K}\cdot\underline{r}}) = 0$$

multiplying by $e^{-i\underline{K}'\cdot\underline{r}}$, integrating over the volume of the crystal W, and dividing through by W, we obtain, since $\lim_{W\to\infty} \frac{1}{W} \int_W e^{i(\underline{K}-\underline{K}')\cdot\underline{r}} d\underline{r} = \delta_{\underline{K},\underline{K}'}$

$$\sum_{\underline{K}} [(|\underline{K}|^2 - E) \delta_{\underline{K},\underline{K}'} + V_{\underline{K}-\underline{K}'}] A_{\underline{K}} = 0 \qquad [6]$$

where $$V_{\underline{K}} = \frac{1}{W} \int_W V(\underline{r}) e^{i\underline{K}\cdot\underline{r}} d\underline{r} \qquad [7]$$

The solution of [6] is equivalent to finding the eigenvalues and eigenvectors of the matrix whose i,j element is

$$|\underline{K}_i|^2 \delta_{\underline{K}_i,\underline{K}_j} + V_{\underline{K}_i-\underline{K}_j}$$

The coefficients $A_{\underline{K}}$ in which we are interested are the elements of the eigenvector corresponding to the lowest eigenvalue.

B. F.C.C. Structure

For the discussion of the face centered cubic structure the origin is chosen to be at one of the atomic sites as shown in figure 2a. The unit cell has a basis of one atom and the space group is O_h^5.

The potential $V(\underline{r})$ in equation [5] is constructed from the $U(r)$ of equation [3] as follows

$$V(\underline{r}) = \sum_{\underline{\tau}} U(|\underline{r}-\underline{\tau}|)$$

where the $\underline{\tau}$ are lattice vectors, and the sum is over all possible $\underline{\tau}$ in the crystal.

Therefore $V_{\underline{K}}$ of equation [7] is given by

$$V_{\underline{K}} = \frac{1}{W} \sum_{\underline{\tau}} e^{i\underline{K}\cdot\underline{\tau}} \int_W U(\underline{r}-\underline{\tau})\, e^{i\underline{K}\cdot(\underline{r}-\underline{\tau})}\, d(\underline{r}-\underline{\tau}) = \frac{1}{\Omega} U_{\underline{K}} \qquad [8]$$

where Ω is the volume of a primitive unit cell, since $e^{i\underline{K}\cdot\underline{\tau}} = 1$ and there are N $\underline{\tau}$ vectors in the crystal.

$$U_{\underline{K}} = \int_W U(\underline{r})\, e^{i\underline{K}\cdot\underline{r}}\, d\underline{r}$$

To evaluate this integral, we use spherical polar coordinates and choose the polar axis to lie along the direction of $\underline{K}$. We then expand $e^{i\underline{K}\cdot\underline{r}}$ as follows

$$e^{i\underline{K}\cdot\underline{r}} = \sum_{\ell=0}^{\infty} (2\ell+1)\, i^{\ell}\, j_{\ell}(Kr)\, P_{\ell}(\cos\theta)$$

where j_{ℓ} is the spherical Bessel function of order ℓ, and $P_{\ell}(\cos\theta)$ is the Legendre polynomial of order ℓ.

Because $U(r)$ is essentially zero beyond a Wigner-Seitz cell, we may replace the integration over W by integration over all space. Then we get for $U_{\underline{K}}$

FIGURE 2a

Unit Cell of F.C.C. Structure

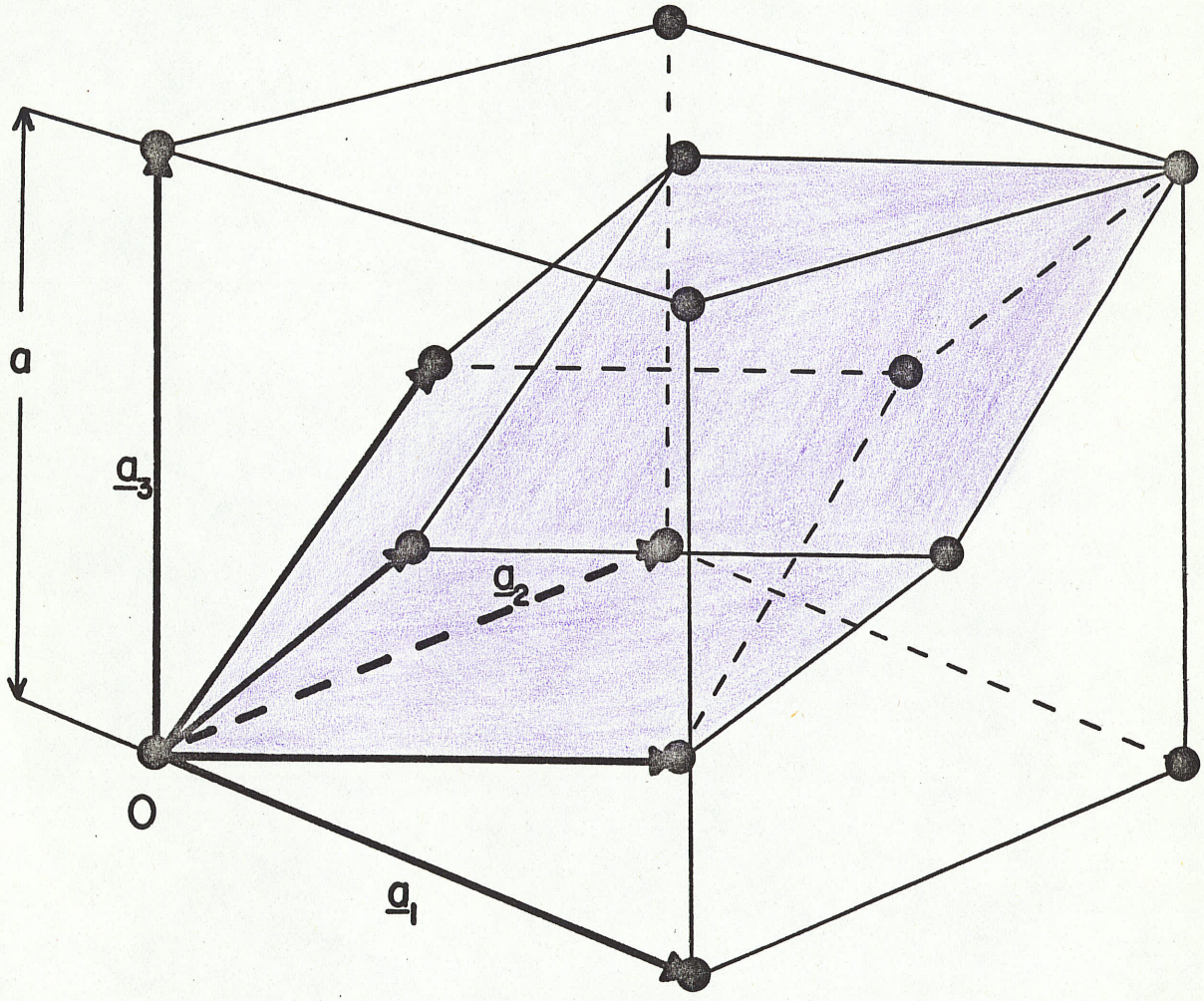
a
$\underline{a}_3$
$\underline{a}_2$
O
$\underline{a}_1$

$$U_{\underline{K}} = \sum_{\ell=0}^{\infty} (2\ell+1)\, i^{\ell} \int_0^{\infty} dr\, r^2\, U(r)\, j_{\ell}(Kr) \int_0^{2\pi} d\Phi \int_0^{\pi} d\theta\, \sin\theta\, P_{\ell}(\cos\theta)$$

but $$\int_0^{\pi} d\theta\, \sin\theta\, P_{\ell}(\cos\theta) = \frac{2}{2\ell+1}\, \delta_{\ell,0}$$

so $$U_{\underline{K}} = 4\pi \int_0^{\infty} dr\, r^2\, U(r)\, j_0(Kr) \qquad [9]$$

This integral was evaluated using Simpson's rule and using equation [3] for U(r).

To reduce the number of independent coefficients in equation [6] we make use of the symmetry of the crystal. The invariance of the positron wavefunction under all lattice translations imposes no restriction on the coefficients $A_{\underline{K}}$, since each of the plane waves $e^{i\underline{K}\cdot\underline{r}}$ is invariant under all lattice translations. The lowest energy eigenfunction of the positron transforms according to the Γ_1 irreducible representation of the space groups. Therefore, in the face centered cubic structure the wavefunction must be invariant under all the operations of the point group O_h. The operations of this group are listed in table I together with their action on an arbitrary function $\psi(\underline{r})$. The vector $\underline{r}$ in real space is specified by Cartesian coordinates x, y, z, i.e.

$$\underline{r} = x\underline{a}_1 + y\underline{a}_2 + z\underline{a}_3$$

where $\underline{a}_1$, $\underline{a}_2$ and $\underline{a}_3$ are as shown in figure 2a.

The operations of this group are all either proper or improper rotations. The action of these operators on the plane wave $e^{i\underline{K}\cdot\underline{r}}$ is to transform it into the plane wave $e^{i\underline{K}'\cdot\underline{r}}$ where $\underline{K}'$ is obtained from $\underline{K}$ by the inverse operation. Therefore $\underline{K}'$ has the same magnitude as $\underline{K}$. Since the wavefunction must remain invariant under the given operation for arbitrary $\underline{r}$, the coefficient $A_{\underline{K}}$ must be equal to $A_{\underline{K}'}$. By application

TABLE I

Operators of the Point Group O_h

$R_1 \quad \psi(\underline{r}) = \psi(x,y,z)$

$R_2 \quad \psi(\underline{r}) = \psi(x,y,-z)$

$R_3 \quad \psi(\underline{r}) = \psi(x,-y,z)$

$R_4 \quad \psi(\underline{r}) = \psi(x,-y,-z)$

$R_5 \quad \psi(\underline{r}) = \psi(-x,y,z)$

$R_6 \quad \psi(\underline{r}) = \psi(-x,y,-z)$

$R_7 \quad \psi(\underline{r}) = \psi(-x,-y,z)$

$R_8 \quad \psi(\underline{r}) = \psi(-x,-y,-z)$

$R_9 \quad \psi(\underline{r}) = \psi(y,x,z)$

$R_{10} \quad \psi(\underline{r}) = \psi(y,x,-z)$

$R_{11} \quad \psi(\underline{r}) = \psi(y,-x,z)$

$R_{12} \quad \psi(\underline{r}) = \psi(y,-x,-z)$

$R_{13} \quad \psi(\underline{r}) = \psi(-y,x,z)$

$R_{14} \quad \psi(\underline{r}) = \psi(-y,x,-z)$

$R_{15} \quad \psi(\underline{r}) = \psi(-y,-x,z)$

$R_{16} \quad \psi(\underline{r}) = \psi(-y,-x,-z)$

$R_{17} \quad \psi(\underline{r}) = \psi(z,x,y)$

$R_{18} \quad \psi(\underline{r}) = \psi(z,x,-y)$

$R_{19} \quad \psi(\underline{r}) = \psi(z,-x,y)$

$R_{20} \quad \psi(\underline{r}) = \psi(z,-x,-y)$

$R_{21} \quad \psi(\underline{r}) = \psi(-z,+x,+y)$

$R_{22} \quad \psi(\underline{r}) = \psi(-z,x,-y)$

$R_{23} \quad \psi(\underline{r}) = \psi(-z,-x,y)$

$R_{24} \quad \psi(\underline{r}) = \psi(-z,-x,-y)$

$R_{25} \quad \psi(\underline{r}) = \psi(x,z,y)$

$R_{26} \quad \psi(\underline{r}) = \psi(x,z,-y)$

$R_{27} \quad \psi(\underline{r}) = \psi(x,-z,y)$

$R_{28} \quad \psi(\underline{r}) = \psi(x,-z,-y)$

$R_{29} \quad \psi(\underline{r}) = \psi(-x,z,y)$

$R_{30} \quad \psi(\underline{r}) = \psi(-x,z,-y)$

$R_{31} \quad \psi(\underline{r}) = \psi(-x,-z,y)$

$R_{32} \quad \psi(\underline{r}) = \psi(-x,-z,-y)$

$R_{33} \quad \psi(\underline{r}) = \psi(y,z,x)$

$R_{34} \quad \psi(\underline{r}) = \psi(y,z,-x)$

$R_{35} \quad \psi(\underline{r}) = \psi(y,-z,x)$

$R_{36} \quad \psi(\underline{r}) = \psi(y,-z,-x)$

$R_{37} \quad \psi(\underline{r}) = \psi(-y,z,x)$

$R_{38} \quad \psi(\underline{r}) = \psi(-y,z,-x)$

$R_{39} \quad \psi(\underline{r}) = \psi(-y,-z,x)$

$R_{40} \quad \psi(\underline{r}) = \psi(-y,-z,-x)$

$R_{41} \quad \psi(\underline{r}) = \psi(z,y,x)$

$R_{42} \quad \psi(\underline{r}) = \psi(z,y,-x)$

$R_{43} \quad \psi(\underline{r}) = \psi(z,-y,x)$

$R_{44} \quad \psi(\underline{r}) = \psi(z,-y,-x)$

$R_{45} \quad \psi(\underline{r}) = \psi(-z,y,x)$

$R_{46} \quad \psi(\underline{r}) = \psi(-z,y,-x)$

$R_{47} \quad \psi(\underline{r}) = \psi(-z,-y,x)$

$R_{48} \quad \psi(\underline{r}) = \psi(-z,-y,-x)$

of all the operations in table I, it can be seen that all reciprocal lattice vectors having the same magnitude must have the same coefficient $A_{\underline{K}}$.

We can now construct new functions

$$\phi_i = \frac{1}{\sqrt{N_i}} \sum_{\substack{\underline{K} \\ |\underline{K}|=C_i}} e^{i\underline{K}\cdot\underline{r}}$$

where N_i is the number of $\underline{K}$ vectors having magnitude C_i. Such a group of $\underline{K}$ vectors will be referred to as a star (Bouckaert, Smoluchowski, and Wigner, 1936) and N_i as the multiplicity. In the cubic case a star may be generated by taking a typical vector (h,k,ℓ) and performing all permutations of indices and signs. (h,k,ℓ) denotes the reciprocal lattice vector $h\underline{a}_1^* + k\underline{a}_2^* + \ell\underline{a}_3^*$ where $\underline{a}_1^*$, $\underline{a}_2^*$, $\underline{a}_3^*$ are as shown in figure 2b. Typical vectors of the first eleven stars in the f.c.c. case are shown in table II along with their magnitudes, their multiplicities, and the value of their coefficients.

We can rewrite equation [4] as

$$\psi_+(\underline{r}) = \sum_i B_i \phi_i \qquad [10]$$

where it is obvious that $B_i = \sqrt{N_i}\, A_{\underline{K}}$ where $|\underline{K}| = C_i$. The equivalent of equation [6] is

$$\sum_j \left[(C_j^2 - E)\delta_{ij} + \frac{1}{\sqrt{N_i N_j}} \sum_{\substack{\underline{K} \\ |\underline{K}|=C_i}} \sum_{\substack{\underline{K}' \\ |\underline{K}'|=C_j}} V_{\underline{K}-\underline{K}'}\right] B_j = 0 \qquad [11]$$

If we use the first eleven ϕ_i in equation [10], we get an 11 × 11 matrix to diagonalize. As can be seen from table II, this includes 149 plane waves in the expansion [4].

FIGURE 2b

Unit Cell of Reciprocal Lattice for F.C.C. Structure

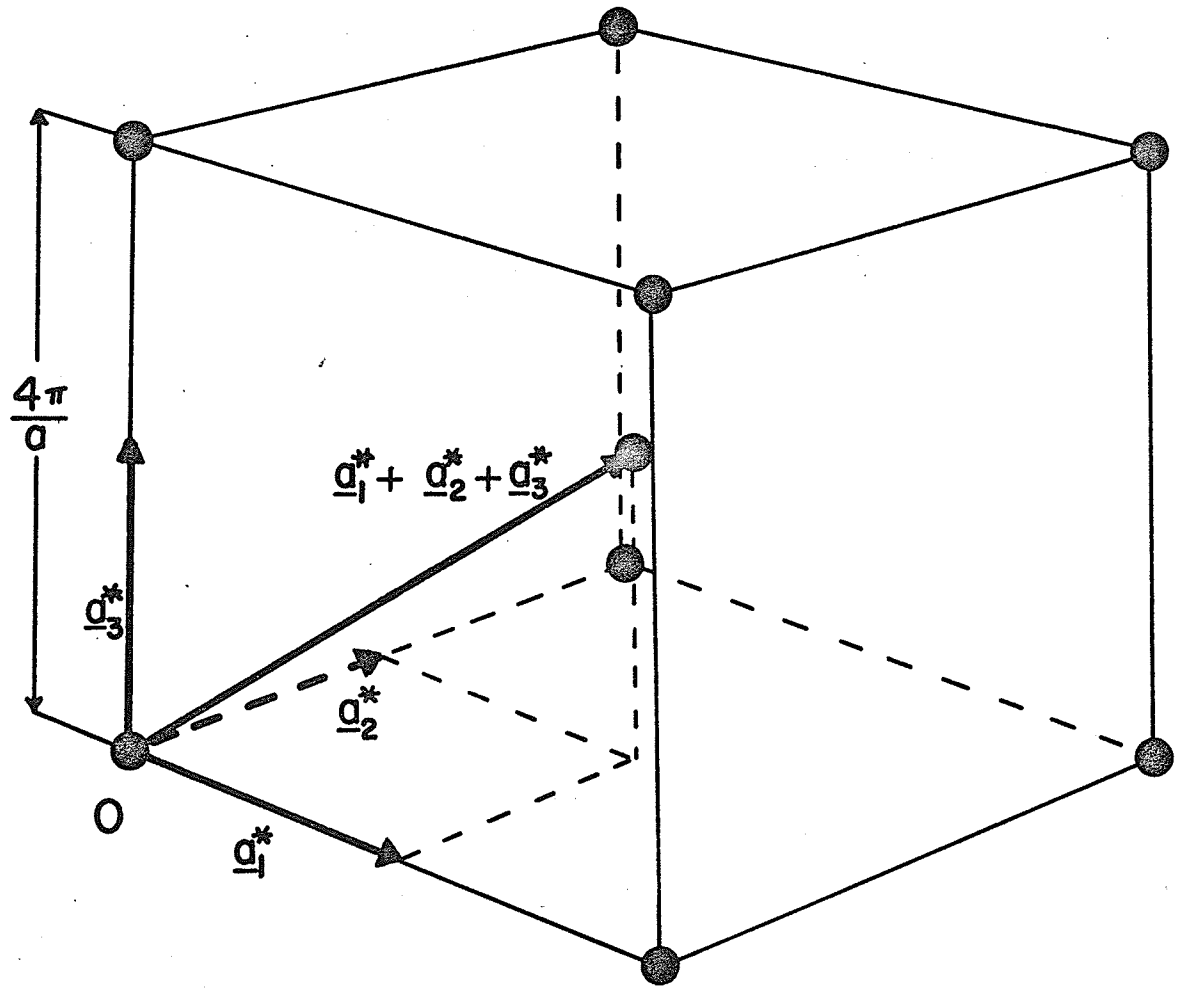
$\frac{4\pi}{a}$
$\underline{a}_1^* + \underline{a}_2^* + \underline{a}_3^*$
$\underline{a}_3^*$
$\underline{a}_2^*$
O
$\underline{a}_1^*$

We can see from equations [8] and [9] that $V_{\underline{K}}$ is real and depends only on the magnitude of $\underline{K}$. Therefore the matrix we wish to diagonalize is a real symmetric matrix.

The matrix elements were calculated using equations [11], [9], and [8], and the resulting matrix was diagonalized using the subroutine EIGEN from the IBM Scientific Subroutine Package (1968). This subroutine calculates the eigenvalues and eigenvectors of a real symmetric matrix using a method originated by Jacobi and adapted by von Neuman for large computers (Ralston and Wilf, 1962)

TABLE II

Stars and Their Coefficients for F.C.C. Case

(h,k,ℓ)	multiplicity N_i	magnitude in units of $2\pi/a$	$A_{\underline{K}} = B_i/\sqrt{N_i}$ copper	gold
0,0,0	1	0	.9730	.9627
1,1,1	8	$\sqrt{3}$	-.0736	-.0885
2,0,0	6	2	-.0397	-.0417
2,2,0	12	$\sqrt{8}$	-.0063	-.0026
3,1,1	24	$\sqrt{11}$	-.0021	+.0009
2,2,2	8	$\sqrt{12}$	-.0015	+.0007
4,0,0	6	$\sqrt{4}$	-.0005	+.0010
3,3,1	24	$\sqrt{19}$	-.0002	+.0012
4,2,0	24	$\sqrt{24}$	-.0000	+.0006
3,3,3	8	$\sqrt{27}$	+.0000	+.0007

Because the matrix of equation [11] is a real symmetric matrix, its eigenvalues and eigenvectors are all real. Therefore all the Fourier coefficients of the positron wavefunction are real.

The Fourier coefficients were calculated using successively more plane waves in the expansion [4], or more accurately, successively more basis functions in the expansion [10], until the changes in the first few coefficients became insignificantly small. It was found that 11 basis functions containing 149 plane waves were adequate for the cases of both gold and copper.

C. H.C.P. Structure

For the discussion of the hexagonal close packed structure the origin is chosen as shown in figure 3. The vectors $\underline{a}_1$ and $\underline{a}_2$ have length a, the distance between nearest neighbours in the same plane. The vector $\underline{a}_3$ which is not shown in the diagram has length c, twice the distance between planes of atoms, and is perpendicular to the vectors $\underline{a}_1$ and $\underline{a}_2$. The primitive unit cell of the h.c.p. structure contains two atoms at the positions $\frac{2}{3}\underline{a}_1 + \frac{1}{3}\underline{a}_2 + \frac{1}{4}\underline{a}_3$ and $\frac{1}{3}\underline{a}_1 + \frac{2}{3}\underline{a}_2 + \frac{3}{4}\underline{a}_3$ as shown in figure 4.

The vectors $\underline{t}_1$, $\underline{t}_2$, and $\underline{t}_4$ in figure 4 are identical to $\underline{a}_1$, $\underline{a}_2$, and $\underline{a}_3$ respectively in figure 3. They form a set of primitive vectors, and they define a primitive unit cell indicated by shading in figure 4. The volume of this unit cell is

$$\Omega = \underline{t}_1 \cdot (\underline{t}_2 \times \underline{t}_4) = \frac{\sqrt{3}}{2} a^2 c$$

The additional vector $\underline{t}_3$ is used in defining a four index notation for describing vectors in the hexagonal system.

FIGURE 3

Choice of Origin for Treatment of H.C.P. Structure
The solid circles represent spheres in a plane c/4 above the origin, the dashed circles represent spheres in a plane c/4 below the origin.

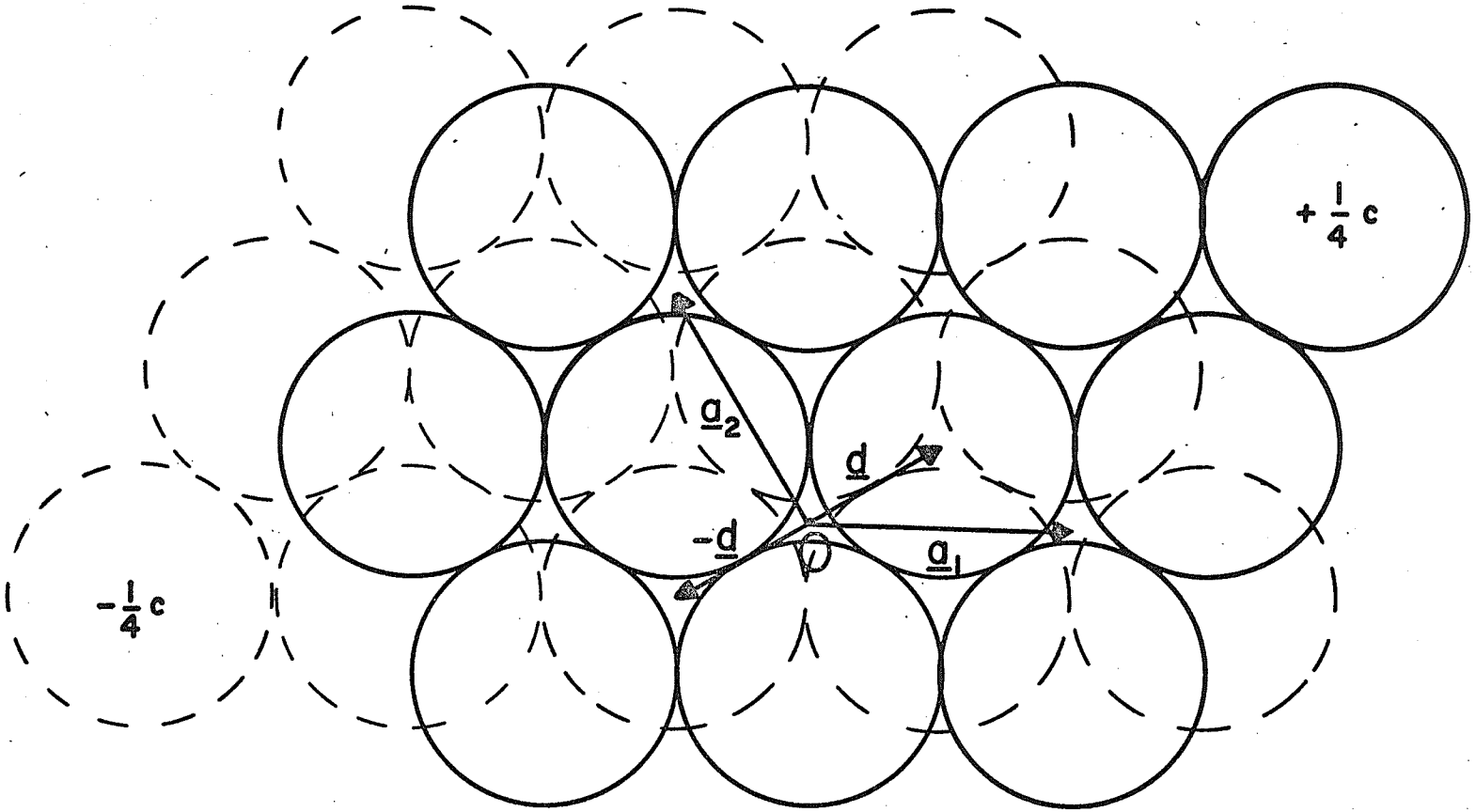
$+\frac{1}{4}c$
$-\frac{1}{4}c$
$\underline{a}_2$
$\underline{d}$
$-\underline{d}$
$\underline{a}_1$
O

FIGURE 4

Unit Cell of H.C.P. Structure

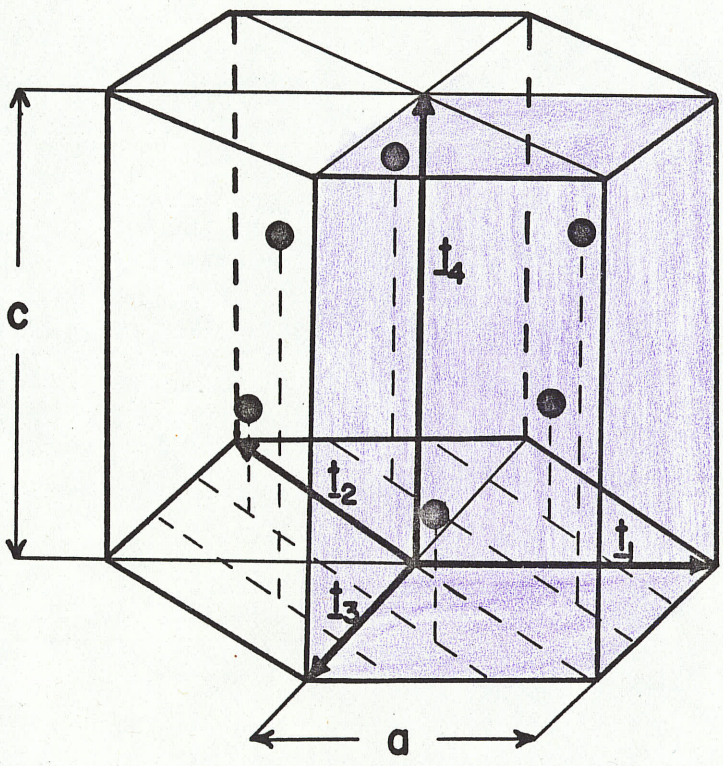
c
t_4
t_2
t_1
t_3
a

We define the quantity (h,k,i,ℓ) as the vector $h\underline{t}_1 + k\underline{t}_2 + i\underline{t}_3 + \ell\underline{t}_4$ with the restriction that we must have $h + k + i = 0$. This system has the advantage that equivalent points and directions are obviously equivalent since they are obtained from each other by permutations of the indices and signs subject to the restriction $h + k + i = 0$.

The potential $V(\underline{r})$ is constructed from the $U(r)$ by the formula

$$V(\underline{r}) = \sum_{\underline{\tau}} [U(\underline{r}-\underline{\tau}-\underline{d}) + U(\underline{r}-\underline{\tau}+\underline{d})]$$

where $\underline{d}$ is the vector $\frac{2}{3}\underline{a}_1 + \frac{1}{3}\underline{a}_2 + \frac{1}{4}\underline{a}_3$ from the origin to one of the atoms as shown in figure 3, and the sum is over all lattice vectors $\underline{\tau}$ of the hexagonal Bravais lattice.

It is easily seen that the equivalent of equation [8] is

$$V_{\underline{K}} = \frac{2\cos(\underline{K}\cdot\underline{d})}{\Omega} U_{\underline{K}} \qquad [12]$$

where Ω is defined above, and $U_{\underline{K}}$ is again given by equation [9].

The space group D_{6h}^4 of the hexagonal close packed metals is non-symmorphic and this complicates the reduction of the number of independent coefficients in the expansion of the positron wavefunction. Again lattice translations leave all the plane waves $e^{i\underline{K}\cdot\underline{r}}$ invariant and thus are no help in the reduction. The remaining operations with no lattice translations consist of rotations (proper and improper) and rotations combined with a nonprimitive translation of $\frac{c}{2}$ along the $\underline{a}_3$ axis.

To discuss the effect of these operations on the plane waves $e^{i\underline{K}\cdot\underline{r}}$, it is necessary to have a clear picture of the reciprocal lattice to the hexagonal space lattice. A single hexagonal cell of the reciprocal lattice is shown in figure 5. The four vectors $\underline{t}_1^*$, $\underline{t}_2^*$, $\underline{t}_3^*$, $\underline{t}_4^*$ define a four index notation for reciprocal lattice vectors in the same way as

FIGURE 5

Unit Cell of Reciprocal Lattice for H.C.P. Structure

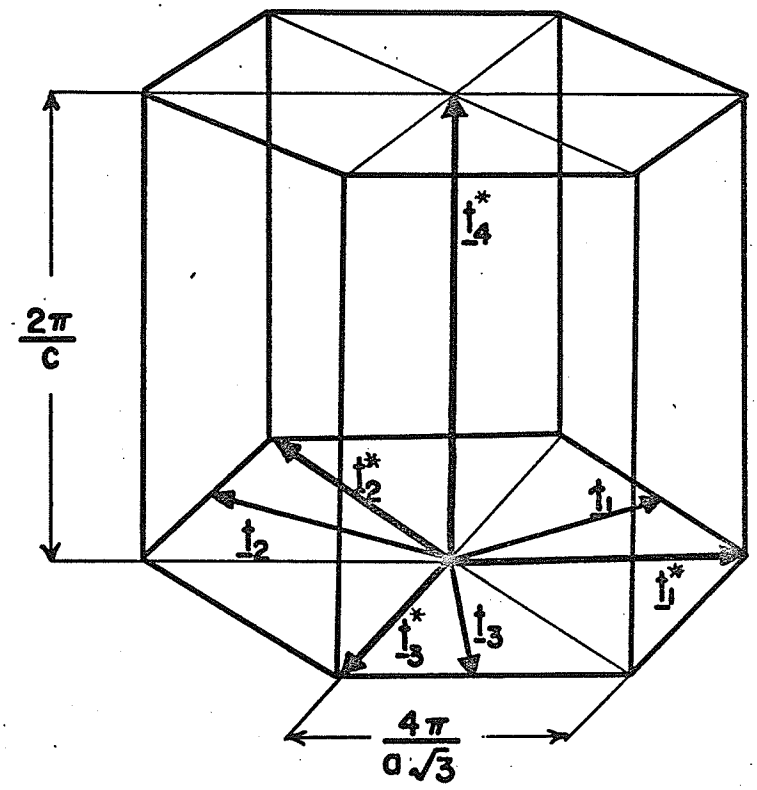
$\frac{2\pi}{c}$
$\underline{t}_4^*$
$\underline{t}_2^*$
$\underline{t}_1$
$\underline{t}_2$
$\underline{t}_1^*$
$\underline{t}_3^*$
$\underline{t}_3$
$\frac{4\pi}{a\sqrt{3}}$

$\underline{t}_1$, $\underline{t}_2$, $\underline{t}_3$, $\underline{t}_4$ do for the real lattice vectors. The vectors $\underline{t}_1$, $\underline{t}_2$, $\underline{t}_3$, $\underline{t}_4$ are shown in figure 5 to indicate the orientation of the reciprocal lattice relative to the real lattice.

The rotations in real space again transform the plane wave $e^{i\underline{K}\cdot\underline{r}}$ into $e^{i\underline{K}'\cdot\underline{r}}$ where $\underline{K}'$is obtained from $\underline{K}$ by applying the inverse rotation in reciprocal space. The non-primitive translation applied to $e^{i\underline{K}\cdot\underline{r}}$ where $\underline{K} = h\underline{t}_1^* + k\underline{t}_2^* + i\underline{t}_3^* + \ell\underline{t}_4^*$ multiplies it by $(-1)^{\ell}$. The operations of the group D_{6h}^4 not involving lattice translations are listed in table III together with their action on an arbitrary function $\psi(\underline{r})$. The vector $\underline{r}$ in real space is specified by the co-ordinates u, v, w in terms of hexagonal axes, i.e.

$$\underline{r} = u\underline{a}_1 + v\underline{a}_2 + w\underline{a}_3$$

where $\underline{a}_1$, $\underline{a}_2$, $\underline{a}_3$ are shown in figure 3.

Figure 6 shows a plane in reciprocal space. With origin chosen at 0, it is clear that the groups of lattice vectors having the same magnitude are those whose ends lie on the same circle about the origin or whose ends lie the same distance above or below the basal plane and whose projections on the basal plane lie on the same circle about the origin. The type of such a group will be specified as the number of the circle on which the group is projected in the basal plane in figure 6. Figure 7 shows the projections of the reciprocal lattice points of different type onto a unit circle in the basal plane. The inner circle corresponds to points from below the basal plane, the outer circle to points from above the basal plane. In the case of a group from the basal plane, the inner and outer circles coincide. Now, by considering table III and figure 7, we can see which points are carried into each

FIGURE 6

Plane in Reciprocal Lattice of Figure 5

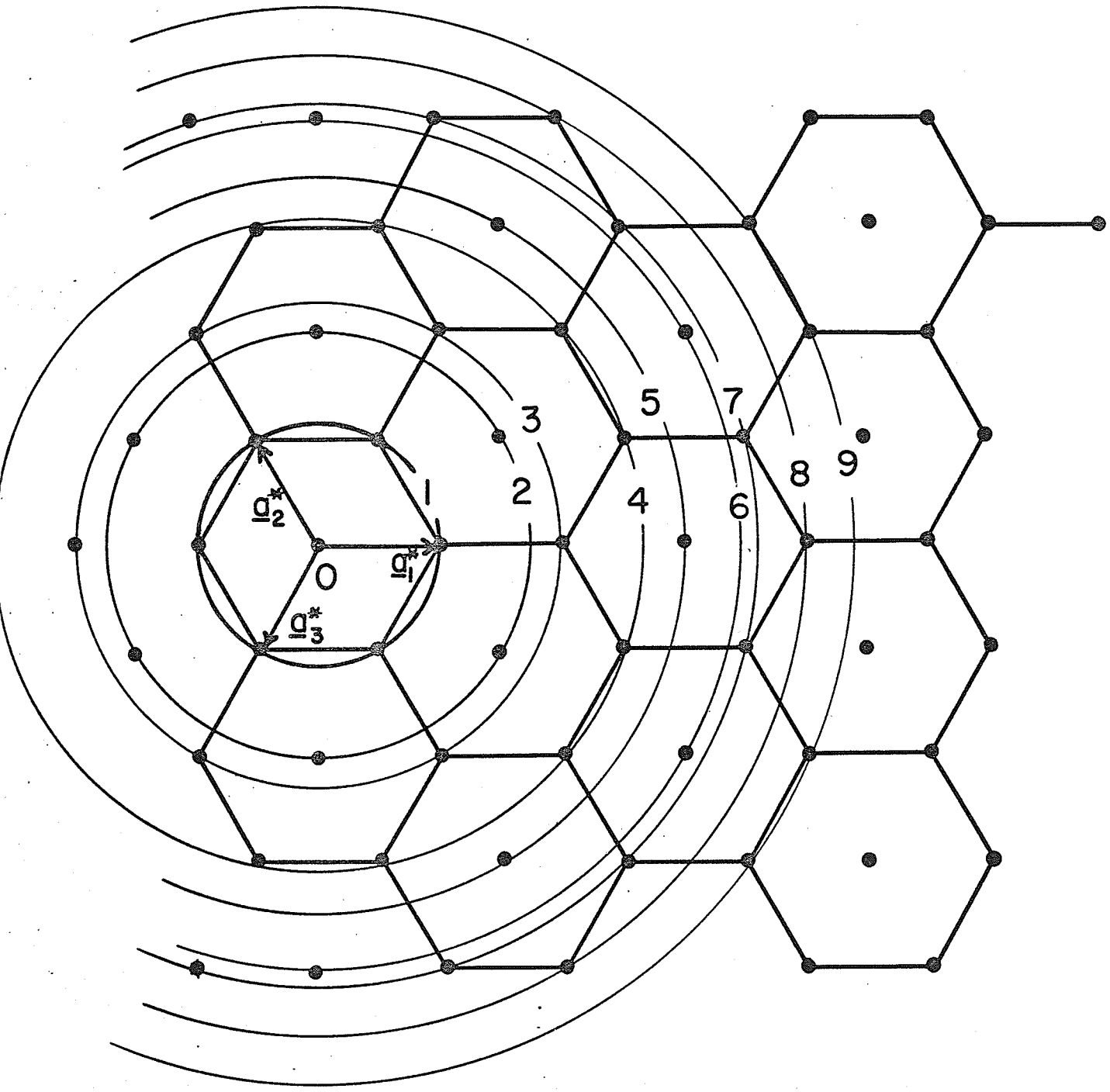
0
1
2
3
4
5
6
7
8
9
$\underline{a}_1^*$
$\underline{a}_2^*$
$\underline{a}_3^*$

FIGURE 7

Projections of Stars onto Unit Circle in Basal Plane for H.C.P. Structure

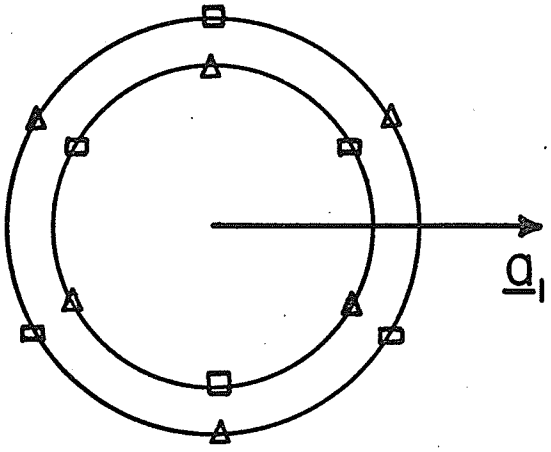

types 1,3,5,8

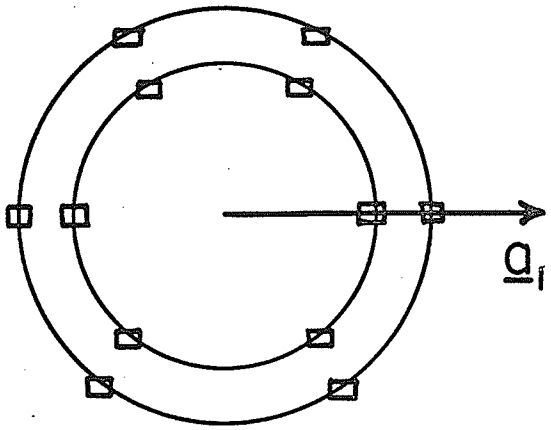

types 2,6

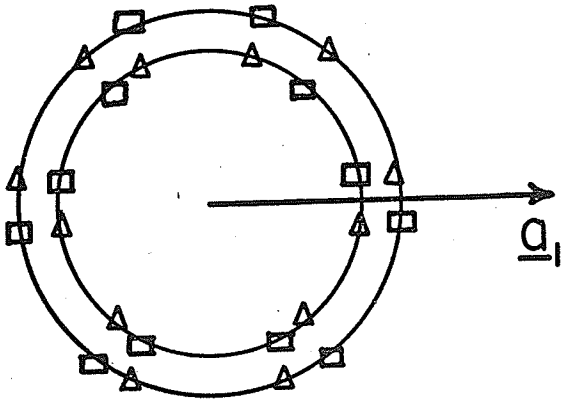

types 4,7,9

TABLE III

Operators of Group D_{6h}^4 not involving Lattice Translations

---

$X_o \quad \psi(\underline{r}) = \quad \psi(u,v,w)$

$X_1 \quad \psi(\underline{r}) = \quad \psi(u-v,u,w+\frac{1}{2})$

$X_{-1} \quad \psi(\underline{r}) = \quad \psi(v,v-u,w+\frac{1}{2})$

$X_2 \quad \psi(\underline{r}) == \quad \psi(-v,u-v,w)$

$X_{-2} \quad \psi(\underline{r}) = \quad \psi(v-u,-u,w)$

$X_3 \quad \psi(\underline{r}) = \quad \psi(-u,-v,w+\frac{1}{2})$

$Y_o \quad \psi(\underline{r}) = \quad \psi(u,u-v,w)$

$Y_1 \quad \psi(\underline{r}) = \quad \psi(v,u,w+\frac{1}{2})$

$Y_{-1} \quad \psi(\underline{r}) = \quad \psi(u-v,-v,w+\frac{1}{2})$

$Y_2 \quad \psi(\underline{r}) = \quad \psi(v-u,v,w)$

$Y_{-2} \quad \psi(\underline{r}) = \quad \psi(-u,-v,w)$

$Y_3 \quad \psi(\underline{r}) = \quad \psi(-u,v-u,w+\frac{1}{2})$

$X_o \quad \psi(\underline{r}) = \quad \psi(u,v,-w+\frac{1}{2})$

$X_1^1 \quad \psi(\underline{r}) = \quad \psi(u-v,u,-w)$

$X_{-1}^1 \quad \psi(\underline{r}) = \quad \psi(v,v-u,-w)$

$X_2^1 \quad \psi(\underline{r}) = \quad \psi(-v,u-v,-w+\frac{1}{2})$

$X_{-2}^1 \quad \psi(\underline{r}) = \quad \psi(v-u,-u,-w+\frac{1}{2})$

$X_3^1 \quad \psi(\underline{r}) = \quad \psi(-u,-v,-w)$

$Y_o^1 \quad \psi(\underline{r}) = \quad \psi(u,u-v,-w+\frac{1}{2})$

$Y_1^1 \quad \psi(\underline{r}) = \quad \psi(v,u,-w)$

$Y_{-1}^1 \quad \psi(\underline{r}) = \quad \psi(u-v,-v,-w)$

$Y_2^1 \quad \psi(\underline{r}) = \quad \psi(v-u,v,-w+\frac{1}{2})$

$Y_{-2}^1 \quad \psi(\underline{r}) = \quad \psi(-v,-u,-w+\frac{1}{2})$

$Y_3^1 \quad \psi(\underline{r}) = \quad \psi(-u,v-u,-w)$

other by the various operations and the relationship of the corresponding coefficients of the positron wavefunction.

The plane waves corresponding to the reciprocal lattice vectors of a group all having the same magnitude are transformed into one another with perhaps a change of sign. In fact it can be seen that if $\underline{K} = (h,k,i,\ell)$ is a typical member of the group, the plane waves corresponding to the reciprocal lattice vectors of the group represented by a square in figure 7 transform into one another with no change of sign and into $(-1)^{\ell}$ times the plane waves corresponding to those reciprocal lattice vectors of the group represented by a triangle.

We again use the argument that for the $\psi_+(\underline{r})$ to be invariant for arbitrary $\underline{r}$ the transformed expansion must be identical term by term. This implies that if $e^{i\underline{K}'\cdot\underline{r}}$ is transformed into $(-1)^{\ell}\, e^{i\underline{K}\cdot\underline{r}}$ then $A_{\underline{K}'} = (-1)^{\ell} A_{\underline{K}}$. The group of all reciprocal lattice vectors having the same magnitude and obtainable from one another by a permutation of signs and indices in the four index notation will again be called a star, and we construct the following functions from the plane waves corresponding to the elements of a star.

$$\Phi_i = \frac{1}{\sqrt{N_i}} \sum_{\substack{\underline{K} \\ |\underline{K}|=C_i}} \theta_{\underline{K}}\, e^{i\underline{K}\cdot\underline{r}} \qquad [13]$$

where $\theta_{\underline{K}}$ for $\underline{K} = (h,k,k,\ell)$ is +1 for all reciprocal lattice vectors represented by a square in figure 7, and is $(-1)^{\ell}$ for all reciprocal lattice vectors represented by a triangle. Otherwise the notation is the same as for the cubic case and again

$$\psi_+(\underline{r}) = \sum_i B_i \Phi_i$$

where $B_i = \sqrt{N_i}\ A_{\underline{K}}$ for $|\underline{K}| = C_i$

It is clear that the star whose typical vector is of the form $(0,0,0,\ell)$ will have coefficient zero when ℓ is odd since the operation X_3' carries $e^{i\underline{K}\cdot\underline{r}}$ into $e^{i(-\underline{K})\cdot\underline{r}}$ giving $A_{\underline{K}} = A_{-\underline{K}}$ whereas X_0' carries $e^{i\underline{K}\cdot\underline{r}}$ into $(-1)^\ell\, e^{i(-\underline{K})\cdot\underline{r}}$ giving $A_{\underline{K}} = (-1)^\ell A_{-\underline{K}} = (-)^\ell A_{\underline{K}}$. The star specified by the vector $(1,-1,0,\ell)$ exhibits the same property since the operation Y_{-1} carries $e^{i\underline{K}\cdot\underline{r}}$ into $(-1)^\ell\, e^{i\underline{K}\cdot\underline{r}}$ giving $A_{\underline{K}} = (-1)^\ell A_{\underline{K}}$.

Typical vectors of the first 25 stars in order of increasing magnitude are shown in table IV for the ideal h.c.p. structure along with their magnitudes, multiplicities, and the value of their coefficients. Magnesium is very close to being ideal h.c.p. but zinc and cadmium have $\frac{c}{a}$ ratios differing substantially from that for ideal h.c.p. Therefore the ordering of some of the higher stars is changed and the stars listed in table IV are not the first 25 stars for zinc and cadmium.

Equation [11] for the cubic case now becomes

$$\sum_j [(C_j^2 - E)\delta_{ij} + \frac{1}{\sqrt{N_i N_j}} \sum_{|\underline{K}|=C_i} \sum_{|\underline{K}'|=C_j} \theta_{\underline{K}}\theta_{\underline{K}'} V_{\underline{K}-\underline{K}'}]B_j = 0 \qquad [14]$$

where $\theta_{\underline{K}}$ is as defined above for equation [13]. $V_{\underline{K}-\underline{K}'}$ is calculated from equations [9] and [12]. If we use the first 25 Φ_i, omitting those whose coefficients we have shown to be zero, we obtain a 20 × 20 matrix to diagonalize. This matrix was diagonalized, and the eigenvalues and eigenvectors obtained in the same way as in the cubic case. It was found that the use of 25 basis functions containing 245 plane waves gave good results for magnesium, zinc and cadmium.

TABLE IV

Stars and Their Coefficients for H.C.P. Case

(h,k,i,ℓ)	multiplicity	magnitude in units of $4\pi/\sqrt{3a}$	$A_K = B_i/\sqrt{N_i}$ magnesium	zinc	cadmium
0,0,0,0	1	0	.9637	.9575	.9521
0,0,0,1	2	.53	0	0	0
$\frac{2}{3},-\frac{1}{3},-\frac{1}{3},0$	6	1	.0432	.0366	.0367
0,0,0,2	2	1.06	.1298	.1649	.1816
$\frac{2}{3},-\frac{1}{3},-\frac{1}{3},1$	12	1.13	-.0462	-.0406	-.0396
$\frac{2}{3},-\frac{1}{3},-\frac{1}{3},2$	12	1.46	-.0073	-.0078	-.0070
0,0,0,3	2	1.59	0	0	0
1,-1,0,0	6	1.73	-.0041	-.0035	-.0024
1,-1,0,1	12	1.81	0	0	0
$\frac{2}{3},-\frac{1}{3},-\frac{1}{3},3$	12	1.88	.0019	.0025	.0012
$\frac{4}{3},-\frac{2}{3},-\frac{2}{3},0$	6	2	.0009	.0005	.0002
1,-1,0,2	12	2.03	.0011	.0010	.0001
$\frac{4}{3},-\frac{2}{3},-\frac{2}{3},1$	12	2.07	-.0012	.0006	-.0001
0,0,0,4	2	2.12	-.0030	-.0012	.0008
$\frac{4}{3},-\frac{2}{3},-\frac{2}{3},2$	12	2.26	-.0004	-.0002	.0001
$\frac{2}{3},-\frac{1}{3},-\frac{1}{3},4$	12	2.35	.0002	-.0002	-.0009
1,-1,0,3	12	2.35	0	0	0
$\frac{4}{3},-\frac{2}{3},-\frac{2}{3},3$	12	2.56	-.0006	-.0002	.0003
$\frac{5}{3},-\frac{4}{3},-\frac{1}{3},0$	12	2.65	.0004	.0003	.0002
0,0,0,5	2	2.65	0	0	0
$\frac{5}{3},-\frac{4}{3},-\frac{1}{3},1$	24	2.70	.0006	-.0001	-.0006
1,-1,0,4	12	2.74	-.0004	.0001	.0007
$\frac{2}{3},-\frac{1}{3},-\frac{1}{3},5$	12	2.83	.0004	.0002	.0010
$\frac{5}{3},-\frac{4}{3},-\frac{1}{3},2$	24	2.85	-.0003	-.0000	.0002
$\frac{4}{3},-\frac{2}{3},-\frac{2}{3},4$	12	2.92	.0003	-.0000	-.0002

2.3 Distributions in Momentum Space

A. General

The probability per unit time that a positron in the state $\frac{1}{\sqrt{w}}\psi_+(\underline{r})$ will annihilate with an electron in a singly occupied Bloch state $\frac{1}{\sqrt{N}} U_{\underline{k}}(\underline{r})\, e^{i\underline{k}\cdot\underline{r}}$ to produce a photon pair with total momentum in the range $d\underline{p}$ at $\underline{p}$ is given by $\rho_{\underline{k}}(\underline{p})d\underline{p}$ (Ferrell 1956, Chang Lee 1958), where

$$\rho_{\underline{k}}(\underline{p}) = \frac{\alpha^3}{8\pi^2 N^2 \Omega}\left|\int_w d\underline{r}\, e^{i(\underline{k}-\underline{p})\cdot\underline{r}}\, \psi_+(\underline{r}) U_{\underline{k}}(\underline{r})\right|^2 \qquad [15]$$

$U_{\underline{k}}(\underline{r})$ is normalized to 1 in a unit cell of volume Ω, while $\psi_+(\underline{r})$ is normalized to Ω in a unit cell. w is the volume of the crystal and is equal to $N\Omega$.

This normalization of the positron wavefunction is equivalent to placing the condition on equation [4] that

$$\sum_{\underline{K}} A_{\underline{K}}^2 = 1 \qquad [16]$$

since by equation [4]

$$\int_\Omega |\psi_+(\underline{r})|^2 d\underline{r} = \frac{1}{N}\int_w \sum_{\underline{K}}\sum_{\underline{K}'} A_{\underline{K}} A_{\underline{K}'}^*\, e^{i(\underline{K}-\underline{K}')\cdot\underline{r}}\, d\underline{r}$$

but the coefficients $A_{\underline{K}}$ are all real, and so

$$\int_\Omega |\psi_+(\underline{r})|^2 d\underline{r} = \frac{w}{N}\sum_{\underline{K}} A_{\underline{K}}^2 = \Omega\sum_{\underline{K}} A_{\underline{K}}^2$$

For the electron wavefunction $U_{\underline{k}}(\underline{r})\, e^{i\underline{k}\cdot\underline{r}}$ we shall use the Bloch tight binding function (Bloch 1928, Peierls 1955, Ziman 1964), which, in the case of one atom per unit cell, is given by

$$U_{\underline{k}}^{\beta}(\underline{r})\, e^{i\underline{k}\cdot\underline{r}} = \sum_{\underline{\tau}} e^{i\underline{k}\cdot\underline{\tau}}\, \Phi_{n\ell m}(\underline{r}-\underline{\tau}) \qquad [17]$$

where n,ℓ,m are the quantum numbers specifying the atomic orbital and β labels the band in the crystal. This expression can easily be seen to satisfy the normalization condition on $U_{\underline{k}}(\underline{r})$ given in section 2.3A.

As long as the overlap between orbitals on neighbouring atoms is small, the resulting bands are narrow relative to the spacing between them for non-degenerate orbitals. The band may then be labelled by the atomic quantum numbers n,ℓ,m. If, however, we have an s-fold degenerate atomic energy level, this level may lead to one band having $s \cdot N$ states if the crystal field does not split the degeneracy, to s bands each having N states if there is complete splitting of the degeneracy, or to some case intermediate between these two.

The Hartree-Fock Slater orbitals having $2\ell+1$-fold degeneracy for each n,ℓ. If these lead to $2\ell+1$ bands which mix different m states then we must use the $(2\ell+1)N$ degenerate orbitals in the sum [17] and it takes on the following form

$$U_{\underline{k}}^{n\ell\mu}(\underline{r})\ e^{i\underline{k}\cdot\underline{r}} = \sum_{\underline{\tau}} \sum_{m} e^{i\underline{k}\cdot\underline{\tau}}\ a_{m\mu}\ \Phi_{n\ell m}(\underline{r}-\underline{\tau}) \qquad [18]$$

where the coefficients $a_{m\mu}$ must be independent of $\underline{\tau}$ for Bloch's theorem to be satisfied. The band is now labelled by n,ℓ,μ where μ runs through $2\ell+1$ values. The value of the coefficients $a_{m\mu}$ are to be determined by a variational calculation. However, for the purposes of the present calculation it is not necessary to determine them explicitly.

We can make the unitary transformation

$$\chi_{n\ell\mu}(\underline{r}) = \sum_{m=-\ell}^{+\ell} a_{m\mu}\ \Phi_{n\ell m}(\underline{r}) \qquad [19]$$

and then equation [18] becomes

$$U_{\underline{k}}^{n\ell\mu}(\underline{r})\, e^{i\underline{k}\cdot\underline{r}} = \sum_{\underline{\tau}} e^{i\underline{k}\cdot\underline{\tau}}\, \chi_{n\ell\mu}(\underline{r}-\underline{\tau}) \qquad [20]$$

In the following section we will assume that the mixing of m states in a band does not occur and shall label the bands by n,ℓ,m. All the results are the same if mixing does occur in the case of closed shell core structures. This may be seen fairly easily, although rather tediously, by using equation [20] in place of equation [17], using the unitarity of the transformation [19] and summing over μ from 1 to $2\ell+1$ in equation [28] instead of over m.

B. F.C.C. Structure

The f.c.c. structure has one atom per unit cell and so equation [17] gives the tight binding function for an electron in the band labelled by n,ℓ,m. Substituting this in equation [15] we get

$$\rho_{\underline{k}}^{n\ell m}(\underline{p}) = \frac{\alpha^3}{8\pi^2 N^2 \Omega} \left| \sum_{\underline{\tau}} e^{i\underline{k}\cdot\underline{\tau}} \sum_{\underline{K}} A_{\underline{K}} \int_w e^{-i(\underline{p}-\underline{K})\cdot\underline{r}}\, \Phi(\underline{r}-\underline{\tau})\, d\underline{r} \right|^2$$

$$= \frac{\alpha^3}{8\pi^2 N^2 \Omega} \left| \sum_{\underline{\tau}} e^{i(\underline{k}+\underline{K}-\underline{p})\cdot\underline{\tau}} \sum_{\underline{K}} A_{\underline{K}}\, B_{n\ell m}(\underline{p}-\underline{K}) \right|^2$$

where $$B_{n\ell m}(\underline{p}-\underline{K}) = \int_w e^{-i(\underline{p}-\underline{K})\cdot\underline{r}}\, \Phi_{n\ell m}(\underline{r})\, d\underline{r} \qquad [21]$$

Using the relation

$$\sum_{\underline{\tau}} e^{i(\underline{k}+\underline{K}-\underline{p})\cdot\underline{\tau}} = N\delta_{\underline{k}-\underline{p},\underline{G}}$$

where $\underline{G}$ is any reciprocal lattice vector, we obtain

$$\rho_{\underline{k}}^{n\ell m}(\underline{p}) = \frac{\alpha^3}{8\pi^2 \Omega} \left| \sum_{\underline{K}} A_{\underline{K}}\, B_{n\ell m}(\underline{p}-\underline{K}) \right|^2 \delta_{\underline{k}-\underline{p},\underline{G}} \qquad [22]$$

The total contribution from the band labelled by n,ℓ,m is obtained by summing over the occupied electron states. There are N $\underline{k}$ states in a band each capable of containing 2 electrons. Each occupied core orbital n,ℓ,m contains 2 electrons since the atom core is assumed to have closed shell structure. The N atoms contribute 2N electrons to the band n,ℓ,m and it is full. Therefore, in the band n,ℓ,m there is one and only one occupied $\underline{k}$ state such that $\underline{k}-\underline{p} = \underline{G}$.

The sum over occupied electron states is twice the sum over occupied $\underline{k}$ states and we obtain

$$\rho^{n\ell m}(\underline{p}) = 2\sum_{\substack{\underline{k} \\ \text{occ.}}} \rho_{\underline{k}}^{n\ell m}(\underline{p}) = \frac{\alpha^3}{4\pi^2\Omega} \left|\sum_{\underline{K}} A_{\underline{K}} B_{n\ell m}(\underline{p}-\underline{K})\right|^2 \qquad [23]$$

The Hartree-Fock-Slater orbital $\Phi_{n\ell m}(\underline{r})$ may be written

$$\Phi_{n\ell m}(\underline{r}) = \frac{P_{n\ell}(r)}{r} Y_{\ell}^{m}(\theta_{\underline{r}},\phi_{\underline{r}}) \qquad [24]$$

where $P_{n\ell}$ is numerically tabulated, $Y_{\ell}^{m}(\theta_{\underline{r}},\phi_{\underline{r}})$ is a spherical harmonic, and r, $\theta_{\underline{r}},\phi_{\underline{r}}$ are the spherical polar coordinates of $\underline{r}$. Using this and the expansion

$$e^{-i\underline{q}\cdot\underline{r}} = 4\pi \sum_{\ell'=0}^{\infty} \sum_{m=-\ell'}^{+\ell'} (-i)^{\ell'} j_{\ell'}(qr) Y_{\ell'}^{m'}(\theta_{\underline{q}},\phi_{\underline{q}}) Y_{\ell'}^{*m'}(\theta_{\underline{r}},\phi_{\underline{r}}) \qquad [25]$$

where q, $\theta_{\underline{q}}$, $\phi_{\underline{q}}$ are the spherical polar coordinates of $\underline{q}$ in the same coordinate system, we may write $B_{n\ell m}(\underline{q})$ as

$$B_{n\ell m}(\underline{q}) = 4\pi \sum_{\ell'=0}^{\infty} \sum_{m'=-\ell'}^{+\ell'} (-i)^{\ell'} \int_{w} d\underline{r}\; j_{\ell'}(qr) Y_{\ell'}^{m'}(\theta_{\underline{q}},\phi_{\underline{q}}) Y_{\ell'}^{*m'}(\theta_{\underline{r}},\phi_{\underline{r}})$$

$$(P_{n\ell}(r)/r) Y_{\ell}^{m}(\theta_{\underline{r}},\phi_{\underline{r}})$$

Then, using the relation

$$\int_0^{2\pi} d\phi_{\underline{r}} \int_0^{\pi} d\theta_{\underline{r}} \sin\theta_{\underline{r}} Y_{\ell'}^{*m'}(\theta_{\underline{r}},\phi_{\underline{r}}) Y_{\ell}^{m}(\theta_{\underline{r}},\phi_{\underline{r}}) = \delta_{mm'}\,\delta_{\ell\ell'}$$

we get

$$B_{n\ell m}(\underline{q}) = 4\pi(-i)^{\ell} Y_{\ell}^{m}(\theta_{\underline{q}},\phi_{\underline{q}}) \int_0^{\infty} dr\, r j_{\ell}(qr) P_{n\ell}(r) \qquad [26]$$

We make the definition

$$I_{n\ell}(\underline{q}) = \int_0^{\infty} dr\, r j_{\ell}(qr) P_{n\ell}(r) \qquad [27]$$

and substitute equation [26] and [27] into equation [23] obtaining after summation over all m values for fixed n,

$$\rho^{n\ell}(\underline{p}) = \sum_{m=-\ell}^{+\ell} \rho^{n\ell m}(\underline{p}) = \frac{4\alpha^3}{\Omega} \sum_{\underline{K}} \sum_{\underline{K}'} A_{\underline{K}} A^*_{\underline{K}'}\, I_{n\ell}(\underline{p}-\underline{K}) I^*_{n\ell}(\underline{p}-\underline{K}') \sum_{m=-\ell}^{\ell}$$

$$Y_{\ell}^{m}(\theta_{\underline{p}-\underline{K}},\phi_{\underline{p}-\underline{K}}) Y_{\ell}^{*m}(\theta_{\underline{p}-\underline{K}'},\phi_{\underline{p}-\underline{K}'}) \qquad [28]$$

By the addition theorem for spherical harmonics

$$\sum_{m=-\ell}^{+\ell} Y_{\ell}^{m}(\theta_{\underline{p}-\underline{K}},\phi_{\underline{p}-\underline{K}}) Y_{\ell}^{*m}(\theta_{\underline{p}-\underline{K}'},\phi_{\underline{p}-\underline{K}'}) = \frac{2\ell+1}{4\pi} P_{\ell}(\cos\alpha_{\underline{p}-\underline{K},\underline{p}-\underline{K}'}) \qquad [29]$$

where $\cos\alpha_{\underline{p}-\underline{K},\underline{p}-\underline{K}'} = (\underline{p}-\underline{K})\cdot(\underline{p}-\underline{K}')/|\underline{p}-\underline{K}'||\underline{p}-\underline{K}|$ [30]

and we get for equation [28], noting that $A_{\underline{K}}$ and $I_{n\ell}(\underline{q})$ are real

$$\rho^{n\ell}(\underline{p}) = \frac{(2\ell+1)\alpha^3}{\pi\Omega} \sum_{\underline{K}} \sum_{\underline{K}'} A_{\underline{K}} A_{\underline{K}'}\, I_{n\ell}(\underline{p}-\underline{K}) I_{n\ell}(\underline{p}-\underline{K}') P_{\ell}(\cos\alpha_{\underline{p}-\underline{K},\underline{p}-\underline{K}'}) \qquad [31]$$

which depends only on the relative orientations of the $\underline{p}-\underline{K}$, and is thus independent of our choice of coordinate system in equations [24] and [25].

This expression can be evaluated in a straight-forward manner using equations [27] and [30]. The total $\rho(\underline{p})$ is then obtained by summing $\rho^{n\ell}(\underline{p})$ over the appropriate core shells n,ℓ.

C. H.C.P. Structure

The h.c.p. structure has a basis of two atoms per unit cell. In this case the expression [17] for the tight binding functions must be modified slightly. Two linearly independent combinations for the tight binding function are given by (Kittel 1963)

$$e^{i\underline{k}\cdot\underline{r}}\, U_{\underline{k}}^{\,b}(\underline{r}) = \frac{1}{\sqrt{2}} \sum_{\underline{\tau}} \{e^{i\underline{k}\cdot(\underline{\tau}+\underline{d})}\, \Phi_{n\ell m}(\underline{r}-\underline{\tau}-\underline{d}) + e^{i\underline{k}\cdot(\underline{\tau}-\underline{d})}\, \Phi_{n\ell m}(\underline{r}-\underline{\tau}+\underline{d})\} \quad [32]$$

and $$e^{i\underline{k}\cdot\underline{r}}\, U_{\underline{k}}^{\,a}(\underline{r}) = \frac{1}{\sqrt{2}} \sum_{\underline{\tau}} \{e^{i\underline{k}\cdot(\underline{\tau}+\underline{d})}\, \Phi_{n\ell m}(\underline{r}-\underline{\tau}-\underline{d}) - e^{i\underline{k}\cdot(\underline{\tau}-\underline{d})}\, \Phi_{n\ell m}(\underline{r}-\underline{\tau}+\underline{d})\} \quad [33]$$

These correspond to the formation of bonding and antibonding orbitals respectively from the orbitals on the two atoms in a unit cell.

The bonding and antibonding orbitals will lead to two bands for each atomic orbital, each having N doubly occupied k-states. But we will now have 4N electrons for these bands so both will be filled.

In the case where there is no overlap between orbitals on the two different atoms in the unit cell, these two functions are degenerate. We must then again make linear combinations of the degenerate functions as in the preceding section. Again the final results are the same as for the non-degenerate case. We will work through this non-degenerate case.

Substituting [4] and [32] into [15] we get

$$\rho_{\underline{k}}^{n\ell mb} = \frac{\alpha^3}{8\pi^2 N^2 \Omega} \left|\frac{1}{\sqrt{2}} \{\sum_{\underline{\tau}} e^{i(\underline{k}+\underline{K}-\underline{p})\cdot(\underline{\tau}+\underline{d})} \sum_{\underline{K}} A_{\underline{K}} \int_W e^{-i(\underline{p}-\underline{K}-\underline{k})\cdot(\underline{r}-\underline{\tau}-\underline{d})} \Phi(\underline{r}-\underline{\tau}-\underline{d}) d(\underline{r}-\underline{\tau}-\underline{d})\right.$$

$$\left. + \sum_{\underline{\tau}} e^{i(\underline{k}+\underline{K}-\underline{p})\cdot(\underline{\tau}-\underline{d})} \sum_{\underline{K}} A_{\underline{K}} \int_W e^{-i(\underline{p}-\underline{K}-\underline{k})\cdot(\underline{r}-\underline{\tau}+\underline{d})} \Phi(\underline{r}-\underline{\tau}+\underline{d}) d(\underline{r}-\underline{\tau}+\underline{d})\}\right|^2$$

$$= \frac{\alpha^3}{16\pi^2\Omega} \left|\sum_{\underline{K}} A_{\underline{K}} B_{n\ell m}(\underline{p}-\underline{K})[e^{i(\underline{k}+\underline{K}-\underline{p})\cdot\underline{d}} + e^{-i(\underline{k}+\underline{K}-\underline{p})\underline{d}}]\delta_{\underline{k}-\underline{p},\underline{G}}\right|^2$$

$$= \frac{\alpha^3}{16\pi^2\Omega} \sum_{\underline{K}} \sum_{\underline{K}'} A_{\underline{K}} A^*_{\underline{K}'} B_{n\ell m}(\underline{p}-\underline{K}) B^*_{n\ell m}(\underline{p}-\underline{K}')[2\cos\theta_1 + 2\cos\theta_2]\delta_{\underline{k}-\underline{p},\underline{G}}$$

where $\theta_1 = (\underline{K}-\underline{K}')\cdot\underline{d}$ $\quad\quad$ $\theta_2 = (2\underline{k}+\underline{K}+\underline{K}'-2\underline{p})\cdot\underline{d}$ similarly from [33] we get

$$\rho_{\underline{k}}^{n\ell ma} = \frac{\alpha^3}{16\pi^2\Omega} \sum_{\underline{K}} \sum_{\underline{K}'} A_{\underline{K}} A_{\underline{K}'} B_{n\ell m}(\underline{p}-\underline{K}) B^*_{n\ell m}(\underline{p}-\underline{K}')[2\cos\theta_1 - 2\cos\theta_2]\delta_{\underline{k}-\underline{p},\underline{G}}$$

Then for the total from the two bands we get

$$\rho_{\underline{k}}^{n\ell m}(\underline{p}) = \frac{\alpha^3}{4\pi^2\Omega} \sum_{\underline{K}} \sum_{\underline{K}'} A_{\underline{K}} A_{\underline{K}'} B_{n\ell m}(\underline{p}-\underline{K}) B^*_{n\ell m}(\underline{p}-\underline{K}') \cos(\underline{K}-\underline{K}')\cdot\underline{d}\,\delta_{\underline{k}-\underline{p},\underline{G}}.$$

We may now use the same procedure as in section 2.1A to sum over $\underline{k}$ occupied and m, obtaining the result

$$\rho^{n\ell}(\underline{p}) = \frac{2(2\ell+1)\alpha^3}{\pi\Omega} \sum_{\underline{K}} \sum_{\underline{K}'} A_{\underline{K}} A^*_{\underline{K}'} I_{n\ell}(\underline{p}-\underline{K}) I_{n\ell}(\underline{p}-\underline{K}') \quad (\cos(\underline{K}-\underline{K}')\cdot\underline{d}) \qquad [34]$$

$$P_\ell \cos(\alpha_{\underline{p}-\underline{K},\underline{p}-\underline{K}'})$$

where $I_{n\ell}(\underline{p}-\underline{K})$, $\cos\alpha_{\underline{p}-\underline{K},\underline{p}-\underline{K}'}$ are as defined in equations [27] and [30] for the cubic case. Again the formula is straight forward to evaluate and the total $\rho(\underline{p})$ is obtained by summing over the appropriate core shells.

2.4 Angular Distributions

Having calculated $\rho(\underline{p})$ we now wish to obtain theoretical angular distributions corresponding to those measured experimentally. We shall regard the experimental arrangement as being a perfect detector, that is having infinitely narrow resolution. Then the most general point detector experiments (Colombino et al 1963) measure the following quantity

$$N(p_y,p_z) = \int_{-\infty}^{\infty} \rho(\underline{p})dp_x \qquad [35]$$

To evaluate this integral, for both the cubic and hexagonal cases, a Cartesian coordinate system was set up in momentum space. For the given coordinates p_y, p_z $\rho(\underline{p})$ was evaluated at a series of values of p_x by the method of the preceding section. The integral was then evaluated by numerical integration.

Long slit detector experiments measure the momentum distribution integrated over two perpendicular directions, that is they measure the following quantity.

$$N(p_z) = \int_{-\infty}^{\infty} \int_{-\infty}^{\infty} \rho(\underline{p})\ dp_x\ dp_y \qquad [36]$$

In the present work we are interested in calculating polycrystalline long slit results. To simulate the polycrystalline sample, $\rho(\underline{p})$ calculated by the method of the preceding section was averaged, for fixed $|\underline{p}|$, over randomly chosen directions. The directions were chosen by means of a pseudo random number generator of the power residue type (Lewis et al 1969). Angular distributions were then obtained from the resulting isotropic $\rho(p)$ by means of the formula (Wallace 1960)

$$N(p_z) = 2\pi \int_{p_z}^{\infty} p\ \rho(p)\ dp \qquad [37]$$

In long slit detector results the quantity p_z is usually expressed as the angle θ in the z, x plane which the movable detector makes with the line from the fixed detector through the sample. As can be seen from figure 1, since each photon has momentum $\approx$ c, this angle θ is given by

$$c\theta = \frac{\theta}{\alpha} = p_z \ .$$

The angle 1 milliradian corresponds to $p_z = \frac{10^{-3}}{\alpha} = .137$ a.u. Similarly in point detector results p_y, p_z are expressed as angles in the y, x and z, x planes respectively. In the point detector results to be presented in this work p_y or θ_y is held equal to zero and the detector is moved in the z, x plane. The counting rate is then presented as a function of the angle in this plane.

CHAPTER III

NUMERICAL RESULTS

3.1 Details of the Numerical Calculations

The functions $P_{n\ell}(r)$ used in equations [3] and [27] were taken from Herman and Skillman (1963) and were read into the computer program for the same mesh of r values as that used by those authors. This resulted in a mesh of 100 points for gold, 90 points for cadmium, and 80 points for zinc, copper, and magnesium. The integrands in equations [3], [9], and [27] were then calculated at these r values and the integrals evaluated by a second order numerical method equivalent to Simpson's rule over a constant interval mesh.

The value of the lattice constants for all five metals were obtained from Table A6 of Barrett and Massalski (1966). The volume of a unit cell and the radius of a Wigner-Seitz sphere were both calculated from the lattice constants.

The $I_{n\ell}$ (q) of equation [27] depend only on the magnitude of $\underline{q}$. These were calculated for a mesh of q values from 0 to 60 milliradians at 1 milliradian intervals. Here q is expressed in the units of momentum used in the presentation of experimental results as explained at the end of the last section. To obtain $I_{n\ell}$ ($\underline{p}$-$\underline{K}$) in equations [31] and [34] the magnitude of $\underline{p}$-$\underline{K}$ was calculated and a linear interpolation used between points in the q-mesh.

The approximation of the positron wavefunction by a finite sum of plane waves is worst very close to the nucleus at an atomic site where the potential is changing very rapidly. Any overestimate of the positron wavefunction in this region leads to increased overlap with high momentum electrons and produces higher large angle tails in the angular distributions.

The Wigner-Seitz approximation, on the other hand, is best in this same region. The approximations of spherical symmetry and independence from other atomic sites are most valid, and the solution is less affected by the artificial boundary condition.

As shown in Appendix II, the positron wavefunction approaches very close to zero at the nucleus in the Wigner-Seitz approximation for all the metals studied other than magnesium. The following prescription was therefore followed in utilizing equations [31] and [34] to calculate $\rho(\underline{p})$. A finite number of plane waves were used and the first Fourier coefficient A_0 was adjusted so that in the cubic case we had

$$\psi_+(\underline{r}) = \sum_{\underline{K}} A_{\underline{K}} = 0$$

or in the hexagonal case

$$\psi_+(\underline{r}+\underline{d}) = \sum_{\underline{K}} A_{\underline{K}}\, e^{i\underline{K}\cdot\underline{d}} = 0$$

or in the case of magnesium, $\psi_+(\underline{r}+\underline{d}) = 0.1$.

All the $A_{\underline{K}}$'s were then renormalized so that

$$\sum_{\underline{K}} A_{\underline{K}}^2 = 1$$

The procedure was repeated using successively more plane waves in equations [31] and [34] until the changes in the angular distributions became negligible. This required 59 plane waves in the cubic case and 69 plane waves in the hexagonal case.

This procedure of adjusting the first Fourier coefficient did not affect the shape of the positron wavefunction since A_0 is just the constant part of the wavefunction. The adjustments which had to be made affected the individual Fourier components by at most about 1%. Thus it is felt that the procedure is physically reasonable.

To evaluate the integral in equation [35] the integrand was computed at the center of cubic cells of side 2 milliradians and the integration over p_x was carried out by Simpson's rule over a range of ±20 milliradians. Doubling the integration range and halving the mesh size resulted in insignificant changes in the shape of $N(p_y,p_z)$.

For the long slit detector results, $\rho(p)$ was calculated at 1 milliradian intervals from 1/2 milliradian to 24 1/2 milliradians. $N(p_z)$ was then evaluated at 1 milliradian intervals for p_z in the range 0 to 24 milliradians. $N(p_z)$ for each successive inward point, starting with the outermost point, was calculated by means of the formula

$$N(\chi_{n-1}) = N(\chi_n) + 2\pi \int_{\chi_{n-1}}^{\chi_n} p\rho(p)dp$$

taking $\int_{\chi_{n-1}}^{\chi_n} p\rho(p)dp = (\chi_n - \chi_{n-1})(\chi_{n-1} + \frac{1}{2}\,\text{mrad})\rho(\chi_{n-1} + \frac{1}{2}\,\text{mrad.})$

In the Wigner-Seitz calculation, described in Appendix I, integration over real space co-ordinates is carried out in the same way as described above and over the same mesh. The momentum space integrations of equations [A4] and [37] were carried out by Simpson's rule, the integrands in both cases being calculated at 1 milliradian intervals from 0 to 24 milliradians.

Again changing the mesh size or the integration range had negligible effect on the final distributions.

The conduction electron contribution calculated on the basis of free electrons, but using the Fourier expansion positron wavefunction, yields for $\rho(\underline{p})$ the expression

$$\rho(\underline{p}) = \frac{\alpha^3}{4\pi^2} \sum_{\underline{Q}} |A_{\underline{Q}}|^2 H(p_F - |\underline{p}-\underline{Q}|) \qquad [38]$$

where p_F is the Fermi momentum and H is the Heaviside step function

$$H(\chi) = \begin{cases} 0 & \chi<0 \\ 1 & \chi>0 \end{cases}$$

This $\rho(\underline{p})$ can be interpreted as being due to a set of Fermi spheres, one situated at each reciprocal lattice point and weighted by the factor $A_{\underline{K}}^2$.

By an obvious generalization, the point detector conduction electron distribution for copper and gold were taken to be due to Fermi surfaces situated at each reciprocal lattice point weighted by $A_{\underline{K}}^2$. The Fermi surfaces were assumed to consist of a sphere having the free electron radius of 5.25 milliradians with cylindrical necks extending to the Brillouin zone boundaries in the 111 directions.

The computer calculation of conduction electron distributions for these surfaces is described by Senicki (1972).

For the point detector results for zinc and magnesium, and for all the long slit results, spherical Fermi surfaces were assumed. In these cases, Kahana's (1963) momentum dependent enhancement factor was also included. $\rho(\underline{p})$ is enhanced by the factor $\varepsilon(\gamma)(\gamma = p/p_F)$ where

$$\varepsilon(\gamma) = a + b\gamma^2 + c\gamma^4$$

The coefficients a, b, c depend on the density of the electron gas and are shown in the table below.

TABLE V

Enhancement Factor Coefficients

Metal	a	b	c	p_F
Magnesium	5.2	1.0	.7	.72
Copper	5.2	1.0	.7	.72
Zinc	4.1	.76	.5	.83
Cadmium	4.9	.94	.6	.74

3.2 Positron Wavefunctions

Figures 8 through 11 show the positron wavefunctions, calculated by the method of section 2.2, along various crystal directions together with a Wigner-Seitz positron wavefunction for copper, gold, zinc and cadmium. These were calculated using the number of plane waves specified in the preceding section and using the adjustment described there. The positron wavefunctions are normalized to Ω in a unit cell.

Also shown on each diagram is the radial wavefunction $R_{n\ell}(r)$ of the outermost core electrons.

$$\Phi_{n\ell m}(\underline{r}) = R_{n\ell}(r) Y_\ell^m(\theta_{\underline{r}}, \phi_{\underline{r}})$$

$R_{n\ell}(r)$ is normalized so that

$$\int_o^\infty r^2 |R_{n\ell}(r)|^2 \, dr = 1.$$

3.3 Polycrystalline Long Slit Results

Figures 12 through 14 show experimental angular distributions for copper, cadmium and zinc together with theoretical core distributions calculated by the method of section 2.3. Figures 15 through 17 show angular distributions for the same metals with theoretical core distributions calculated by the Wigner-Seitz method.

FIGURE 8

Positron Wavefunction and Radial 3d Wavefunction in Copper

--- Fourier Expansion Positron Wavefunction

—— Wigner-Seitz Positron Wavefunction

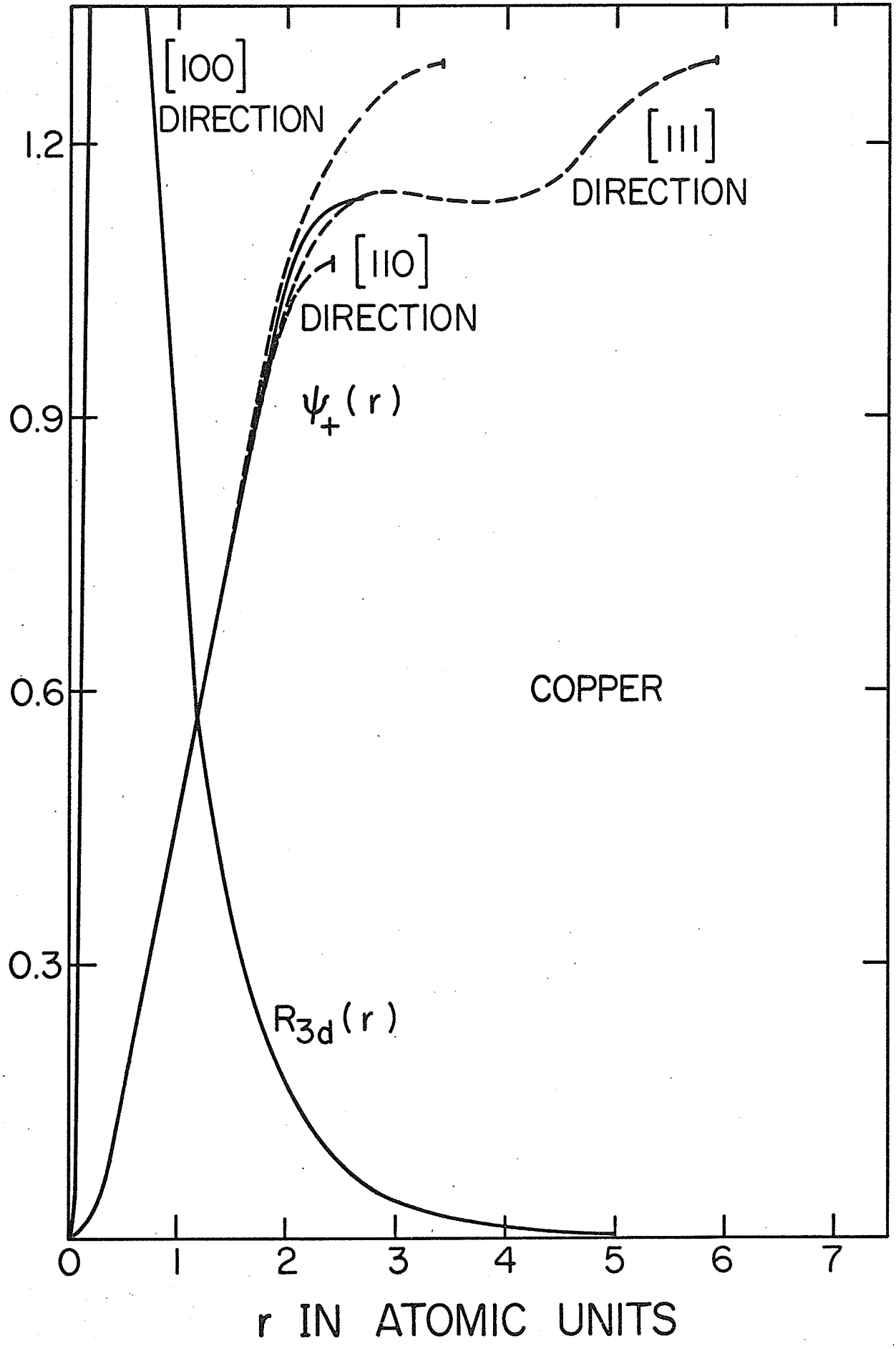
[100]
DIRECTION
[111]
DIRECTION
[110]
DIRECTION
$\psi_+(r)$
COPPER
$R_{3d}(r)$
1.2
0.9
0.6
0.3
0
1
2
3
4
5
6
7
r IN ATOMIC UNITS

FIGURE 9

Positron Wavefunction and Radial 5d Wavefunction in Gold

--- Fourier expansion positron wavefunction

—— Wigner-Seitz positron wavefunction

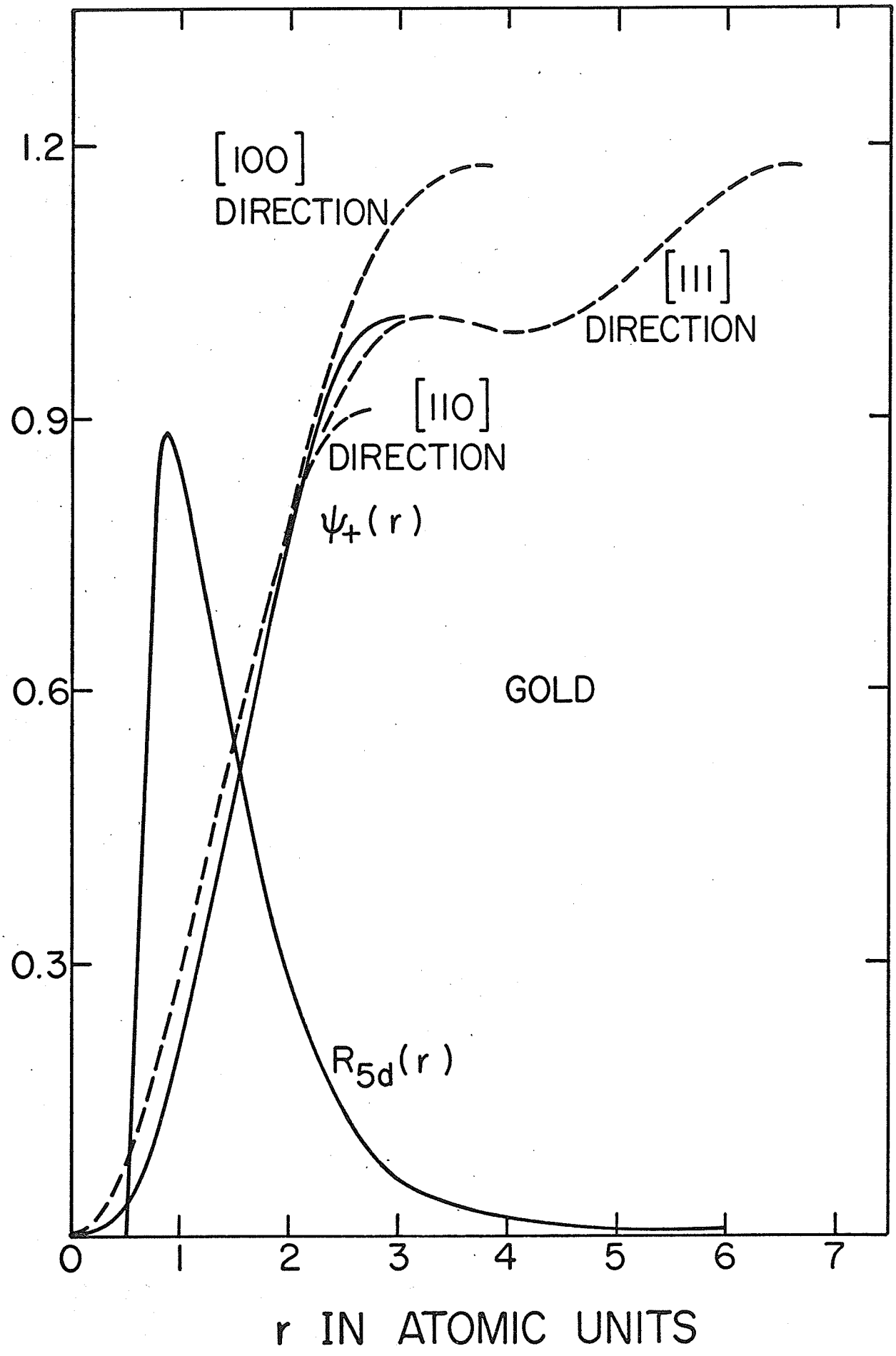
1.2
0.9
0.6
0.3
0
1
2
3
4
5
6
7
[100]
DIRECTION
[111]
DIRECTION
[110]
DIRECTION
$\psi_+(r)$
GOLD
$R_{5d}(r)$
r IN ATOMIC UNITS

FIGURE 10

Positron Wavefunction and Radial 3d Wavefunction in Zinc

--- Fourier Expansion Positron Wavefunction

—— Wigner-Seitz Positron Wavefunction

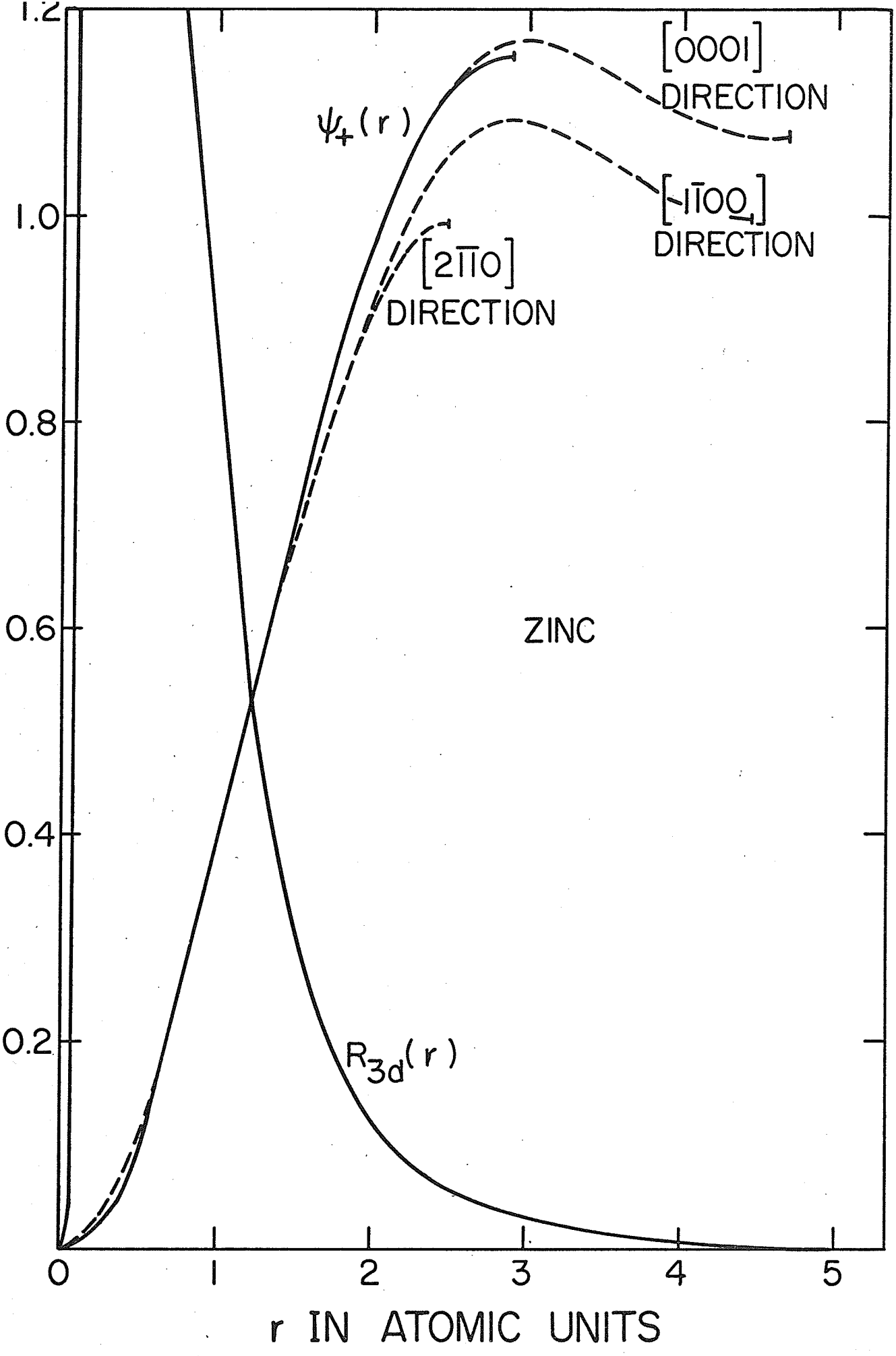
1.2
1.0
0.8
0.6
0.4
0.2
0
1
2
3
4
5
[0001]
DIRECTION
$\psi_+(r)$
[1$\bar{1}$00]
DIRECTION
[2$\bar{1}\bar{1}$0]
DIRECTION
ZINC
$R_{3d}(r)$
r IN ATOMIC UNITS

FIGURE 11

Positron Wavefunction and Radial 4d Wavefunction in Cadmium

--- Fourier Expansion Positron Wavefunction

—— Wigner-Seitz Positron Wavefunction

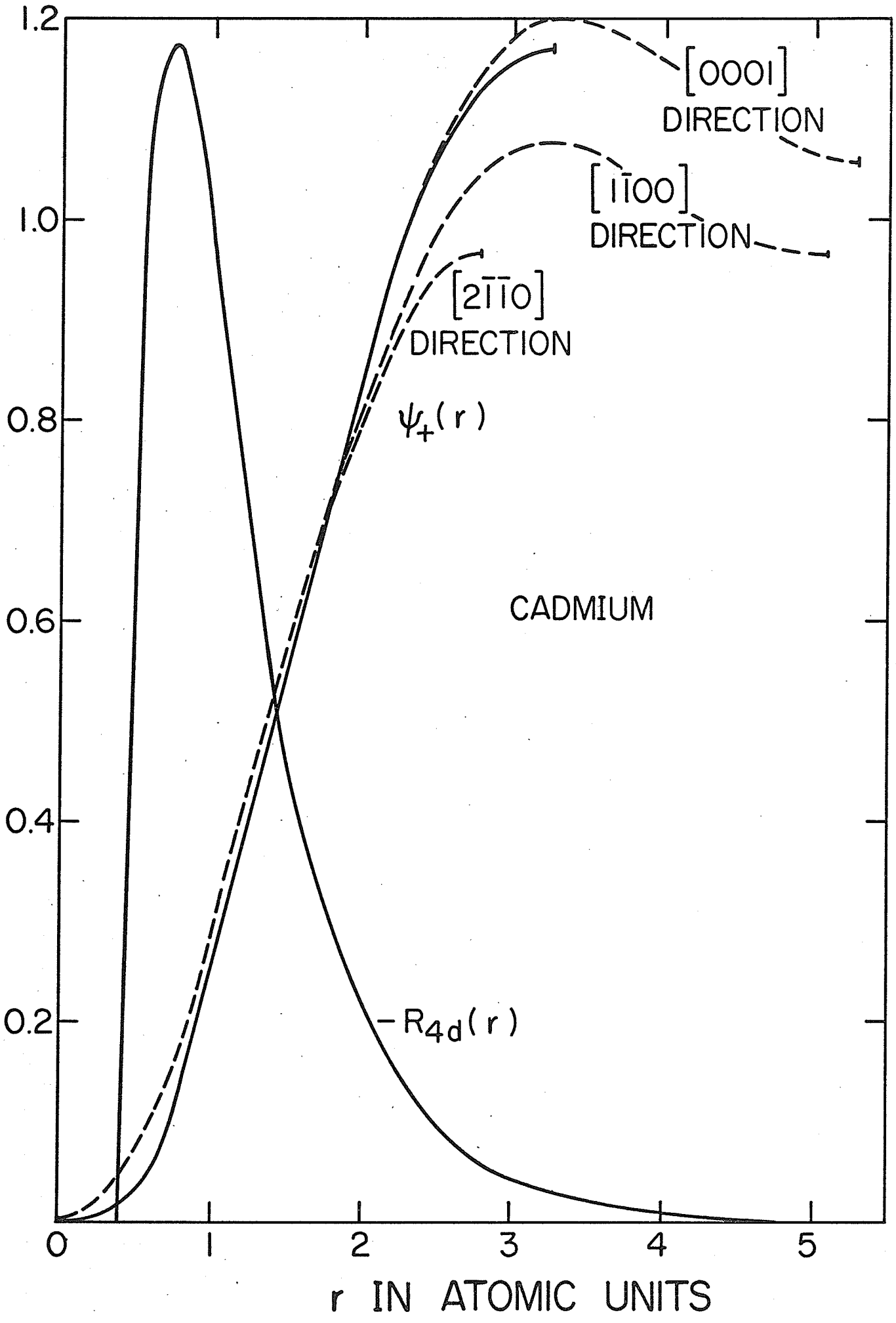
1.2
1.0
0.8
0.6
0.4
0.2
0
1
2
3
4
5
r IN ATOMIC UNITS
[0001]
DIRECTION
[1$\bar{1}$00]
DIRECTION
[2$\bar{1}\bar{1}$0]
DIRECTION
$\psi_+(r)$
CADMIUM
$-R_{4d}(r)$

As has been stated in chapter I, the present independent particle model calculation will not give the correct annihilation rate for either core or conduction electrons. Because of their different abilities to respond to the positron field, core electrons and conduction electrons will require the application of different enhancement rates. In the absence of any theoretical calculation to indicate what the enhancement rates should be, the core distributions have been normalized to give the best fit to the experimental distributions at large angles and then the conduction distributions have been normalized to give the best fit at small angles.

The experimental results are from Berko and Plaskett (1958) for copper, from Connors et al (1971) for cadmium, and from Mogensen and Trumpy (1969) for zinc. The angular resolution is about .5 milliradians for the zinc and cadmium results and about 1.1 milliradians for copper. The statistical error is less than 1% on all points.

3.4 Single Crystal Point Detector Results

Figures 18 through 25 show a comparison of the two types of core annihilation calculation with experimental data for gold, copper, zinc and magnesium. Figures 22 and 24 for zinc and magnesium also show a comparison between conduction distributions with and without the application of Kahana's (1963) momentum dependent enhancement factor. The core and conduction distributions have been arbitrarily normalized in the same way as for the long slit distributions to obtain the best fit to the experimental distributions.

The experimental results are those of Senicki (1972). The angular resolution is approximately 1.5 milliradians. The statistical error in the points varies from less than 1% at the peak to between 5% and 7% in the far core.

FIGURE 12

Long Slit Detector Angular Distribution in Copper

—— Experimental Distribution

--- Theoretical Distributions Calculated Using the Method of Chapter II Including Enhancement of Conduction Electrons

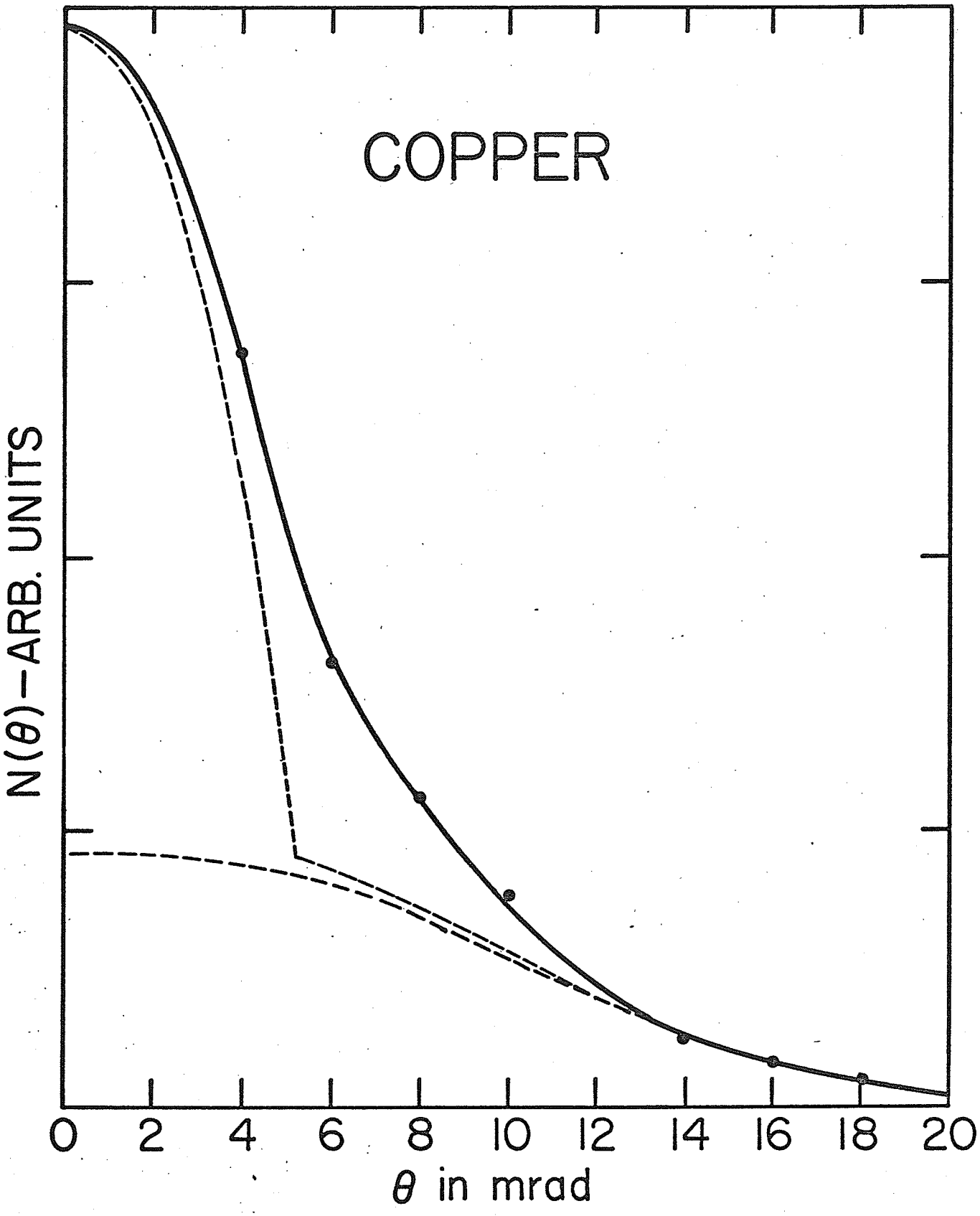
COPPER
N(θ)—ARB. UNITS
0
2
4
6
8
10
12
14
16
18
20
θ in mrad

FIGURE 13

Long Slit Detector Angular Distribution in Cadmium

● Experimental Points

--- Theoretical Distributions Calculated Using Method of Chapter II Without Enhancement of Conduction Electrons

—— Total Theoretical Distribution Including Conduction Enhancement

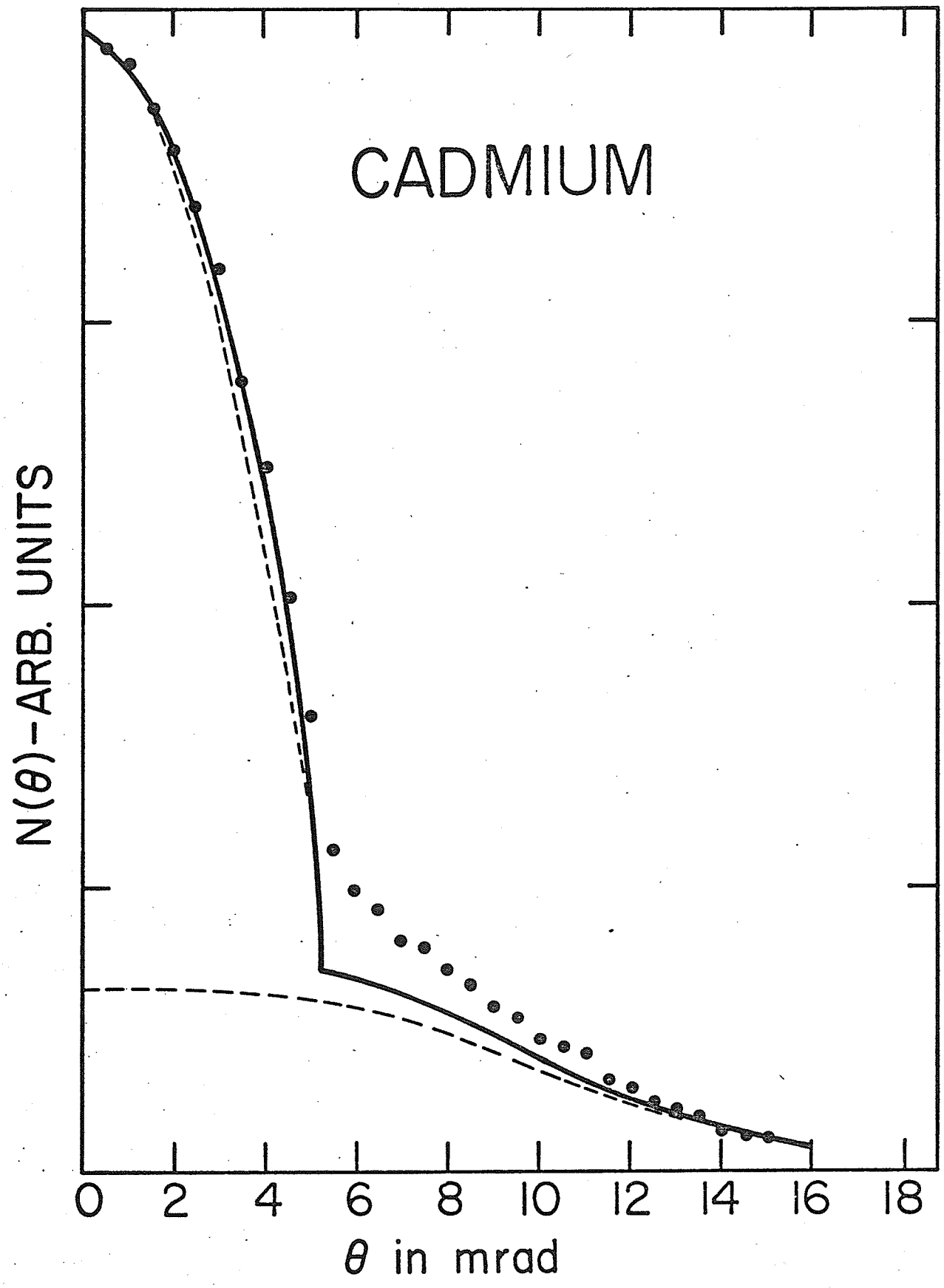
CADMIUM
N(θ)-ARB. UNITS
0
2
4
6
8
10
12
14
16
18
θ in mrad

FIGURE 14

Long Slit Detector Angular Distribution in Zinc

• Experimental Points

--- Theoretical Distributions Calculated Using Method of Chapter II Without Enhancement of Conduction Electrons.

—— Total Theoretical Distribution Including Conduction Enhancement

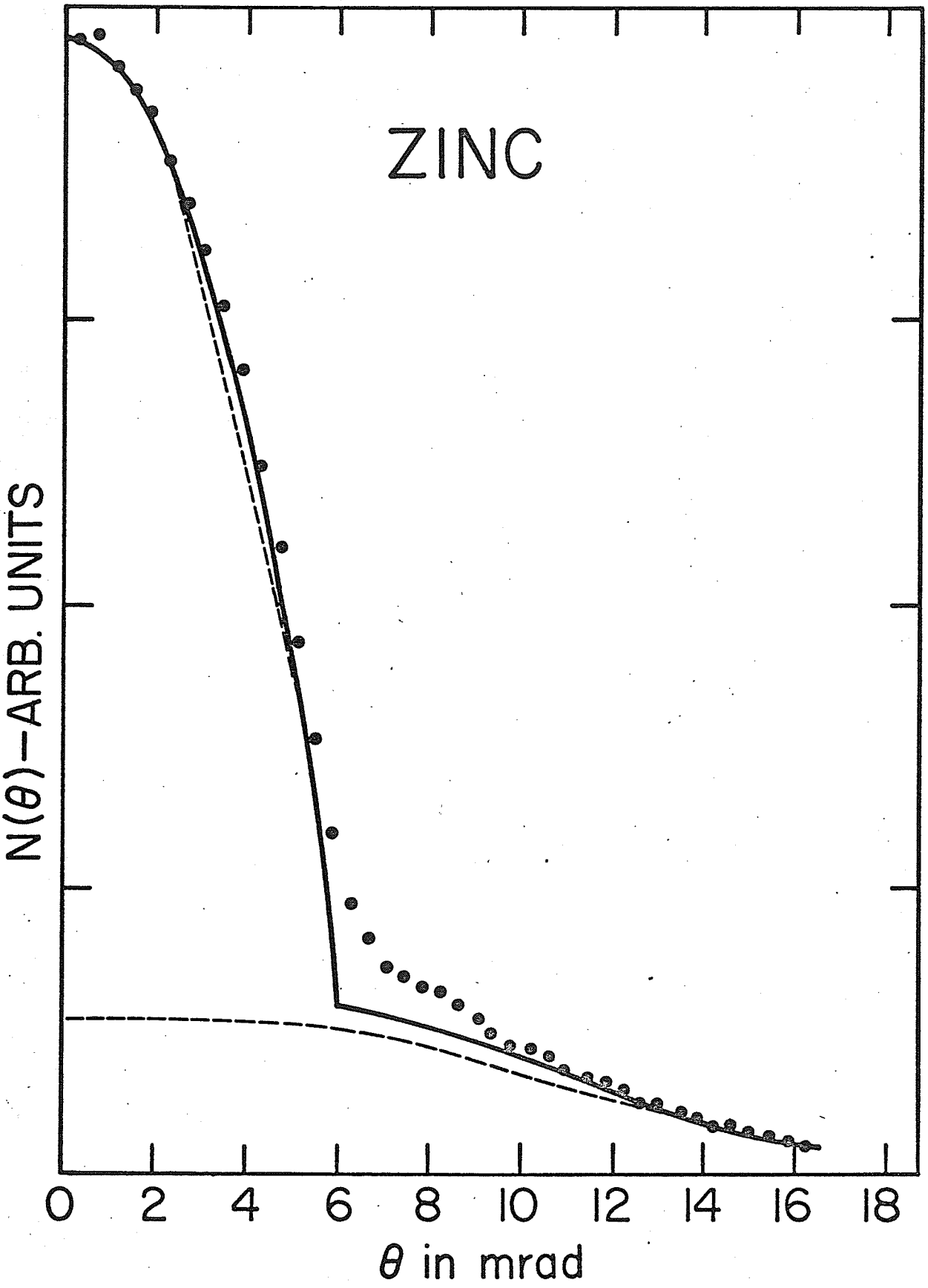
ZINC
N(θ)—ARB. UNITS
0
2
4
6
8
10
12
14
16
18
θ in mrad

FIGURE 15

Long Slit Detector Angular Distribution in Copper

—— Experimental Distribution

--- Theoretical Distributions Calculated in the Wigner-Seitz Approximation Including Enhancement of Conduction Electrons

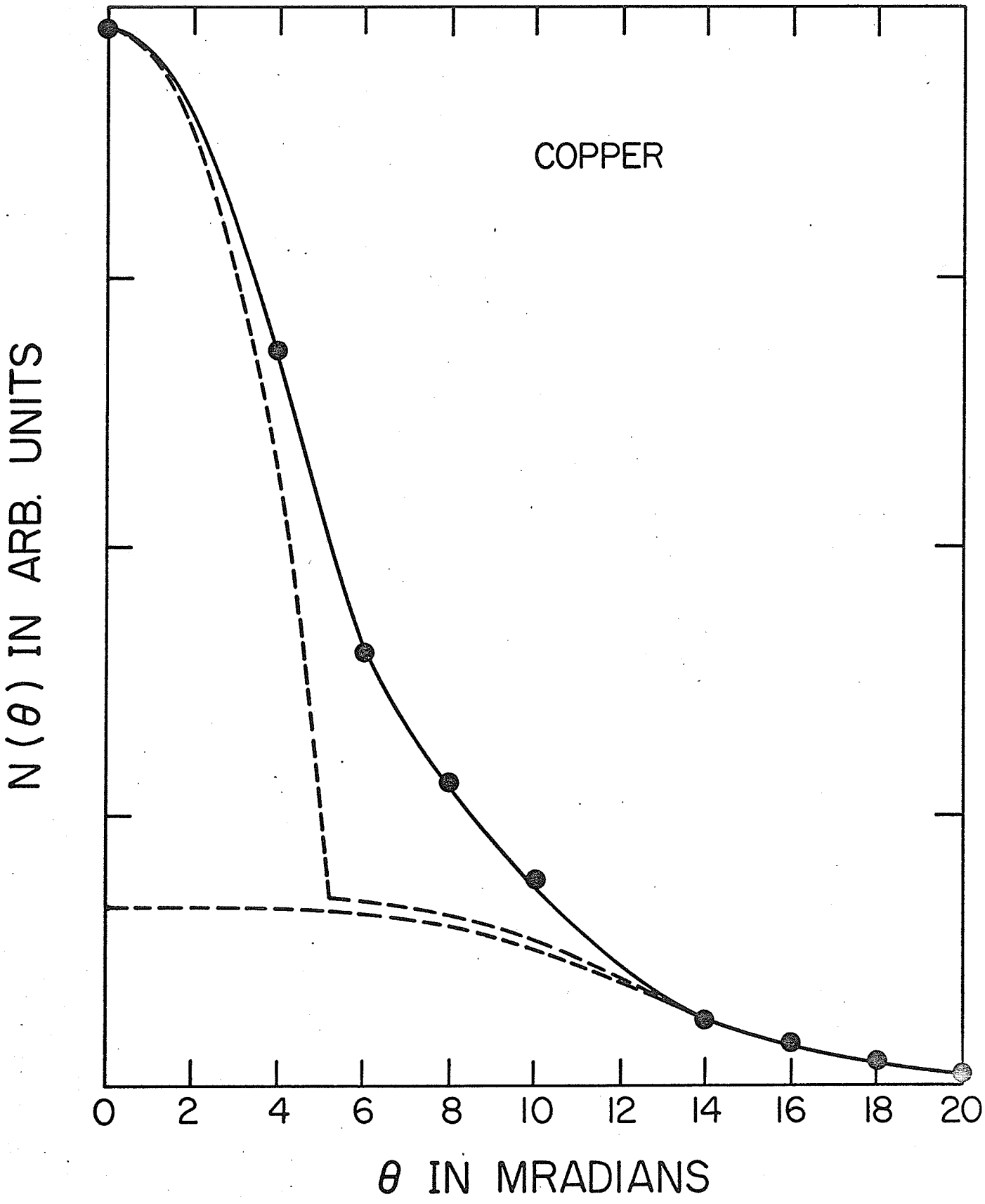
COPPER
N(θ) IN ARB. UNITS
0
2
4
6
8
10
12
14
16
18
20
θ IN MRADIANS

FIGURE 16

Long Slit Detector Angular Distribution in Cadmium

● Experimental Distributions

--- Theoretical Distributions Calculated in the Wigner-Seitz Approximation Without Enhancement of Conduction Electrons.

—— Total Theoretical Distribution Including Conduction Enhancement

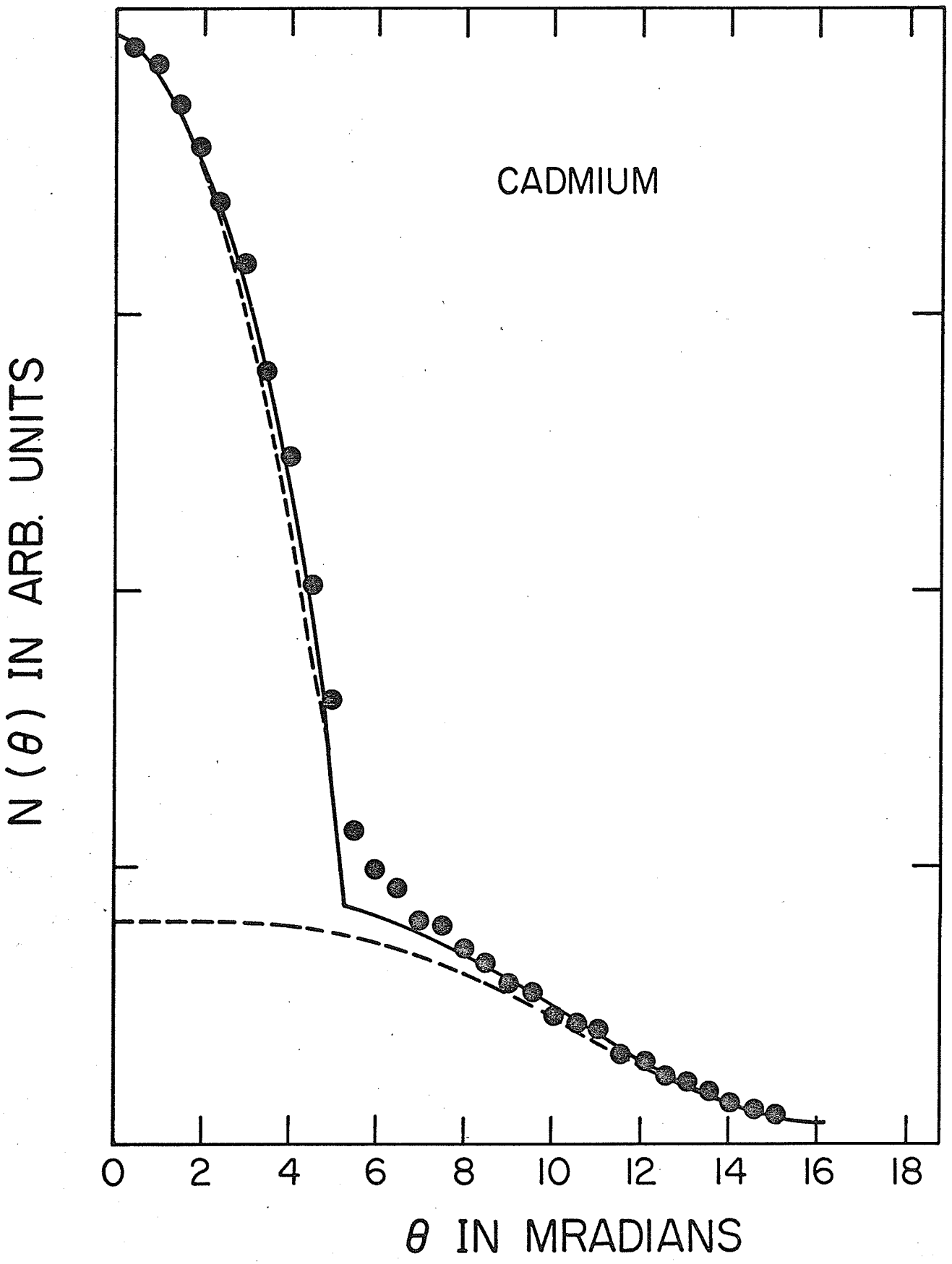
CADMIUM
N(θ) IN ARB. UNITS
0
2
4
6
8
10
12
14
16
18
θ IN MRADIANS

FIGURE 17

Long Slit Detector Angular Distributions for Zinc

● Experimental Points

--- Theoretical Distributions Calculated in the Wigner-Seitz Approximation Without Enhancement of Conduction Electrons.

—— Total Theoretical Distribution Including Conduction Enhancement

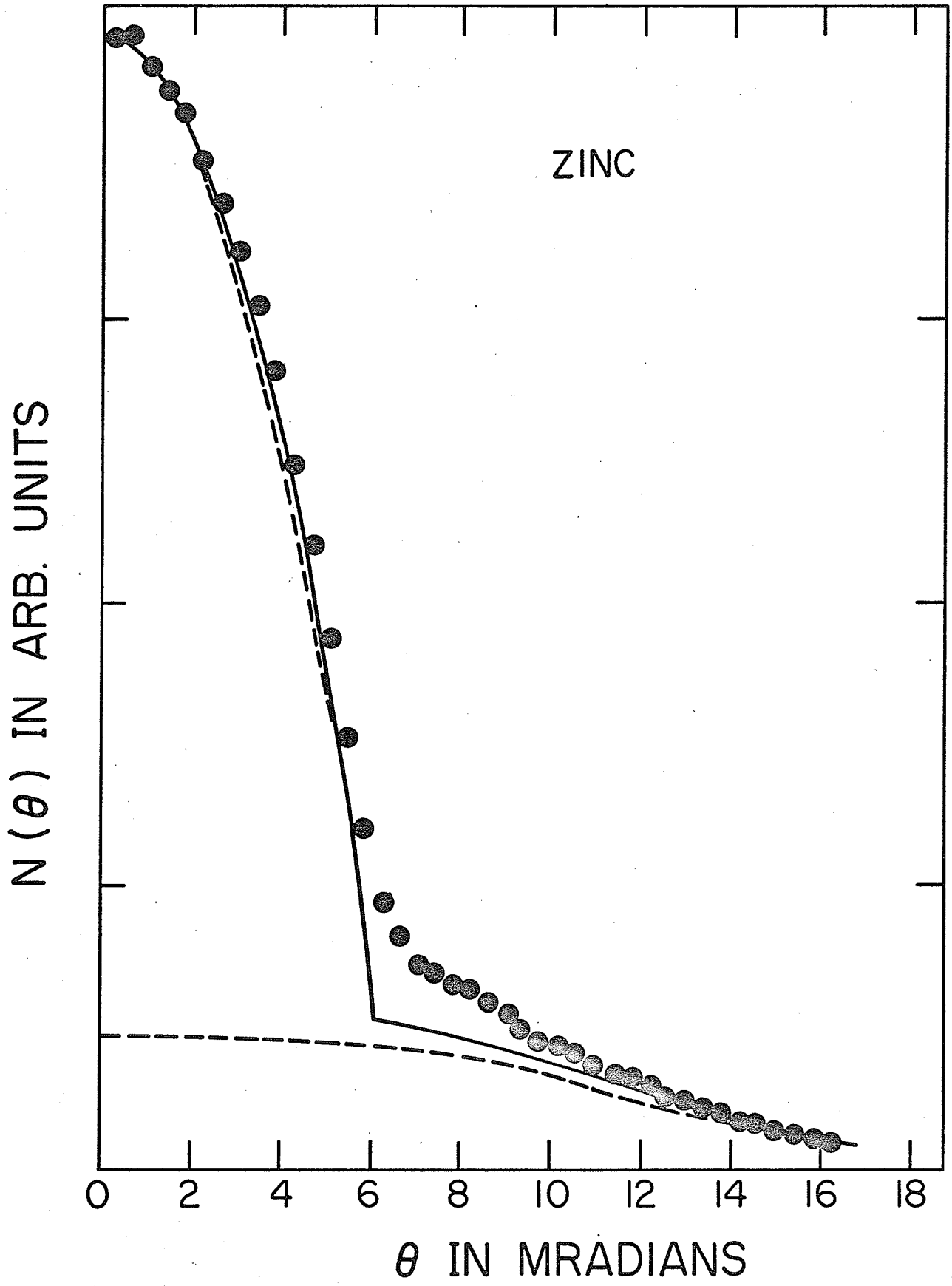
ZINC
N(θ) IN ARB. UNITS
0
2
4
6
8
10
12
14
16
18
θ IN MRADIANS

FIGURE 18

Point Detector Angular Distribution for Copper

● Experimental Points

A Distribution Calculated from Fourier Expansion Positron Wavefunction

B Distribution Calculated from Wigner-Seitz Positron Wavefunction

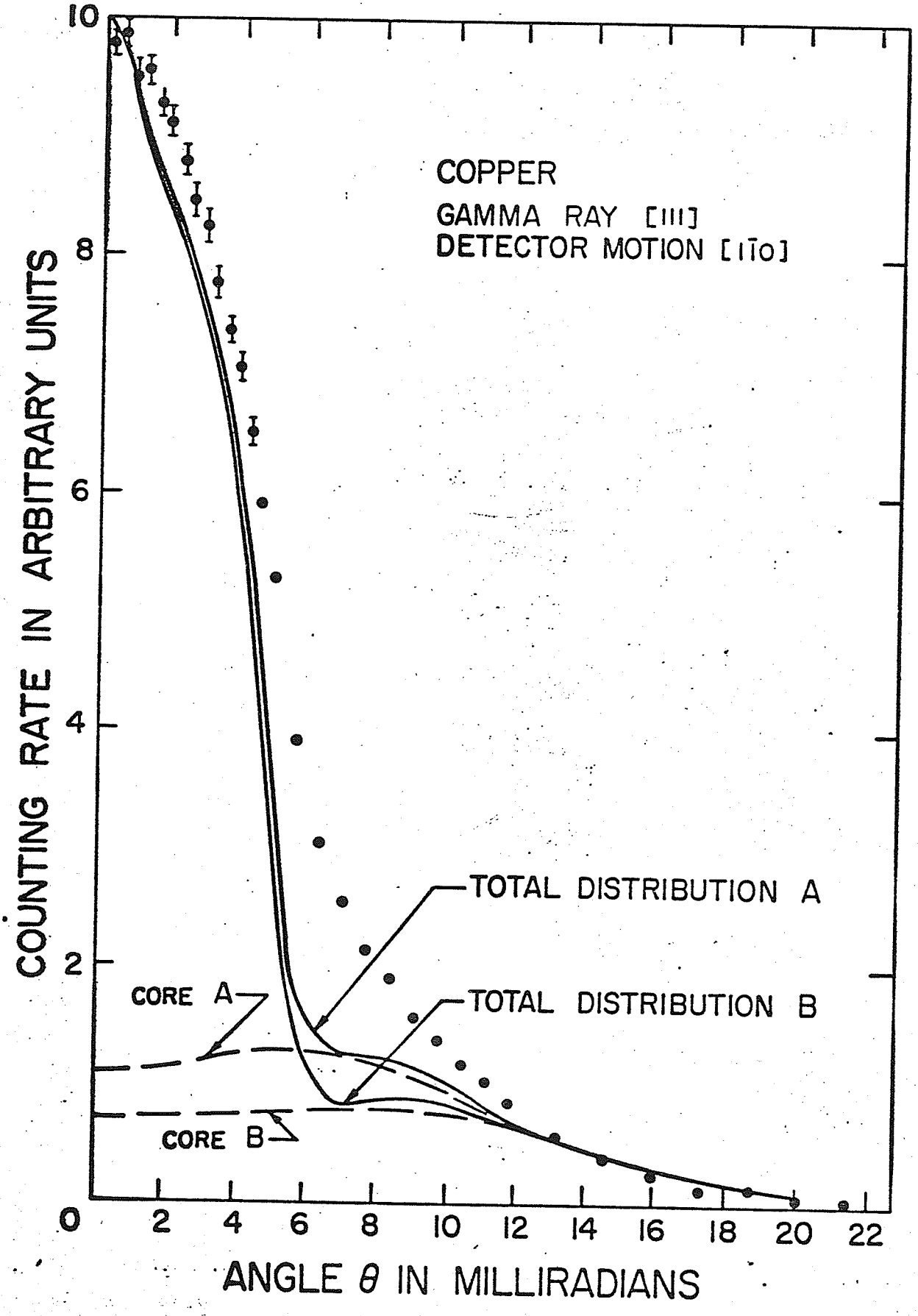
COPPER
GAMMA RAY [111]
DETECTOR MOTION [1$\bar{1}$0]
TOTAL DISTRIBUTION A
TOTAL DISTRIBUTION B
CORE A
CORE B
COUNTING RATE IN ARBITRARY UNITS
ANGLE θ IN MILLIRADIANS
0
2
4
6
8
10
12
14
16
18
20
22

FIGURE 19

Core Angular Distributions for Copper

● Experimental Points

--- Calculated from F.E. Positron Wavefunction

—— Calculated from W.S. Positron Wavefunction

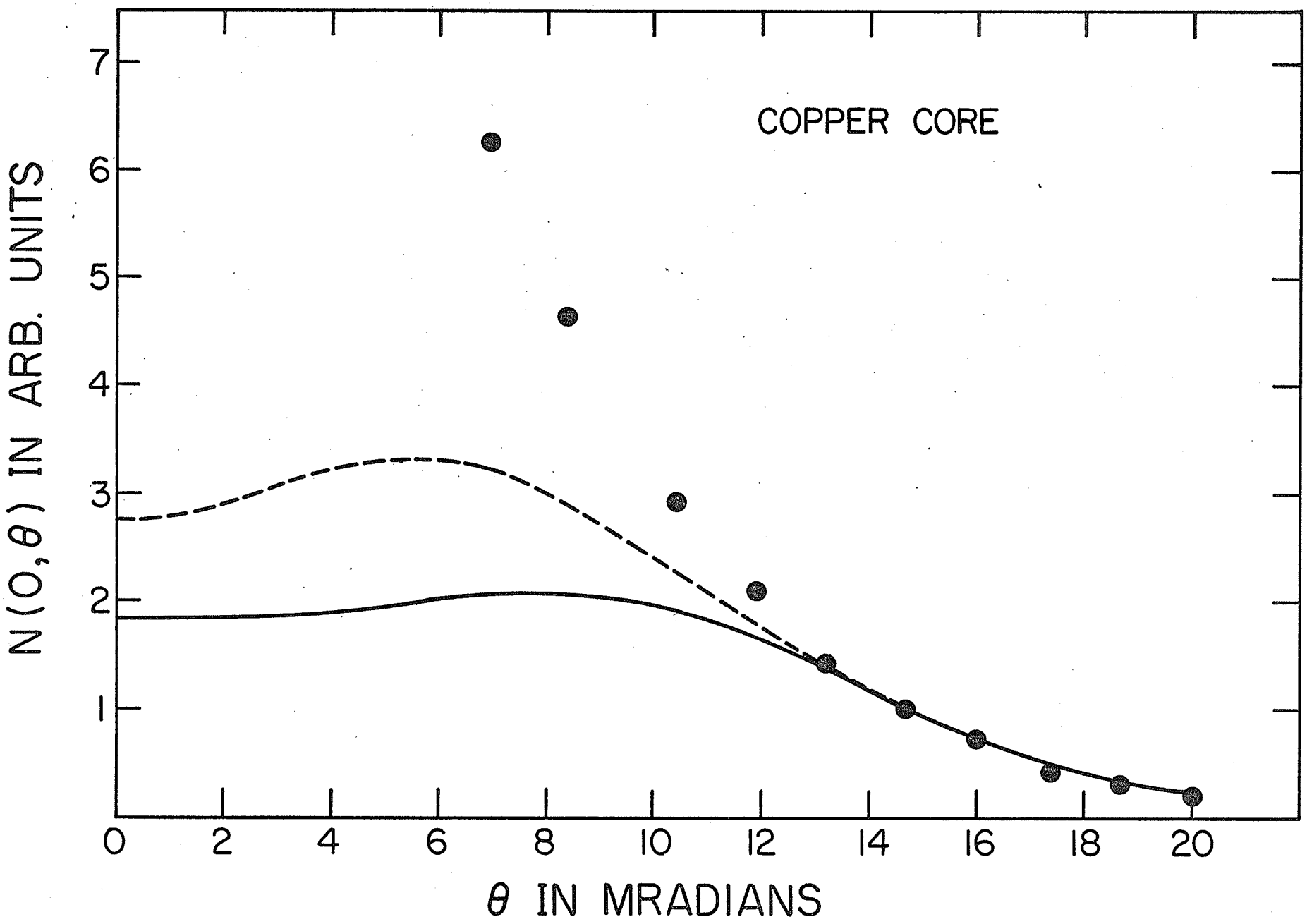
COPPER CORE
N(O,θ) IN ARB. UNITS
θ IN MRADIANS
0
2
4
6
8
10
12
14
16
18
20
1
2
3
4
5
6
7

FIGURE 20

Point Detector Angular Distribution for Gold

● Experimental Points

A Distribution Calculated From Wigner-Seitz Positron Wavefunction

B Distribution Calculated from Fourier Expansion Positron Wavefunction

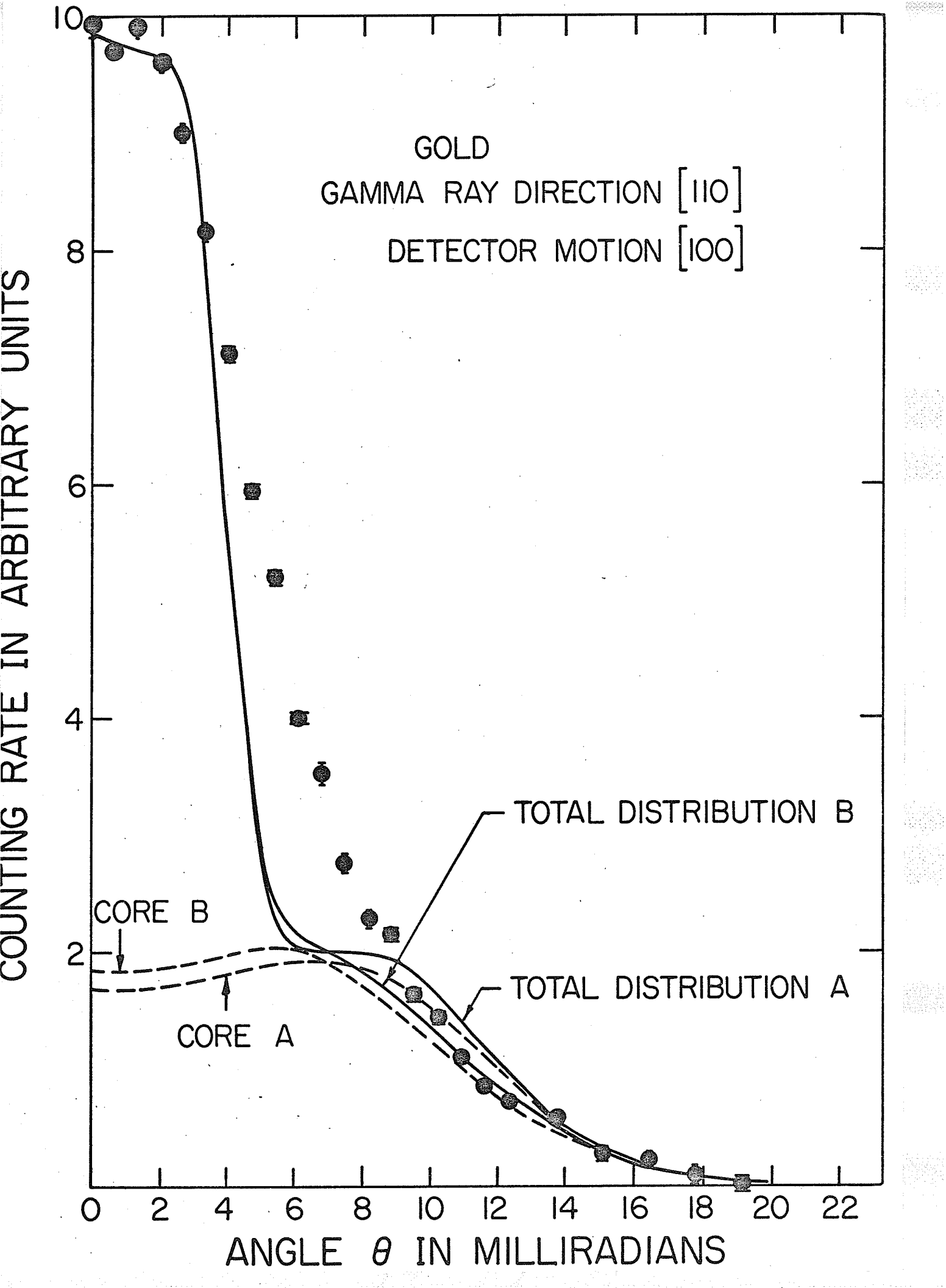
GOLD
GAMMA RAY DIRECTION [110]
DETECTOR MOTION [100]
TOTAL DISTRIBUTION B
TOTAL DISTRIBUTION A
CORE B
CORE A
COUNTING RATE IN ARBITRARY UNITS
ANGLE θ IN MILLIRADIANS
10
8
6
4
2
0
2
4
6
8
10
12
14
16
18
20
22

FIGURE 21

Core Angular Distribution for Gold

● Experimental Points

--- Calculated from F.E. Positron Wavefunction

—— Calculated from W.S. Positron Wavefunction

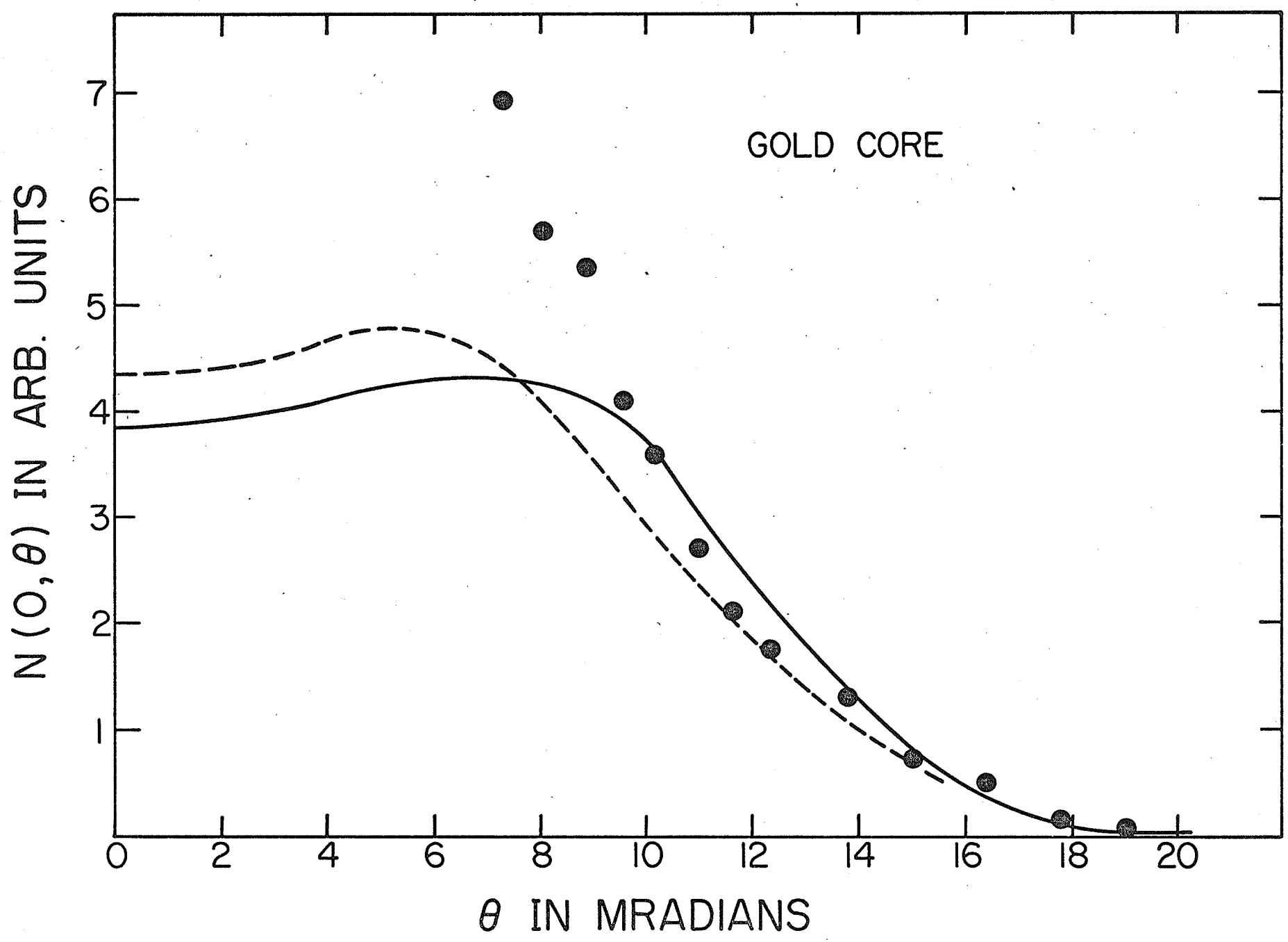
GOLD CORE
N(O,θ) IN ARB. UNITS
θ IN MRADIANS
0
2
4
6
8
10
12
14
16
18
20
1
2
3
4
5
6
7

FIGURE 22

Point Detector Angular Distribution for Magnesium

● Experimental Points

--- Core Distribution Calculated from Fourier Expansion Positron Wavefunction

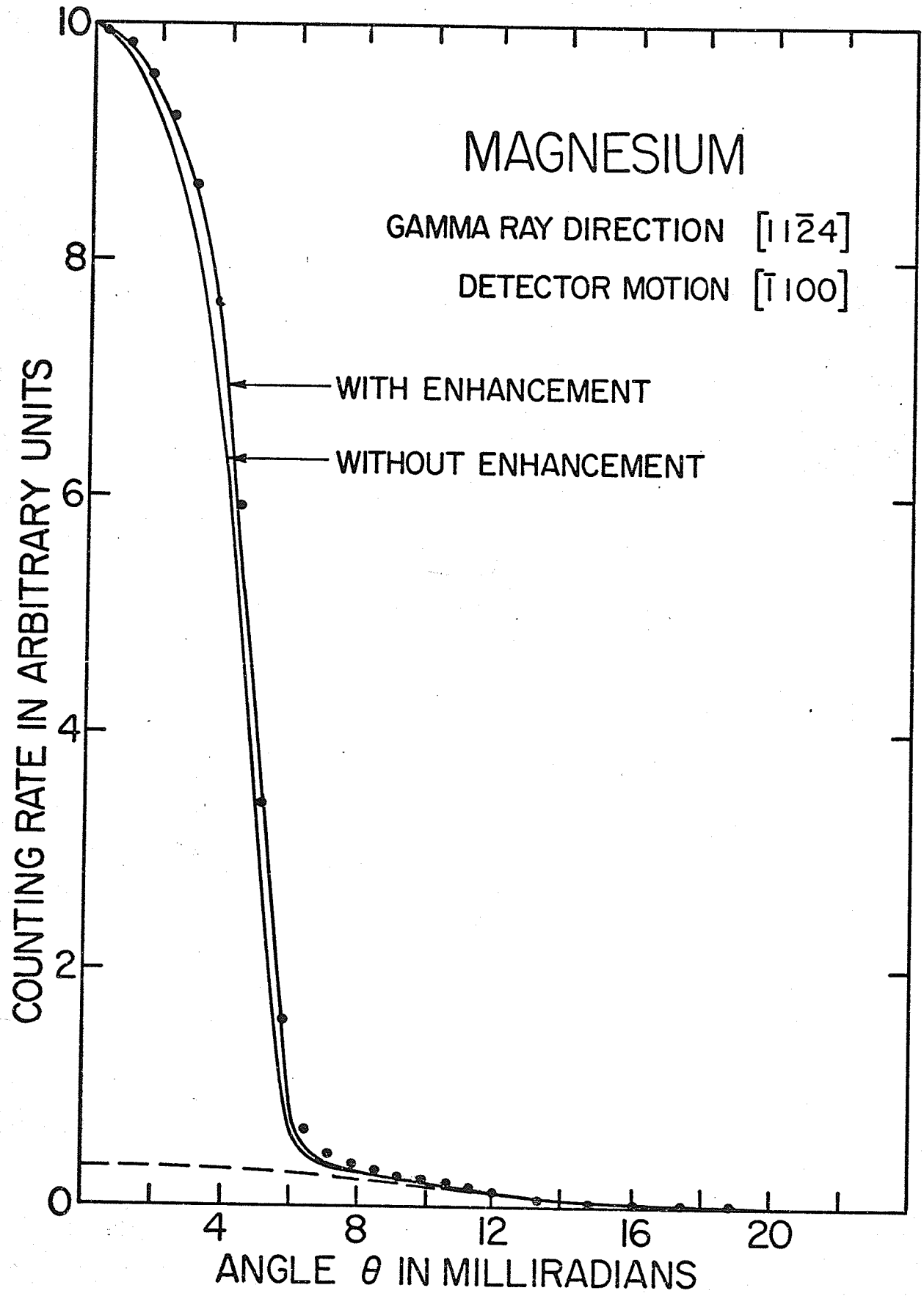
MAGNESIUM
GAMMA RAY DIRECTION [11$\bar{2}$4]
DETECTOR MOTION [$\bar{1}$100]
WITH ENHANCEMENT
WITHOUT ENHANCEMENT
COUNTING RATE IN ARBITRARY UNITS
ANGLE θ IN MILLIRADIANS
0
2
4
6
8
10
4
8
12
16
20

FIGURE 23

Core Angular Distribution for Magnesium

● Experimental Points

--- Calculated from F.E. Positron Wavefunction

—— Calculated from W.S. Positron Wavefunction

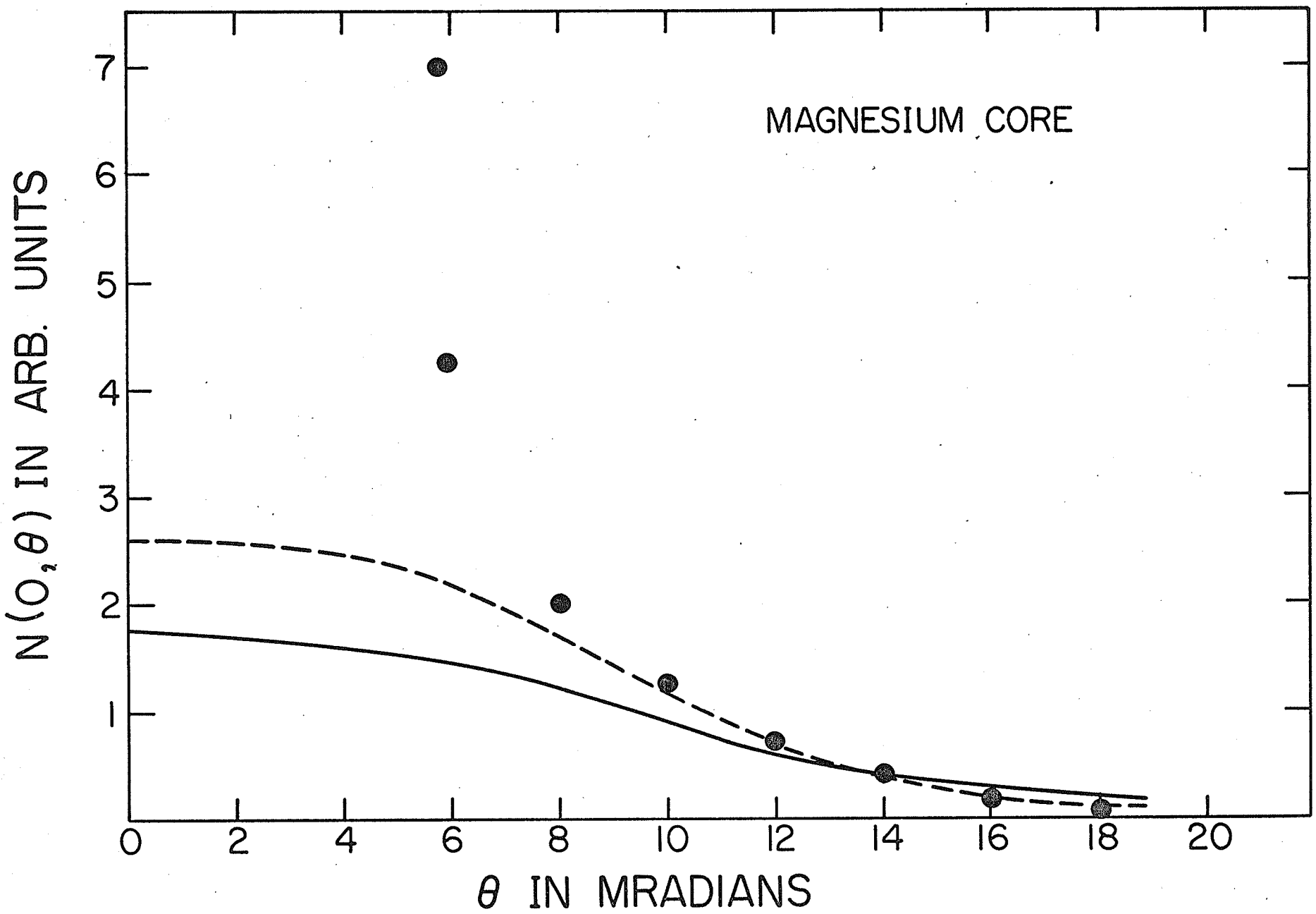
MAGNESIUM CORE
N(O,θ) IN ARB. UNITS
θ IN MRADIANS
0
2
4
6
8
10
12
14
16
18
20
1
2
3
4
5
6
7

FIGURE 24

Point Detector Angular Distribution for Zinc

● Experimental Points

A Distribution Calculated from Wigner-Seitz Positron Wavefunction

B Distribution Calculated from Fourier Expansion Positron Wavefunction

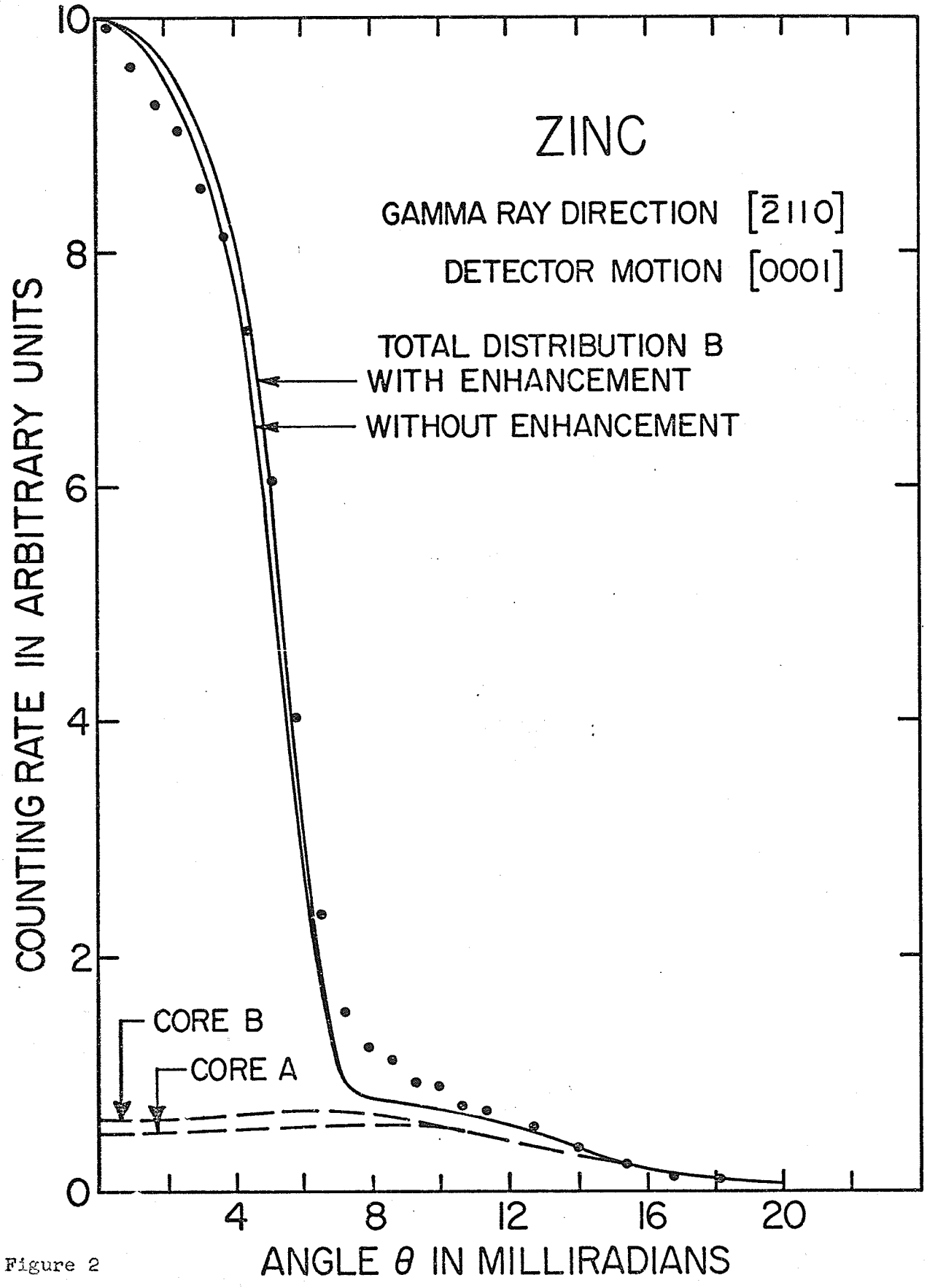
ZINC
GAMMA RAY DIRECTION [$\bar{2}$110]
DETECTOR MOTION [0001]
TOTAL DISTRIBUTION B
WITH ENHANCEMENT
WITHOUT ENHANCEMENT
CORE B
CORE A
COUNTING RATE IN ARBITRARY UNITS
ANGLE θ IN MILLIRADIANS
0
2
4
6
8
10
4
8
12
16
20

Figure 2

FIGURE 25

Core Angular Distributions for Zinc

● Experimental Points

--- Calculated from F.E. Positron Wavefunction

—— Calculated from W.S. Positron Wavefunction

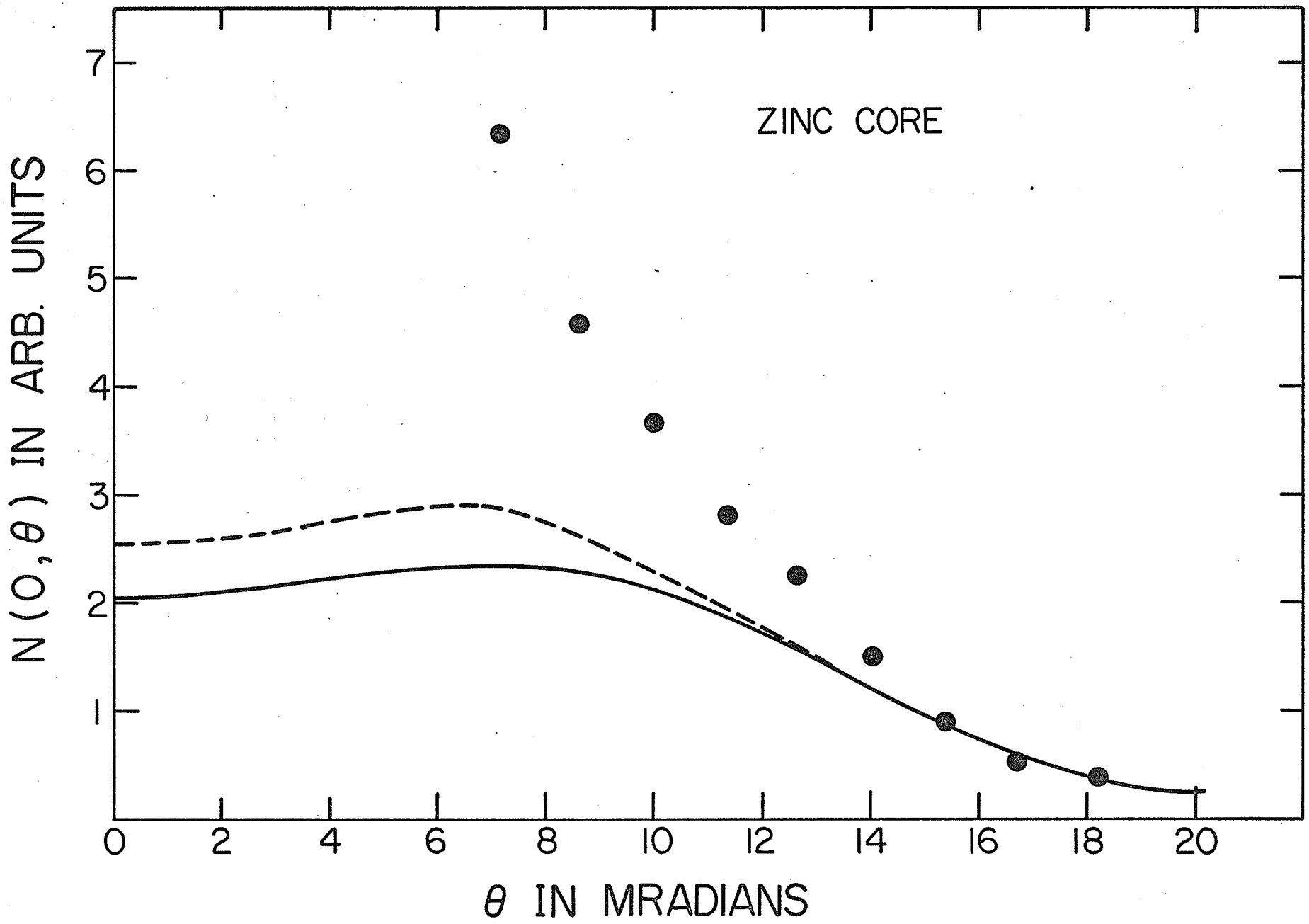
ZINC CORE
N(O,θ) IN ARB. UNITS
θ IN MRADIANS
0
2
4
6
8
10
12
14
16
18
20
1
2
3
4
5
6
7

CHAPTER IV

DISCUSSION AND CONCLUSIONS

The positron wavefunction was calculated for aluminum and compared with the results of Stroud and Ehrenreich (1968). The value of V_{111} calculated by the present method differed by about 10% from their value. The higher Fourier components of the potential agreed to within the accuracy of their presentation of their results. The positron wavefunction agreed to within 1% at all r values over the directions for which it was calculated.

The deviation of experimental and Hartree-Fock values for the X-ray form factors for low $\underline{K}$ values is well known (Weiss 1966). However, it would appear that the resulting deviation in crystal potential has very little effect on the positron wavefunction.

The positron wavefunctions for copper and gold (figures 8 and 9) show a shape similar to that for aluminum. This shape, characteristic of the f.c.c. lattice, allows the positron to heap up in the interstitial regions along [111] directions.

The positron wavefunction in gold is pushed out more at low r values than is that of copper because of the higher z value for gold. In this case, the Fourier expansion wavefunction deviates more from the Wigner-Seitz one near the nucleus. The Fourier expansion wavefunction could probably be improved in this region by including more plane waves in the expansion. However, the shape of the final distributions appears to be insensitive to the exact shape of the positron wavefunction in this region as long as the wavefunction goes to zero at the nucleus. This is physically reasonable since the positron wavefunction is then very small and because the wavefunction occupies a very small volume near the nucleus.

The positron wavefunctions for zinc and cadmium (figures 10 and 11) exhibit shapes quite different from those for copper and gold. The peaks in the interstitial regions are pushed in towards the atomic sites and secondary minima are found in the interstitial regions along the [0001] and [$1\bar{1}00$] directions.

Cadmium, with a higher z than zinc, again shows a greater difference between the Fourier expansion wavefunction and the Wigner-Seitz wavefunction at low r values. The positron wavefunction for magnesium (not shown) is almost identical to that of zinc.

The deviation of the positron wavefunction from a plane wave may be characterized by the parameter δ, where

$$\delta = \sum_{\underline{K} \neq 0} A_{\underline{K}}^2$$

The values of δ for the five metals studied are shown below

TABLE VI

Deviation of Positron Wavefunctions from a Plane Wave

Metal	δ
Copper	.053
Gold	.073
Zinc	.083
Cadmium	.094
Magnesium	.071

The deeper an electron is in the core, the better it is approximated by the tight binding function. The deeper core electrons also have the highest momentum. Therefore, the core calculations based on tight binding functions will be best at high momentum. It is for this reason that the calculated core distributions were normalized to the high momentum part of the curves.

The core distributions calculated with the Fourier expansion positron wavefunctions are generally higher at low momentum than those calculated with the Wigner-Seitz positron wavefunction. This is due to the increased overlap of the positron wavefunction with the lower momentum core electrons in the interstitial regions.

The present Wigner-Seitz results are better than those of previous calculations. Berko and Plaskett did not renormalize the individual core and valence parts of the distributions and consequently their total distribution contained too much core contribution. Rockmore and Stewart (1967) did normalize their core and conduction contributions separately. Their result in magnesium is not very satisfactory (compare figure 23 of present work with figure 1 of Rockmore and Stewart, 1967). The present results avoid the use of a "fudge" factor such as that used by Rockmore and Stewart (1967).

The better results are probably due to the better Hartree-Fock-Slater approximations to the atomic wavefunctions. The finer integration mesh of r values may also be partially responsible.

The Fourier expansion wavefunction results are better than the Wigner-Seitz results in all cases. In cadmium and gold, although the Wigner-Seitz distributions appear to be as good, they have a tendency to ride high in the region 8 to 14 milliradians. Since we have neglected higher momentum contributions (Berko and Plaskett 1958) to the conduction electron distributions and these contributions will come in just in this region, the present theoretical curves should fall below the experimental curves.

The agreement between the experimental and theoretical curves for zinc, cadmium and magnesium is excellent, and any remaining discrepancies

may be plausibly attributed to higher momentum components in the conduction electron wavefunctions and the effect of finite resolution and temperature. In copper and gold the discrepancies are too large to be accounted for by these effects.

It is known, however, that the tight binding functions are not as good an approximation for the core electrons in copper and gold as in zinc, cadmium and magnesium (Heine 1967, Friedel 1967). As pointed out by Melngailis (1970), a spreading of the d wave functions in real space will lead to more peaking at low angles. This will increase the core in gold and copper and lead to a better fit to the experimental curves. The spreading of the d wavefunctions would also make proper treatment of the positron wavefunction in the interstitial regions more important.

It can be seen from the results presented that the more realistic positron wavefunction accounts for as much of the discrepancy between Wigner-Seitz results and experiment as remains to be accounted for by higher momentum components in the conduction electron wavefunctions.

The Fourier expansion positron wavefunctions can be used to look for anisotropies in the core contributions. Preliminary results on long slit distributions for zinc did not show the same anisotropies as the experimental results of Mogensen and Trumpy (1969). However, the anisotropies in the experimental results were close to the statistical uncertainties. Also, the higher momentum components, which are important for the long slit detector geometry, have been neglected.

In the case of point detector distributions for copper, the present results indicate an increase in counting rate at $\theta_z = 0$ of about 6 1/2% when the γ-ray direction is along a [110] axis over that

when the γ-ray direction is along a [111] or [100] axis. This is in excellent agreement with the rotating crystal results of Williams et al (1968) assuming that 50% of the counting rate is due to core electrons when the γ-ray direction is along a [100] axis.

The experimental distributions for cadmium exhibit a significant change in shape over the temperature range $110^{o}K \rightarrow 300^{o}K$. One measure of the shape of a distribution is

$$h = \frac{N(p_z = 0)}{\int_{-\infty}^{\infty} N(p_z) dp_z}$$

For Cd h(T) increases by 4% between $110^{o}K$ and $300^{o}K$. Core distributions were calculated at the endpoints of this range using expansion coefficients for the lattice parameters from Lonsdale (1962). The combined change in h(T) from the change in the calculated core distribution and the change predicted by the free electron approximation for the conduction electrons was $\sim$ 1 1/2%. It would appear therefore that the observed changes are associated with dynamic effects such as the thermal motion of the lattice sites.

From the definition preceding equation [15] we can see that the total annihilation rate into any momentum is given by

$$\lambda = \int_{\Gamma} \rho(\underline{p}) d\underline{p} = \int_{-\infty}^{\infty} dp_z \; N(p_z)$$

where $N(p_z)$ is given by equation [36]. So, from the long slit distributions we can calculate the annihilation rates for core and conduction electrons. The present calculations give annihilation rates for core electrons roughly the same as for Wigner-Seitz distributions. Using the experimental lifetimes of Mackenzie et al (1967) and of

Weisberg and Berko (1966) and using the figures 12-14 to determine the relative ratios of core and conduction annihilation, the enhancement rates were determined for core and valence electrons.

TABLE VII

Valence and Core Enhancement Factors

Metal	ε_V	ε_C
Cu	$\sim$ 4.6	$\sim$ 1.4
Cd	$\sim$ 5.0	$\sim$ 1
Zn	$\sim$ 4.0	$\sim$ 1

These results are physically reasonable. Carbotte and Salvadori (1967) calculated core enhancement rates in sodium and found them much smaller than conduction enhancement rates. The conduction rate in zinc is expected to be less enhanced than in copper or cadmium because the electron gas is denser. Copper having less conduction enhancement than cadmium agrees with a suggestion of West (1971). Since there is more core annihilation in copper, there is more screening and less enhancement. Core rates are in agreement with what was said about tight binding. The core electrons in copper, being less tightly bound, can respond more to the positron field, leading to greater enhancement than for either zinc or magnesium.

Thus we feel that the present method of calculating angular distributions can be used to separate the core and valence contributions with considerable confidence. In cases such as gold and copper where tight binding functions are poorest it would be worth attempting to construct single particle wavefunctions with less tightly bound character.

There are three significant conclusions from this work.

1. Hartree-Fock charge distributions are as good for computing positron wavefunctions as are the X-ray charge distributions.
2. A good description of experimental angular distributions can be obtained without sophisticated treatment of electronic structure.
3. A correct positron wavefunction is as important as higher momentum electronic components in explaining discrepancies between independent particle model calculations and experiment.

APPENDIX I

THE WIGNER-SEITZ APPROXIMATION

In the Wigner-Seitz approximation (Ziman 1964) the positron wavefunction is assumed to be spherically symmetric inside a sphere of radius r_s about each atomic site. The radius r_s is chosen so that the volume of the sphere is equal to the volume per atom in the crystal.

The spherically symmetric potential around an atom is calculated by the method of equation [3]. From the Schrodinger equation for the positron wavefunction $\psi_+(r)$ we can obtain the following differential equation for $R_+(r) = r\psi_+(r)$

$$R_+''(r) + (E-U(r))R_+(r) = 0 \qquad [A1]$$

The units in equation [A1] are the same as those described in section 2.1. If we assume that $\psi_+(r)$ must remain finite at $r = 0$, we have the inner boundary condition that $R_+(0) = 0$. Equation [A1] is then integrated outward in a standard manner (Hartree 1952) subject to the outer boundary condition

$$\frac{d}{dr}\frac{R_+(r)}{r} = 0 \quad \text{at } r = r_s.$$

The momentum distribution in the Wigner-Seitz approximation may be obtained from equation [15] again using the tight binding function [17]. Assuming for the moment that $\psi_+(\underline{r})$ still depends on $\underline{r}$ and is periodic in the crystal

$$\rho_{\underline{k}}^{n\ell m}(\underline{p}) = \frac{\alpha^3}{8\pi^2 N^2 \Omega}\left|\sum_{\underline{\tau}} e^{i\underline{k}\cdot\underline{\tau}} \int_W e^{-i\underline{p}\cdot\underline{r}}\, \Phi_{n\ell m}(\underline{r}-\underline{\tau})\psi_+(\underline{r})d\underline{r}\right|^2$$

$$= \frac{\alpha^3}{8\pi^2\Omega}\left|\int_W e^{-i\underline{p}\cdot\underline{r}}\, \Phi_{n\ell m}(\underline{r})\psi_+(\underline{r})d\underline{r}\right|^2 \delta_{\underline{k}-\underline{p},\underline{\alpha}} \qquad [A2]$$

To evaluate the integral in equation [A2], we again use equations [24] and [25] and integrate over the angular variables, but now insert the Wigner-Seitz positron wavefunction $\psi_+(\underline{r}) = \frac{R_+(r)}{r}$ for $r<r_s$, $\psi_+(\underline{r}) = 0$ for $r>r_s$.

$$\int_W e^{-i\underline{p}\cdot\underline{r}} \Phi_{n\ell m}(\underline{r}) \frac{R_+(r)}{r} d\underline{r} = 4\pi(-i)^{\ell} Y_{\ell}^{m}(\theta_{\underline{p}},\phi_{\underline{p}}) \int_0^{r_s} dr\ j_{\ell}(pr) P_{n\ell}(r) R_+(r)$$

Summing over m from $-\ell$ to $+\ell$ and over occupied electron states yields

$$\rho^{n\ell}(\underline{p}) = \frac{(2\ell+1)\alpha^3}{\pi\Omega} \left| \int_0^{r_s} dr\ j_{\ell}(pr) P_{n\ell}(r) R_+(r) \right|^2 \qquad [A3]$$

$\rho(\underline{p})$ is again obtained by summing n and ℓ over the appropriate core shells.

Since this $\rho(\underline{p})$ depends only on the magnitude p, as can easily be seen from equation [A3], the integrations over momentum space to obtain angular distributions may be transformed into single integrations over the variable p.

The result of such a transformation of equation [36] for the long slit detector configuration is given by equation [37]. The equivalent transformation of equation [35] for the point detector geometry gives

$$N(p_y,p_z) = 2\int_{p_o}^{\infty} \rho(p) \frac{pdp}{\sqrt{p^2-p_o^2}} \qquad [A4]$$

where $p_o = \sqrt{p_y^2+p_z^2}$

This formula is not amenable to numerical integration as it stands since the integrand is undefined at p_o. To put it into a useful form, we taken an interval Δ, small enough that $\rho(p)$ changes very little from p_o to $p_o + \Delta$, and rewrite [A4] as

$$N(p_y,p_z) = 2\rho(p_o) \int_{p_o}^{p_o+\Delta} \frac{pdp}{\sqrt{p^2-p_o^2}} + 2\int_{p_o+\Delta}^{\infty} \rho(p) \frac{pdp}{\sqrt{p^2-p_o^2}} \qquad [A5]$$

The integrand in the second integral is now defined over the entire range of integration and the first integral can be evaluated analytically yielding $2\rho(p_o)\sqrt{2p_o\Delta+\Delta^2}$.

APPENDIX II

BEHAVIOUR OF THE POSITRON WAVEFUNCTION IN THE NEIGHBOURHOOD OF r=0

The Schrodinger equation, in the units of section 2.1, for the positron wavefunction is

$$\nabla^2\psi_+(\underline{r}) + (E-V(\underline{r}))\psi_+(\underline{r}) = 0 \qquad [A6]$$

At very small values of r the positron wavefunction will be spherically symmetric and the potential $V(\underline{r})$ will be very close to $\frac{2Z}{r}$. The radial Wigner-Seitz differential equation [A1] will be

$$\frac{d^2R_+(r)}{dr^2} + (E - \frac{2Z}{r})R_+(r) = 0 \qquad [A7]$$

The point r = 0 is a regular singular point for this differential equation and it is well known (Mathews and Walker 1965) that we can then find a solution of the form

$$R_+(r) = r^S \sum_{n=0}^{\infty} a_n r^n \quad a_0 \neq 0 \qquad [A8]$$

Substituting this is the equation [A7] we obtain the indicial equation S(S-1) = 0, whose roots are S = 0,1. Only the solution with S = 1 satisfies the boundary condition $R_+(0) = 0$.

We then have

$$\psi_+(r) = \frac{R_+(r)}{r} = \sum_{n=0}^{\infty} a_n r^n$$

and $\psi_+(0) = a_0$.

Substituting equation [A8] in equation [A7] with S = 1, we obtain the recursion relation

$$a_{n+1} = \frac{1}{(n+1)(n+2)} \left(2Z\, a_n - E\, a_{n-1}\right) \qquad [A10]$$

Since we expect the Wigner-Seitz solution of Appendix I to be good for small values of r, we may use it together with the recursion relation [A10] to determine a_o.

With a finite number of terms in equation [A9], we use the recursion relation [A10] to express $R_+(r)$ in terms of only a_o and powers of r. Then using the value of $R_+(r)$ for the smallest value of r in the mesh used in the solution of Appendix I, we solve for a_o. Successively more terms were used in equation [A9] until the value of a_o converged. The values are shown below.

Metal	a_o
Mg	.01049
Cu	.00089
Zn	.00062
Cd	.00005
Au	<.00001

APPENDIX III

Computer Program for F.C.C. Crystals

```
C
C
C
C      THIS PROGRAM CALCULATES POSITRON WAVEFUNCTION COEFFICIENTS
C      FOR FCC METALS AND USES THEM TO CALCULATE POINT DETECTOR
C      ANGULAR DISTRIBUTIONS
C
C
C
       REAL NORM,ASUM(5),PSI(100)
       REAL LTVEC(30,3),KLAT1(48),KLAT2(48),KLAT3(48),R(100),
      1RWFCN(5,5,100),SIGMA(100),Z(100),INTEG(100),SMALVR(100),
      2MATRIX( 400 ),EIGVEC( 400 ),VK(100),LATPAR
       REAL NRMLZ1,NRMLZ2,NRMLZ3,RHOINT(100),P1(100),RHO(200),NK(20),
      2KSTARX(15,48),KSTARY(15,48),KSTARZ(15,48),A(5,5,100),QQ(100)
       INTEGER        NSTAR(20)
       REAL*8 X1,XK(100)
       INTEGER*2 DUMMY(120),ELNAM(40)
       COMMON R,SIGMA,SMALVR,NRVAL,ATNO,Z
       COMMON/B/KLAT1,KLAT2,KLAT3,LTVEC
       COMMON/C/RWFCN
       COMMON/D/EIGVEC
       COMMON/E/NSTAR,KSTARX,KSTARY,KSTARZ
       COMMON/F/A,QQ
       EQUIVALENCE(ELNAM(1),DUMMY(81))
C*****************************************************************************
C
C            INITIALIZE R_DEPENDENT ARRAYS
C
       DO 23    I=1,100
       DO 22    N=1,5
       DO 22    L=1,5
    22 RWFCN(N,L,I)=0.0
       R(I)=0.0
       SIGMA(I)=0.0
       Z(I)=0.0
       INTEG(I)=0.0
    23 SMALVR(I)=0.0
C
C      ***************************************************************
C
       READ(5,1)(ELNAM(I),  I=1,40),ATNO,NRVAL,NMIN,NMAX,VALEL,LATPAR
     1 FORMAT(40A1,3X,F2.0,2X,I3,2(4X,I1),4X,F1.0,5X,F5.4)
C
C            ELNAM=NAME OF ELEMENT BEING STUDIED IN ALPHAMERIC FORM
C            ATNO = ATOMIC NOMBER OF SAID ELEMENT
C            NRVAL = NUMBER OF R VALUES IN TABULATION OF ELECTRONIC WAVEFUNCT
C            NMAX = NUMBER OF SHELLS IN CORE OF ATOM
C            LATPAR = LATTICE PARAMETER
C
C      ***************************************************************
C
       READ(5,2) NKVAL,NVK
     2 FORMAT(2(2X,I3))
C            NKVAL IS THE NUMBER OF STARS USED IN THE CALCULATION
C            NVK IS THE CORRESPONDING NUMBER OF  FOURIER COEFF'S OF THE POT'L
C
       READ(5,3)((LTVEC(I,J),  J=1,3),    I=1,NKVAL)
     3 FORMAT(16(2X,3F1.0))
```

```
C
C
C
C
      READ(5,33)(NK(I),    I=1,NKVAL)
   33 FORMAT(16F5.0)
C
C           LTVEC = COMPONENTS OF RECIPROCAL LATTICE VECTORS
C           NK = MULTIPLICITY OF GIVEN STAR
C
      R(1)=0.0
      I=1
      D=.01
 1001 CONTINUE
      DO 1002    J=1,10
      I=I+1
 1002 R(I)=R(I-1)+D
      IF(I-NRVAL)1003,1004,1004
 1003 D=2.0*D
      GO TO 1001
 1004 CONTINUE
      CORFAC=ATNO**.333333333
      CORFAC=.88534138/CORFAC
      DO 1005    I=1,NRVAL
 1005 R(I)=R(I)*CORFAC
      DO 6     N=1,NMAX
      DO 6    L=1,N
      READ(5,5)(RWFCN(N,L,I),   I=1,NRVAL)
    5 FORMAT(10F8.4)
    6 CONTINUE
C
C           R = RADIAL  CO-ORDINATE
C           RWFCN = RADIAL WAVE FUNCTION
C
      READ(5,17) (XK(I),    I=1,NVK)
   17 FORMAT(16F5.0)
C
C           XK = SQUARE OF MODULUS OF K CORRESPONDING TO  I'TH K VALUE
C
C
C     ***************************************************************
C
C           THE NEXT SECTION COMPUTES THE FOURIER COEFF'S OF THE POTENTIAL
C
      LATPAR=LATPAR/.52917
      RECIP=6.283185/LATPAR
      RSEITZ=.390796*LATPAR
      VOL=(LATPAR*LATPAR*LATPAR)/4.0
      RHOCOR=50.26548*VALEL/(LATPAR*LATPAR*LATPAR)
      DO 9     I=1,NRVAL
      SIGMA(I)=0.0
      DO 7      N=1,NMAX
      DO 7    L=1,N
      L1=L-1
    7 SIGMA(I)=SIGMA(I)-2.0*(2.0*FLOAT(L1)+1.0)*RWFCN(N,L,I)*RWFCN(N,L,I
     1)
    9 CONTINUE
      CALL VINTEG
```

```
C
C
C
C
      ISEITZ=1
   46 DO 50    I=1,NVK
      XK(I)=DSQRT(XK(I))*RECIP
   47 CALL EVAL(XK(I),INTEG)
   48 CALL QTFG(R,INTEG,Z,NRVAL)
   49 SMALVK=Z(NRVAL)
   50 VK(I)=SMALVK/VOL
C
C     VK(I)=FOURIER COEFFICIENT OF POTENTIAL CORR SPONDI G TO I'TH
C     LARGEST K VALUE
C
      WRITE(6,7042) ISEITZ,RSEITZ
 7042 FORMAT('1','R(',I2,') < RSEITZ =',F5.3)
      WRITE(6,7043)(I,SMALVR(I),I=1,NRVAL)
 7043 FORMAT('0',6(' ','V(',I2,')=',F10.4,4X))
      WRITE(6,60)(I, VK(I),    I=1,NVK)
   60 FORMAT('0',2(10X,'VK(',I2,')=',F10.6))
C     **********************************************************************
C
C
C          THIS SECTION PERMUTES SIGNS AND INDICES, FINDS THE CORRESPONDINC
C          VK'S, AND COMPUTES THE MATRIX ELEMENTS OF MATRIX TO BE
C     DIAGONALIZED
C
      DO 159    J=1,NKVAL
      CALL PERMUT(J,KSTOR,0)
      NSTAR(J)=KSTOR
      DO 181      JJ=1,KSTOR
      KSTARX(J,JJ)=KLAT1(JJ)*RECIP
      KSTARY(J,JJ)=KLAT2(JJ)*RECIP
  181 KSTARZ(J,JJ)=KLAT3(JJ)*RECIP
      DO 159     M=J,NKVAL
  144 JM=J+(M*M-M)/2
  145 MATRIX(JM)=0.0
  146 DO 159    MM=1,KSTOR
  147 C1=LTVEC(M ,1)-KLAT1(MM)
  148 C2=LTVEC(M ,2)-KLAT2(MM)
  149 C3=LTVEC(M ,3)-KLAT3(MM)
  150 X1=C1*C1+C2*C2+C3*C3
      X1=DSQRT(X1)*RECIP
  151 DO 155     JVK=1,NVK
  152 IF(X1.NE.XK(JVK))GO TO 155
  153 I=JVK
  154 GO TO 158
  155 CONTINUE
  156 WRITE(6,157) J,M,MM
  157 FORMAT('0','MODULUS DOES NOT CORRESPOND TO ANY OF THE GIVEN MODULI
     1 FOR J =',I3,3X,'M=',I3,3X,'MM=',I3)
  158 CONTINUE
  159 MATRIX(JM)=MATRIX(JM)+VK(I)*SQRT(NK(M)/NK(J))
  160 DO 164    I=1,NKVAL
      DIAG=0.0
  161 DO 162    J=1,3
  162 DIAG=DIAG+LTVEC(I,J)*LTVEC(I,J)
```

```
C
C
C
C
  163 DIAG=DIAG*RECIP*RECIP
      II=I+(I*I-I)/2
  164 MATRIX(II)=MATRIX(II)+DIAG
      WRITE(6,201)
  201 FORMAT('1','ORIGINAL MATRIX')
      DO 203    I=1,NKVAL
      IJ1=(I*I-I)/2 +1
      IJN=(I*I+I)/2
      WRITE(6,202) (MATRIX(IJ),  IJ=IJ1,IJN)
  202 FORMAT('0',11(F10.5,2X))
  203 CONTINUE
      CALL OUT(MATRIX,EIGVEC,NKVAL)
      J=NKVAL
      SUMSQ=0.0
      SUM=0.0
      DO 62    I=1,NKVAL
      IJ =(J-1)*NKVAL +I
      SUMSQ=SUMSQ+EIGVEC(IJ) *EIGVEC(IJ)
   62 SUM=SUM+EIGVEC(IJ) *SQRT(NK(I))
      WRITE(6,63) J,SUMSQ,J,SUM
   63 FORMAT('0','SUMSQ(',I2,')=',F10.6,10X,'SUM(',I2,')=',F10.6)
C
C
C     **********************************************************************
C
C     A1,A2,A3,;B1,B2,B3;C1,C2,C3 SPECIFY THE GAMMA RAY DIRECTION
C     ,POINT DETECTOR MOTION, AND LONG SLIT DETECTOR MOTION
C     NPPTS IS THE NUMBER OF POINTS TO BE CALCULATED IN DISTRIBUTION
C     NPPTS1 IS THE NUMBER OF POINTS IN THE INTEGRAL OVER PX
C     IZERO SPECIFIES STARTING POINT
C     RANGE SPECIFIES INTEGRATION RANGE
C     NK9 IS THE NUMBER OF PLANE WAVES USED TO CALCULATE THE
C     ANGULAR DISTRIBUTIONS
C
C
      READ(5,166)A1,A2,A3,B1,B2,B3,C1,C2,C3,NPPTS,NPPTS1,IZERO,RANGE,NK9
  166 FORMAT(3(4X,3F2.0),3I5,F5.0,I5)
C
C     **********************************************************************
C
C     THE FOLLOWING SECTION RENORMALIZES THE POSITRON COEFFICIENTS
C
        SUM=0.0
      SUMSQ=0.0
      DO 64    I=1,NK9
      IJ=(J-1)*J+I
      SUMSQ=SUMSQ+EIGVEC(IJ) *EIGVEC(IJ)
   64 SUM=SUM+EIGVEC(IJ) *SQRT(NK(I))
      WRITE(6,65) NK9,SUMSQ,NK9,SUM
   65 FORMAT('0','SUMSQ(',I2,')=',F10.6,10X,'SUM(',I2,')=',F10.6)
      IJ=(J-1)*J+1
      EIGVEC(IJ)=EIGVEC(IJ)-SUM
      SUMSQ=0.0
      DO 66    I=1,NK9
```

```
C
C
C
C
      IJ=(J-1)*J+I
   66 SUMSQ=SUMSQ+EIGVEC(IJ) *EIGVEC(IJ)
      DEN=SQRT(SUMSQ)
      DO 67    I=1,NK9
      IJ=(J-1)*J+I
      EIGVEC(IJ)=EIGVEC(IJ)/DEN
      OUTPUT=EIGVEC(IJ)/SQRT(NK(I))
   67 WRITE(6,68) I,OUTPUT
   68 FORMAT('0','A(',I2,') =',F10.5)
C
C     **********************************************************************
C
C     THE FOLLOWING SECTION CALCULATES ISUB N,L(Q)
C
      DO 221       N=1,NMAX
      DO 221       L=1,N
      TEMP=-1.0
      DO 221       I=1,60
      TEMP=TEMP+1.0
      QQ(I)=TEMP*.137038
      CALL FOLD(N,L,NRVAL,QQ(I),INTEG)
      CALL QTFG(R,INTEG,Z,NRVAL)
  221 A(N,L,I)=Z(NRVAL)
      WRITE(6,250)
  250 FORMAT('1',5(10X,'ASUM',6X))
      DO 252    I=1,60
      DO 251    N=1,NMAX
      ASUM(N)=0.0
      DO 251     L=1,N
  251 ASUM(N)=(2.0*FLOAT(L-1)+1.)*A(N,L,I)*A(N,L,I)+ASUM(N)
  252 WRITE(6,253)(ASUM(N),  N=1,NMAX)
  253 FORMAT(' ',5(F15.5,5X))
C
C     **********************************************************************
C
C     THE NEXT SECTION PERFORMS THE INTEGRATIONS OVER MOMENTUM SPACE
C     FOR POINT DETECTOR SINGLE XTAL DISTRIBUTIONS. THIS SEGMENT
C     IS USED FOR BOTH  FCC AND HCP  PROGRAMS.
C
      NKVAL=NK9
      WRITE(6,174)
  174 FORMAT('1','POINT GEOMETRY ANGULAR DISTRIBUTION'///)
      WRITE(6,175)B1,B2,B3,A1,A2,A3
  175 FORMAT('0',20X,'DETECTOR MOVING ALONG ',3F3.0,'AXIS,',5X,'GAMMA
     1RAYS ALONG',3F3.0,'AXIS'///)
      WRITE(6,177)
  177 FORMAT('0',7X,' DETECTOR',14X,'COUNT')
      WRITE(6,176)
  176 FORMAT(' ',7X,' POSITION',14X,' RATE')
      H1=(2.0*RANGE)/(FLOAT(NPPTS1-1))
      H2=20.0/FLOAT(NPPTS-1)
      PPTS=FLOAT((NPPTS1+1)/2)
      NRMLZ1=SQRT(A1*A1+A2*A2+A3*A3)
      NRMLZ2=SQRT(B1*B1+B2*B2+B3*B3)
```

```
C
C
C
C
      XINCR1= H1*A1/NRMLZ1
      H1=H1*.137038
      H2=H2*.137038
      YINCR1= H1*A2/NRMLZ1
      ZINCR1= H1*A3/NRMLZ1
      XINCR2=H2*B1/NRMLZ2
      YINCR2=H2*B2/NRMLZ2
      ZINCR2=H2*B3/NRMLZ2
      ZE=IZERO
      PXPDR=ZE*XINCR2
      PYPDR=ZE*YINCR2
      PZPDR=ZE*ZINCR2
      DO 171    K=1,NPPTS
      PXPDR=PXPDR+XINCR2
      PYPDR=PYPDR+YINCR2
      PZPDR=PZPDR+ZINCR2
      PXINT=PXPDR-PPTS*XINCR1
      PYINT=PYPDR-PPTS*YINCR1
      PZINT=PZPDR-PPTS*ZINCR1
      DO 165      L=1,NPPTS1
      PXINT=PXINT+XINCR1
      PYINT=PYINT+YINCR1
      PZINT=PZINT+ZINCR1
  165 CALL CALC(NMIN,NMAX,NKVAL,NRVAL,RECIP,PXINT,PYINT,PZINT,RHO(L))
      CALL QUADR(RHO,NPPTS1,H1,S,IER)
  169 PPD=FLOAT(K+IZERO)*H2/.137038
  170 RHOPD=S
      WRITE(6,179)PPD,RHOPD
  179 FORMAT('0',2(6X,F10.4))
  171 CONTINUE
      STOP
      END
```

```
C
C
C
C
      SUBROUTINE PERMUT(J,KSTOR,ICHK)
C
C     THIS SUBPROGRAM GENERATES THE STARS  FOR THE CUBIC CASE
C     BY PERFORMING ALL PERMUTATIONS OF SIGNS AND INDICES ON THE
C     LATTICE VECTORS READ IN
C
      REAL LTVEC(30,3),KLAT1(48),KLAT2(48),KLAT3(48),K11,K12,K13
      COMMON/B/KLAT1,KLAT2,KLAT3,LTVEC
      KSTOR=0
  541 DO 543     J1=1,3
      K11=-LTVEC(J,J1)
      IF(J1.NE.1)GO TO 107
  101 DO 140     J2=2,3
      K12=-LTVEC(J,J2)
  102 IF(J2.NE.2)GO TO 105
  103 K13=-LTVEC(J, 3)
  104 GO TO 121
  105 K13=-LTVEC(J,2)
  121 CONTINUE
  122 DO  140     LL1=1,2
  123 K11=-K11
  124 DO 140     LL2=1,2
  125 K12=-K12
  126 DO 140   LL3=1,2
  127 K13=-K13
  128 KSTOR=KSTOR+1
  129 KLAT1(KSTOR)=K11
  130 KLAT2(KSTOR)=K12
  131 KLAT3(KSTOR)=K13
  132 IF(KSTOR.EQ.1)GO TO 140
  133 KSTORM=KSTOR-1
  134 DO 139   KKK=1,KSTORM
  135 IF(KLAT1(KSTOR).NE.KLAT1(KKK))GO TO 139
  136 IF(KLAT2(KSTOR).NE.KLAT2(KKK))GO TO 139
  137 IF(KLAT3(KSTOR).NE.KLAT3(KKK))GO TO 139
  138 KSTOR=KSTOR-1
      GO TO 140
  139 CONTINUE
  140 CONTINUE
      GO TO 543
  107 IF(J1.NE.2)GO TO 115
  108 DO 240   J3=1,3
      IF(J3.EQ.2) GO TO 240
  109 K12=-LTVEC(J,J3)
  110 IF(J3.NE.1)GO TO 113
  111 K13=-LTVEC(J,3)
  112 GO TO 221
  113 K13=-LTVEC(J,1)
  221 CONTINUE
  222 DO  240     LL1=1,2
  223 K11=-K11
  224 DO 240     LL2=1,2
  225 K12=-K12
  226 DO 240   LL3=1,2
```

```
C
C
C
C
  227 K13=-K13
  228 KSTOR=KSTOR+1
  229 KLAT1(KSTOR)=K11
  230 KLAT2(KSTOR)=K12
  231 KLAT3(KSTOR)=K13
  232 IF(KSTOR.EQ.1)GO TO 240
  233 KSTORM=KSTOR-1
  234 DO 239   KKK=1,KSTORM
  235 IF(KLAT1(KSTOR).NE.KLAT1(KKK))GO TO 239
  236 IF(KLAT2(KSTOR).NE.KLAT2(KKK))GO TO 239
  237 IF(KLAT3(KSTOR).NE.KLAT3(KKK))GO TO 239
  238 KSTOR=KSTOR-1
      GO TO 240
  239 CONTINUE
  240 CONTINUE
      GO TO 543
  115 DO 340     J4=1,2
  116 K12=-LTVEC(J,J4)
  117 IF(J4.NE.1)GO TO 120
  118 K13=-LTVEC(J,2)
  119 GO TO 321
  120 K13=-LTVEC(J,1)
  321 CONTINUE
  322 DO  340     LL1=1,2
  323 K11=-K11
  324 DO 340     LL2=1,2
  325 K12=-K12
  326 DO 340   LL3=1,2
  327 K13=-K13
  328 KSTOR=KSTOR+1
  329 KLAT1(KSTOR)=K11
  330 KLAT2(KSTOR)=K12
  331 KLAT3(KSTOR)=K13
  332 IF(KSTOR.EQ.1)GO TO 340
  333 KSTORM=KSTOR-1
  334 DO 339   KKK=1,KSTORM
  335 IF(KLAT1(KSTOR).NE.KLAT1(KKK))GO TO 339
  336 IF(KLAT2(KSTOR).NE.KLAT2(KKK))GO TO 339
  337 IF(KLAT3(KSTOR).NE.KLAT3(KKK))GO TO 339
  338 KSTOR=KSTOR-1
      GO TO 340
  339 CONTINUE
  340 CONTINUE
  543 CONTINUE
      IF(ICHK.EQ.0) GO TO 143
  141 WRITE(6,142) (LTVEC(J,I),   I=1,3), KSTOR
  142 FORMAT('0','MULTIPLICITY OF KVECTOR',3F2.0,5X,'=',I3)
  143 CONTINUE
      RETURN
      END
```

```
C
C
C
C
      SUBROUTINE CALC(NMIN,NMAX,NKVAL,NRVAL,RECIP,PX,PY,PZ,RHO)
C
C     THIS SUBPROGRAM CALCULATES THE MOMENTUM SPACE DENSITY
C     FOR THE FCC CASE AT THE CO-ORDINATES PX,PY,PZ
C
      REAL R(100),EIGVEC(400),KSTARX(15,48),KSTARY(15,48),KSTARZ(15,48),
     2A(5,5,100),QQ(100)
      INTEGER NSTAR(20)
      COMMON/D/EIGVEC
      COMMON/E/NSTAR,KSTARX,KSTARY,KSTARZ
      COMMON/F/A,QQ
      RHO=0.0
      DO 11    N=NMIN,NMAX
      DO 11      L=1,N
      IF(L-2)51,52,53
   53 IF(L-4)54,55,56
   51 SUM=0.0
      DO 1       JJ=1,NKVAL
      KSTOR=NSTAR(JJ)
      WT=KSTOR
      WT=SQRT(WT)
      JM=110+JJ
      WT=EIGVEC(JM)/WT
      DO 1       KK=1,KSTOR
      QX1=PX-KSTARX(JJ,KK)
      QY1=PY-KSTARY(JJ,KK)
      QZ1=PZ-KSTARZ(JJ,KK)
      Q1=SQRT(QX1*QX1+QY1*QY1+QZ1*QZ1)
    7 IF(Q1-QQ(1))2,4,4
    4 DO 21      I=1,60
      J=I
      IF(Q1-QQ(I))23,22,21
   21 CONTINUE
    3 TERM=A(N,L,60)
      GO TO 24
   22 TERM=A(N,L,J)
      GO TO 24
   23 TERM=A(N,L,J-1)+((Q1-QQ(J-1))/(QQ(J)-QQ(J-1)))*(A(N,L,J)-A(N,L,J-1
     1))
   24 TERM=TERM*WT
    5 SUM = SUM+TERM
    1 CONTINUE
      RHO=RHO+SUM*SUM
      GO TO 11
   52 SUM=0.0
      DO 101     JJ=1,NKVAL
      KSTOR=NSTAR(JJ)
      WT=KSTOR
      WT=SQRT(WT)
      JM=110+JJ
      WT=EIGVEC(JM)/WT
      DO 101     KK=1,KSTOR
      QX1=PX-KSTARX(JJ,KK)
      QY1=PY-KSTARY(JJ,KK)
```

```
C
C
C
C
      QZ1=PZ-KSTARZ(JJ,KK)
      Q1=SQRT(QX1*QX1+QY1*QY1+QZ1*QZ1)
  107 IF(Q1-QQ(1))2,104,104
  104 DO 121    I=1,60
      J=I
      IF(Q1-QQ(I))123,122,121
  121 CONTINUE
  103 TERM1=A(N,L,60)
      GO TO 124
  122 TERM1=A(N,L,J)
      GO TO 124
  123 TERM1=A(N,L,J-1)+((Q1-QQ(J-1))/(QQ(J)-QQ(J-1)))*(A(N,L,J)-A(N,L,J-
     11))
  124 TERM1=TERM1*WT
      DO 101    LL=1,NKVAL
      KSTOR1=NSTAR(LL)
      WT1=KSTOR1
      WT1=SQRT(WT1)
      JM=110+LL
      WT1=EIGVEC(JM)/WT1
      DO 101    MM=1,KSTOR1
      QX2=PX-KSTARX(LL,MM)
      QY2=PY-KSTARY(LL,MM)
      QZ2=PZ-KSTARZ(LL,MM)
      Q2=SQRT(QX2*QX2+QY2*QY2+QZ2*QZ2)
  125 IF(Q2-QQ(1))2,126,126
  126 DO 127    I=1,60
      J=I
      IF(Q2-QQ(I))129,128,127
  127 CONTINUE
  130 TERM2=A(N,L,60)
      GO TO 131
  128 TERM2=A(N,L,J)
      GO TO 131
  129 TERM2=A(N,L,J-1)+((Q2-QQ(J-1))/(QQ(J)-QQ(J-1)))*(A(N,L,J)-A(N,L,J-
     11))
  131 TERM2=TERM2*WT1
      IF(Q1*Q2.NE.0.0) GO TO 132
      U=1.0
      GO TO 133
  132 U=(QX1*QX2+QY1*QY2+QZ1*QZ2)/(Q1*Q2)
  133 SUM=TERM1*TERM2*U+SUM
  101 CONTINUE
      RHO =RHO+3.0*SUM
      GO TO 11
   54 SUM=0.0
      DO 201    JJ=1,NKVAL
      KSTOR=NSTAR(JJ)
      WT=KSTOR
      WT=SQRT(WT)
      JM=110+JJ
      WT=EIGVEC(JM)/WT
      DO 201    KK=1,KSTOR
      QX1=PX-KSTARX(JJ,KK)
```

```
C
C
C
C
      QY1=PY-KSTARY(JJ,KK)
      QZ1=PZ-KSTARZ(JJ,KK)
      Q1=SQRT(QX1*QX1+QY1*QY1+QZ1*QZ1)
  207 IF(Q1-QQ(1))2,204,204
  204 DO 221    I=1,60
      J=I
      IF(Q1-QQ(I))223,222,221
  221 CONTINUE
  203 TERM1=A(N,L,60)
      GO TO 224
  222 TERM1=A(N,L,J)
      GO TO 224
  223 TERM1=A(N,L,J-1)+((Q1-QQ(J-1))/(QQ(J)-QQ(J-1)))*(A(N,L,J)-A(N,L,J-
     11))
  224 TERM1=TERM1*WT
      DO 201    LL=1,NKVAL
      KSTOR1=NSTAR(LL)
       WT1=KSTOR1
      WT1=SQRT(WT1)
      JM=110+LL
       WT1=EIGVEC(JM)/WT1
      DO 201    MM=1,KSTOR1
      QX2=PX-KSTARX(LL,MM)
      QY2=PY-KSTARY(LL,MM)
      QZ2=PZ-KSTARZ(LL,MM)
      Q2=SQRT(QX2*QX2+QY2*QY2+QZ2*QZ2)
  225 IF(Q2-QQ(1))2,226,226
  226 DO 227    I=1,60
      J=I
      IF(Q2-QQ(I))229,228,227
  227 CONTINUE
  230 TERM2=A(N,L,60)
      GO TO 231
  228 TERM2=A(N,L,J)
      GO TO 231
  229 TERM2=A(N,L,J-1)+((Q2-QQ(J-1))/(QQ(J)-QQ(J-1)))*(A(N,L,J)-A(N,L,J-
     11))
  231 TERM2=TERM2*WT1
      IF(Q1*Q2.NE.0.0) GO TO 232
      U=1.0
      GO TO 233
  232 U=(QX1*QX2+QY1*QY2+QZ1*QZ2)/(Q1*Q2)
  233 SUM=SUM+TERM1*TERM2*(1.5*L*L-.5)
  201 CONTINUE
      RHO=RHO+5.0*SUM
      GO TO 11
   55 SUM=0.0
      DO 301    JJ=1,NKVAL
      KSTOR=NSTAR(JJ)
      WT=KSTOR
      WT=SQRT(WT)
      JM=110+JJ
      WT=EIGVEC(JM)/WT
      DO 301    KK=1,KSTOR
```

```
C
C
C
C
      QX1=PX-KSTARX(JJ,KK)
      QY1=PY-KSTARY(JJ,KK)
      QZ1=PZ-KSTARZ(JJ,KK)
      Q1=SQRT(QX1*QX1+QY1*QY1+QZ1*QZ1)
  307 IF(Q1-QQ(1))2,304,304
  304 DO 321    I=1,60
      J=I
      IF(Q1-QQ(I))323,322,321
  321 CONTINUE
  303 TERM1=A(N,L,60)
      GO TO 324
  322 TERM1=A(N,L,J)
      GO TO 324
  323 TERM1=A(N,L,J-1)+((Q1-QQ(J-1))/(QQ(J)-QQ(J-1)))*(A(N,L,J)-A(N,L,J-
     11))
  324 TERM1=TERM1*WT
      DO 301    LL=1,NKVAL
      KSTOR1=NSTAR(LL)
        WT1=KSTOR1
      WT1=SQRT(WT1)
      JM=110+LL
      WT1=EIGVEC(JM)/WT1
      DO 301    MM=1,KSTOR1
      QX2=PX-KSTARX(LL,MM)
      QY2=PY-KSTARY(LL,MM)
      QZ2=PZ-KSTARZ(LL,MM)
      Q2=SQRT(QX2*QX2+QY2*QY2+QZ2*QZ2)
  325 IF(Q2-QQ(1))2,326,326
  326 DO 327    I=1,60
      J=I
      IF(Q2-QQ(I))329,328,327
  327 CONTINUE
  330 TERM2=A(N,L,60)
      GO TO 231
  328 TERM2=A(N,L,J)
      GO TO 331
  329 TERM2=A(N,L,J-1)+((Q2-QQ(J-1))/(QQ(J)-QQ(J-1)))*(A(N,L,J)-A(N,L,J-
     11))
  331 TERM2=TERM2*WT1
      IF(Q1*Q2.NE.0.0) GO TO 332
      U=1.0
      GO TO 333
  332 U=(QX1*QX2+QY1*QY2+QZ1*QZ2)/(Q1*Q2)
  333 SUM=SUM+TERM1*TERM2*(2.5*L*L*U-1.5*U)
  301 CONTINUE
      RHO =RHO+7.0*SUM
   11 CONTINUE
      RETURN
    2 WRITE(6,10)
   10 FORMAT('0','ERROR IN INPUT TO SUBROUTINE CALC, Q < 0')
   56 RETURN
      END
```

APPENDIX IV

Computer Program for H.C.P. Crystals

```
C
C
C
C
C
C     THIS PROGRAM CALCULATES THE FOURIER COEFFICIENTS OF THE
C     POSITRON WAVEFUNCTION FOR THE HCP STRUCTURE.
C
      REAL R(100),RWFCN(4,4,100),SIGMA(100),Z(100),INTEG(100),
     1SMALVR(100),VK(200),KSTARX(25,24),
     2KSTARY(25,24),KSTARZ(25,24),NK(25),LATPR1,LATPR2
      REAL*8 MATRIX(325),EIGVEC(625)
      INTEGER NSTAR(40)
      REAL*8 X,XK(200),TEST
      INTEGER*2 DUMMY(120),ELNAM(40)
      COMMON R,SIGMA,SMALVR,NRVAL,ATNO,Z
      EQUIVALENCE(ELNAM(1),DUMMY(81))
C*********************************************************************
C
C
C           INITIALIZE R-DEPENDENT ARRAYS
C
      DO 23    I=1,100
      DO 22    N=1,4
      DO 22    L=1,4
   22 RWFCN(N,L,I)=0.0
      R(I)=0.0
      SIGMA(I)=0.0
      Z(I)=0.0
      INTEG(I)=0.0
   23 SMALVR(I)=0.0
C
C
C*********************************************************************
      READ(5,1)(ELNAM(I),I=1,40),ATNO,NRVAL,NMIN,NMAX,VALEL,LATPR1,
     1LATPR2
    1 FORMAT(40A1,3X,F2.0,3X,I2,4X,2(I1,4X),F1.0,5X,2F5.4)
C
C           ELNAM=NAME OF ELEMENT BEING STUDIED IN ALPHAMERIC FORM
C           ATNO = ATOMIC NUMBER OF SAID ELEMENT
C           NRVAL = NUMBER OF R VALUES IN TABULATION OF ELECTRONIC WAVEFUNCT
C           NMIN= PRINCIPAL QUANTUM NUMBER OF LOWEST CORE SHELL CONSIDERED
C           NMAX= PRINCIPAL QUANTUM NUMBER OF HIGHEST CORE SHELL CONSIDERED
C           LATPR1,LATPR2=LATTICE PARAMETERS IN A & C DIRECTIONS
C
C*********************************************************************
C
      READ(5,2) NKVAL
    2 FORMAT( (2X,I3))
C
C           NKVAL IS THE NUMBER OF STARS USED IN THE CALCULATION
C
C
      READ(5,3)(NSTAR(J),J=1,NKVAL)
    3 FORMAT(20(2X,I2))
      DO 25     I=1,NKVAL
      N=NSTAR(I)
   25 READ(5,4)(KSTARX(I,JJ),KSTARY(I,JJ),KSTARZ(I,JJ), JJ=1,N)
```

```
C
C
C
C
    4 FORMAT(3(4X,3F2.0))
C
      R(1)=0.0
      I=1
      D=.01
 1001 CONTINUE
      DO 1002   J=1,10
      I=I+1
 1002 R(I)=R(I-1)+D
      IF(I-NRVAL)1003,1004,1004
 1003 D=2.0*D
      GO TO 1001
 1004 CONTINUE
      CORFAC=ATNO**.333333333
      CORFAC=.88534138/CORFAC
      DO 1005   I=1,NRVAL
 1005 R(I)=R(I)*CORFAC
      DO 6    N=1,NMAX
      DO 6   L=1,N
      READ(5,5)(RWFCN(N,L,I),  I=1,NRVAL)
    5 FORMAT(10F8.4)
    6 CONTINUE
C
C           R = RADIAL  CO-ORDINATE
C           RWFCN = RADIAL WAVE FUNCTION
C
C*************************************************************************
C
C
C
C           THE NEXT SECTION COMPUTES THE FOURIER COEFF'S OF THE POTENTIAL
C
C
      LATPR1=LATPR1/.52917
      LATPR2=LATPR2/.52917
      RECIP1=7.255192/LATPR1
      RECIP2=6.283185/LATPR2
      VOL=.866026*LATPR1*LATPR1*LATPR2
      RSEITZ=.492373*VOL**.3333333
      RHOCOR=25.132741*VALEL/VOL
      VOL=VOL/2.0
      DO 9    I=1,NRVAL
      SIGMA(I)=0.0
      DO 7     N=1,NMAX
      DO 7   L=1,N
      L1=L-1
    7 SIGMA(I)=SIGMA(I)-2.0*(2.0*FLOAT(L1)+1.0)*RWFCN(N,L,I)*RWFCN(N,L,I
     1)
    9 CONTINUE
      CALL VINTEG
      ISEITZ=1
      DO 43   I=1,NRVAL
      IF(R(I)- RSEITZ)41,42,42
C
```

```
C
C
C
C
C       SMALVR(I)= RV(R)  FOR R=R(I)
C
   41 SMALVR(I)=SMALVR(I)-(R(I)*RSEITZ*RSEITZ-.333333*R(I)*R(I)*R(I))
     1*RHOCOR
      ISEITZ=I
      GO TO 43
   42 SMALVR(I)=SMALVR(I)-RHOCOR*.666666*RSEITZ*RSEITZ*RSEITZ
   43 CONTINUE
      WRITE(6,2000) ISEITZ,RSEITZ
 2000 FORMAT('1','R(',I2,') < RSEITZ=',F5.3)
      WRITE(6,2001)(I,SMALVR(I),I=1,NRVAL)
 2001 FORMAT('0',6(' ','V(',I2,')=',F10.4,4X))
      DO 183   J=1,NKVAL
  183 NK(J)=NSTAR(J)
      I=1
      XK(1)=0.0
      CALL EVAL(XK(1),INTEG)
      CALL QTFG(R,INTEG,Z,NRVAL)
      SMALVK=Z(NRVAL)
      VK(1)=SMALVK/VOL
C
C       VK(I)=FOURIER COMPONENT OF POTENTIAL CORRESPONDING
C       TO K IN I'TH STAR
C
C
C       **********************************************************************
C
C       THIS SECTION CALCULATES THE MATRIX ELEMENTS OF THE MATRIX
C       TO BE DIAGONALIZED
C
      DO 10     J=1,NKVAL
      DO 10     M=J,NKVAL
      JM=J+(M*M-M)/2
      MATRIX(JM)=0.0
      JJF=NSTAR(J)
      MMF=NSTAR(M)
      IEXP1=KSTARZ(J,1)
      IEXP2=KSTARZ(M,1)
      ICH1=JJF/2
      ICH2=MMF/2
      DO 10     JJ=1,JJF
      ISGN1=1
      IF(JJ.GT.ICH1) ISGN1=(-1)**IEXP1
   13 DO 10   MM=1,MMF
      ISGN2=1
      IF(MM.GT.ICH2) ISGN2=(-1)**IEXP2
   14 I=I+1
      XKX=KSTARX(J,JJ)-KSTARX(M,MM)
      XKY=KSTARY(J,JJ)-KSTARY(M,MM)
      XKZ=KSTARZ(J,JJ)-KSTARZ(M,MM)
      PHASE=(XKX/1.5-XKY/3.0+XKZ/4.)*6.283185
      XKX=XKX-.5*XKY
      XKY=.866026*XKY
      XKX=XKX*RECIP1
```

```
C
C
C
C
      XKY=XKY*RECIP1
      XKZ=XKZ*RECIP2
      XK(I)=XKX*XKX+XKY*XKY+XKZ*XKZ
      XK(I)=DSQRT(XK(I))
      LM=I-1
      DO 15   L=1,LM
      TEST=DABS(XK(I)-XK(L))
      IF(TEST.GT.0.00001) GO TO 15
      MATRIX(JM)=MATRIX(JM)+ISGN1*ISGN2*VK(L)*(1.0*COS(PHASE))/SQRT(NK(M
     1)*NK(J))
      I=I-1
      GO TO 10
   15 CONTINUE
      CALL EVAL(XK(I),INTEG)
      CALL QTFG(R,INTEG,Z,NRVAL)
      SMALVK=Z(NRVAL)
      VK(I)=SMALVK/VOL
      MATRIX(JM)=MATRIX(JM)+ISGN1*ISGN2*VK(L)*(1.0*COS(PHASE))/SQRT(NK(M
     1)*NK(J))
   10 CONTINUE
      NVK=I
      WRITE(6,59)
   59 FORMAT('1')
      WRITE(6,60)(I, VK(I),    I=1,NVK)
   60 FORMAT('0',2(10X,'VK(',I2,')=',F10.6))
  160 DO 164   I=1,NKVAL
      XKX=(KSTARX(I,1)-.5*KSTARY(I,1))*RECIP1
      XKY=KSTARY(I,1)*.866026*RECIP1
      XKZ=KSTARZ(I,1)*RECIP2
      DIAG=XKX*XKX+XKY*XKY+XKZ*XKZ
      II=I+(I*I-I)/2
  164 MATRIX(II)=MATRIX(II)+DIAG
      WRITE(6,201)
  201 FORMAT('1','ORIGINAL MATRIX')
C
C      **********************************************************************
C
C     THE NEXT SECTION COMPUTES THE SUM OF THE SQUARES OF THE
C     POSITRON COEFFICIENTS AND THE VALUE OF THE POSITRON WAVEFUNCTION
C     AT THE NUCLEUS.
C
      I1=NKVAL-10
      DO 203   I=I1,NKVAL
      IJN=(I*I+I)/2
      IJ1=IJN+I1-I
      WRITE(6,202) (MATRIX(IJ),  IJ=IJ1,IJN)
  202 FORMAT('0',11(F10.5,2X))
  203 CONTINUE
      CALL OUT(MATRIX,EIGVEC,NKVAL)
      II=1
  261 II=II+1
      SUMSQ=0.0
      SUM=0.0
      DO 262     I=1,II
```

```
C
C
C
C
      IEXP1=KSTARZ(I,1)
      IJ=NKVAL*(NKVAL-1)+I
      SUMSQ=SUMSQ+EIGVEC(IJ)*EIGVEC(IJ)
      KSTOR=NSTAR(I)
      TEMP=0.0
      ICH1=KSTOR/2
      DO  162     K=1,KSTOR
      ISGN1=1
      IF(K.GT.ICH1) ISGN1=(-1)**IEXP1
      PHASE=(KSTARX(I,K)/1.5-KSTARY(I,K)/3.0+KSTARZ(I,K)/4.0)*6.283185
  162 TEMP=TEMP+COS(PHASE)*ISGN1
  262 SUM=SUM+EIGVEC(IJ)*TEMP/SQRT(NK(I))
      WRITE(6,263)II,SUMSQ,II,SUM
  263 FORMAT(' ','SUMSQ(',I2,')=',F8.5,'SUM(',I2,')=',F8.5)
      IF(II-NKVAL)261,264,264
  264 CONTINUE
      STOP
      END
```

```
C
C
C
C
C     THIS PROGRAM CALCULATES LONG SLIT DETECTOR ANGULAR DISTRIBUTIONS
C     FOR POLYCRYSTALLINE HCP METALS USING THE POSITRON COEFFICIENTS
C     CALCULATED BY THE PRECEDING PROGRAM
      REAL PSI(100)
      REAL NORM
      REAL R(100),RWFCN(4,4,100),Z(100),INTEG(100),EIGVEC(40),
     1KSTARX(40,12),KSTARY(40,12),KSTARZ(40,12),RHO(100)
     3,NK(40),LATPR1,LATPR2,A(4,4,100),QQ(100),NRMLZ1,NRMLZ2,NRMLZ3
      REAL P2(100),RHOFIN(100)
      INTEGER NSTAR(40)
      INTEGER*2 DUMMY(120),ELNAM(40)
      COMMON R
      COMMON/C/RWFCN
      COMMON/D/EIGVEC,LATPR1,LATPR2
      COMMON/E/NSTAR,KSTARX,KSTARY,KSTARZ
      COMMON/F/A,QQ
      EQUIVALENCE(ELNAM(1),DUMMY(81))
C*****************************************************************************
C
C
C           INITIALIZE R-DEPENDENT ARRAYS
C
      DO 23    I=1,100
      DO 22    N=1,4
      DO 22    L=1,4
   22 RWFCN(N,L,I)=0.0
      R(I)=0.0
      Z(I)=0.0
   23 INTEG(I)=0.0
C
C
C*****************************************************************************
C
      READ(5,1)(ELNAM(I),I=1,40),ATNO,NRVAL,NMIN,NMAX,VALEL,LATPR1,
     1LATPR2
    1 FORMAT(40A1,3X,F2.0,3X,I2,4X,2(I1,4X),F1.0,5X,2F5.4)
C
C           ELNAM=NAME OF ELEMENT BEING STUDIED IN ALPHAMERIC FORM
C           ATNO = ATOMIC NUMBER OF SAID ELEMENT
C           NRVAL = NUMBER OF R VALUES IN TABULATION OF ELECTRONIC WAVEFUNC
C           NMIN= PRINCIPAL QUANTUM NUMBER OF LOWEST CORE SHELL CONSIDERED
C           NMAX= PRINCIPAL QUANTUM NUMBER OF HIGHEST CORE SHELL CONSIDERED
C           LATPR1,LATPR2=LATTICE PARAMETERS IN A & C DIRECTIONS
C
C*****************************************************************************
C
      READ(5,2) NKVAL
    2 FORMAT( (2X,I3))
C
C           NKVAL IS THE NUMBER OF STARS USED IN THE CALCULATION
C
C
      READ(5,3)(NSTAR(J),J=1,NKVAL)
    3 FORMAT(20(2X,I2))
```

```
C
C
C
C
      DO 25     I=1,NKVAL
      N=NSTAR(I)
   25 READ(5,4)(KSTARX(I,JJ),KSTARY(I,JJ),KSTARZ(I,JJ), JJ=1,N)
    4 FORMAT(8(4X,3F2.0))
      R(1)=0.0
      I=1
      D=.01
 1001 CONTINUE
      DO 1002    J=1,10
      I=I+1
 1002 R(I)=R(I-1)+D
      IF(I-NRVAL)1003,1004,1004
 1003 D=2.0*D
      GO TO 1001
 1004 CONTINUE
      COREAC=ATNO**.333333333
      COREAC=.88534138/COREAC
      DO 1005    I=1,NRVAL
 1005 R(I)=R(I)*COREAC
      DO 6     N=1,NMAX
      DO 6    L=1,N
      READ(5,5)(RWFCN(N,L,I),   I=1,NRVAL)
    5 FORMAT(10F8.4)
    6 CONTINUE
C
C           R = RADIAL  CO-ORDINATE
C           RWFCN = RADIAL WAVE FUNCTION
C
C
C*************************************************************************
C
C
      LATPR1=LATPR1/.52917
      LATPR2=LATPR2/.52917
      VOL=.433013*LATPR1*LATPR1*LATPR2
      RECIP1=7.255192/LATPR1
      RECIP2=6.283185/LATPR2
      DO 183     I=1,NKVAL
  183 NK(I)=NSTAR(I)
      READ(5,166)A1,A2,A3,B1,B2,B3,C1,C2,C3,NPPTS,NPPTS1,IZERO,RANGE,NK9
  166 FORMAT(3(4X,3F2.0),3I5,F5.0,I5)
      READ(5,7)(EIGVEC(IJ),IJ=1,NKVAL)
    7 FORMAT(10F8.5)
      J=NKVAL
      SUMSQ=0.0
        SUM=0.0
      DO 5060    I=1,NKVAL
      SUMSQ=SUMSQ+EIGVEC(I) *EIGVEC(I)
      KSTOP=NSTAR(I)
      TEMP=0.0
      DO 5162     K=1,KSTOP
      PHASE=(KSTARX(I,K)/1.5-KSTARY(I,K)/3.0+KSTARZ(I,K)/4.0)*6.283185
 5162 TEMP=TEMP+COS(PHASE)
 5060 SUM=SUM+EIGVEC(I) *TEMP/SQRT(NK(I))
```

```
C
C
C
C
      WRITE(6,5061) J,SUMSQ,J,SUM
 5061 FORMAT('0','SUMSQ(',I2,')=',F10.6,10X,'SUM(',I2,')=',F10.6)
      SUMSQ=0.0
        SUM=0.0
C
C     ***************************************************************************
C
C     THIS SECTION RENORMALIZES THE COEFFICIENTS OF THE POSITRON
C     WAVEFUNCTION
C
      DO 62    I=1,NKS
      IEXP1=KSTARZ(I,1)
      SUMSQ=SUMSQ+EIGVEC(I) *EIGVEC(I)
      KSTOR=NSTAR(I)
      TEMP=0.0
      ICH1=KSTOR/2
      DO 162     K=1,KSTOR
      ISGN1=1
      IF(K.GT.ICH1) ISGN1=(-1)**IEXP1
      PHASE=(KSTARX(I,K)/1.5-KSTARY(I,K)/3.0+KSTARZ(I,K)/4.0)*6.283185
  162 TEMP=TEMP+COS(PHASE)*ISGN1
   62 SUM=SUM+EIGVEC(I) *TEMP/SQRT(NK(I))
      WRITE(6,63) NKS,SUMSQ,NKS,SUM
   63 FORMAT('0','SUMSQ(',I2,')=',F10.6,10X,'SUM(',I2,')=',F10.6)
      EIGVEC(1)=EIGVEC(1)-SUM
      SUMSQ=0.0
      DO 64    I=1,NKS
   64 SUMSQ=SUMSQ+       EIGVEC(I)*EIGVEC(I)
      DEN=SQRT(SUMSQ)
      DO 65    I=1,NKS
   65 EIGVEC(I)=EIGVEC(I)/DEN
      DO 992      J=1,NKS
      KSTOR=NSTAR(J)
      DO 992    K=1,KSTOR
      KSTARX(J,K)=(KSTARX(J,K)+KSTARY(J,K)/1.732052)/RECIP1
        KSTARY(J,K)=KSTARY(J,K)/(.866026*RECIP1)
  992 KSTARZ(J,K)=KSTARZ(J,K)/RECIP2
 7004 CONTINUE
C
C     ***************************************************************************
C
C     THE FOLLOWING SECTION CALCULATES AND PRINTS THE POSITRON
C     WAVEFUNCTION ALONG THE DIRECTION A1,A2,A3 IN CARTESIAN
C     COORDINATES IN MOMENTUM SPACE.
C
      NORM=SQRT(A1*A1+A2*A2+A3*A3)
      DO 719    I=1,NPVAL
  719 PSI(I)=0.0
      DO 721      J=1,NKS
      IEXP1=KSTARZ(J,1)
      TEST=FLOAT(IEXP1)
      IF(KSTARZ(J,1)-TEST-.5)173,173,172
  172 IEXP1=IEXP1+1
  173 CONTINUE
```

```
C
C
C
C
      KSTOR=NSTAR(J)
      ICH1=KSTOR/2
      EIG=EIGVEC(J)/SQRT(NK(J))
      DO 721    K=1,KSTOR
      ISGN1=1
      IF(K.GT.ICH1) ISGN1=(-1)**IEXP1
      PHASE=(KSTARX(J,K)/1.5-KSTARY(J,K)/3.0+KSTARZ(J,K)/4.0)*6.283185
      CP=COS(PHASE)
      SP=SIN(PHASE)
      KSTARX(J,K)=KSTARX(J,K)*RECIP1
      KSTARY(J,K)=KSTARY(J,K)*RECIP1
      KSTARZ(J,K)=KSTARZ(J,K)*RECIP2
      KSTARX(J,K)=KSTARX(J,K)-.5*KSTARY(J,K)
  720 KSTARY(J,K)=KSTARY(J,K)*.866026
      DO 721    I=1,NRVAL
      ARG=(KSTARX(J,K)*A1+KSTARY(J,K)*A2+KSTARZ(J,K)*A3)*R(I)/NORM
  721 PSI(I)=PSI(I)+ISGN1*EIG*(COS(ARG)*CP+SIN(ARG)*SP)
      WRITE(6,723)
  723 FORMAT(' ',6(5X,'X',9X,'F(X)',3X))
      WRITE(6,722) (R(I),PSI(I),   I=1,NRVAL)
  722 FORMAT(' ',6(' ',F9.4,F11.5))
C
C     ***************************************************************
C     FOLLOWING SECTION CALCULATES ISUBN(Q) AT 1 MRAD INTERVALS
C
      DO 221       L=1,N
      TEMP=-1.0
      DO 221       I=1,60
      TEMP=TEMP+1.0
      QQ(I)=TEMP*.137038
      CALL FOLD(N,L,NRVAL,QQ(I),INTEG)
      CALL QTFG(R,INTEG,Z,NRVAL)
  221 A(N,L,I)=Z(NRVAL)
C
C     ***************************************************************
C
C     THE FOLLOWING SECTION CALCULATES POLYXTAL LONG SLIT DISTNS.
C     SUBROUTINE RANDRO IS DESCRIBED BY LEWIS(1969). IT IS A PSEUDO
C     RANDOM NUMBER GENERATOR OF THE POWER RESIDUE TYPE. SAMPLING REGION
C     HERE IS FOR A HEXAGONAL CRYSTAL. WITH A CHANGED SAMPLING REGION
C     THE SAME SEGMENT IS USED FOR FCC POLYXTAL DISTRIBUTIONS.
C
      NKVAL=NK2
      WRITE(6,701)(ELNAM(I),I=1,40)
  701 FORMAT('1',10X,'POLYCRYSTALLINE ANGULAR DISTRIBUTION',10X,40A1//)
      WRITE(6,703)
  703 FORMAT('0',7X,'DETECTOR',14X,'COUNT')
      WRITE(6,704)
  704 FORMAT(' ',7X,'POSITION',14X,'RATE')
      DO 169    I=1,50
  169 PHO(I)=0.0
      READ(5,192) IMAX
  192 FORMAT(I5)
      DO 171    I=1,25
```

```
C
C
C
C
      ICOUNT=0
      NUM=0
      P=I
      P=P-.5
      P=P*.137038
  170 CALL RANDRO(X)
      THETA=1.5707963*X
      CALL RANDRO(X)
      PHI=2.0943951*X
      S=SIN(THETA)
      PX=P*S*COS(PHI)
      PY=P*S*SIN(PHI)
      PZ=P*COS(THETA)
      CALL CALC (NMIN,NMAX,NKVAL,NRVAL,RECIP,PX,PY,PZ,TEMP)
      TEMP=TEMP*P
      ICOUNT=ICOUNT+1
      RHO(I)=(RHO(I)*NUM+TEMP)/(NUM+1)
      NUM=NUM+1
      IF(ICOUNT.LT.IMAX) GO TO 170
  171 CONTINUE
      TEMP=0.0
      DO 190   J=1,25
      P2(J)=J-1
      I=26-J
      TEMP=TEMP+RHO(I)
  190 RHOFIN(I)=TEMP*6.283185
      DO 191     J=1,25
  191 WRITE(6,1173) P2(J),RHOFIN(J)
 1173 FORMAT('0',2(6X,F10.4))
      COEF=.18940/VOL
      CALL QUADR(RHOFIN,25,COEF,AREA,IER)
      WRITE(6,199) VOL,AREA
  199 FORMAT('1','VOLUME PER ATOM =',F20.8,10X,'ANNIHILATION RATE X10F-9
     1 =',F20.8)
      STOP
       END
```

```
C
C
C
C
      SUBROUTINE CALC(NMIN,NMAX,NKVAL,NRVAL,RECIP,PX,PY,PZ,RHO)
C
C     THIS SUBROUTINE CALCULATES MOMENTUM SPACE DENSITIES FOR
C     HCP STRUCTURE AT POINT PX,PY,PZ IN MOMENTUM SPACE IN CARTESIAN
C      COORDINATES
C
      REAL EIGVEC( 40),KSTARX(40,12),KSTARY(40,12),KSTARZ(40,12) ,
     2A(4,4,100),QQ(100),LATPR1,LATPR2
      INTEGER NSTAR(40)
      COMMON/D/EIGVEC,LATPR1,LATPR2
      COMMON/S/NSTAR,KSTARX,KSTARY,KSTARZ
      COMMON/F/A,QQ
      RHO=0.0
      DO 11    N=NMIN,NMAX
      DO 11     L=1,N
      IF(L-2)51,52,53
   53 IF(L-4)54,55,56
   51 SUM1=0.0
      SUM2=0.0
      DO 1      JJ=1,NKVAL
      KSTOR=NSTAR(JJ)
      WT=KSTOR
      WT=SQRT(WT)
      WT=EIGVEC(JJ)/WT
      DO 1      KK=1,KSTOR
      PHASE1=(LATPR1*KSTARX(JJ,KK)/1.732052+LATPR2*KSTARZ(JJ,KK)/4.0)
      QX1=PX-KSTARX(JJ,KK)
      QY1=PY-KSTARY(JJ,KK)
      QZ1=PZ-KSTARZ(JJ,KK)
      Q1=SQRT(QX1*QX1+QY1*QY1+QZ1*QZ1)
    7 IF(Q1-QQ(1))2,4,4
    4 DO 21      I=1,60
      J=I
      IF(Q1-QQ(I))23,22,21
   21 CONTINUE
    3 TERM=A(N,L,60)
      GO TO 24
   22 TERM=A(N,L,J)
      GO TO 24
   23 TERM=A(N,L,J-1)+((Q1-QQ(J-1))/(QQ(J)-QQ(J-1)))*(A(N,L,J)-A(N,L,J-1
     1))
   24 TERM11= TERM*WT*SIN(PHASE1)
      TERM12=TERM*WT*COS(PHASE1)
      SUM1=SUM1+TERM11
    1 SUM2=SUM2+TERM12
      RHO=RHO+(SUM1*SUM1+SUM2*SUM2)
      GO TO 11
   52 SUM1=0.0
      SUM2=0.0
      DO 101    JJ=1,NKVAL
      KSTOR=NSTAR(JJ)
      WT=KSTOR
      WT=SQRT(WT)
      WT=EIGVEC(JJ)/WT
```

```
C
C
C
C
      DO 101    KK=1,KSTOR
      PHASE1=(LATPR1*KSTARX(JJ,KK)/1.732052+LATPR2*KSTARZ(JJ,KK)/4.0)
      QX1=PX-KSTARX(JJ,KK)
      QY1=PY-KSTARY(JJ,KK)
      QZ1=PZ-KSTARZ(JJ,KK)
      Q1=SQRT(QX1*QX1+QY1*QY1+QZ1*QZ1)
  107 IF(Q1-QQ(1))2,104,104
  104 DO 121    I=1,60
      J=I
      IF(Q1-QQ(I))123,122,121
  121 CONTINUE
  103 TERM1=A(N,L,60)
      GO TO 124
  122 TERM1=A(N,L,J)
      GO TO 124
  123 TERM1=A(N,L,J-1)+((Q1-QQ(J-1))/(QQ(J)-QQ(J-1)))*(A(N,L,J)-A(N,L,J-
     11))
  124 TERM11= TERM1*WT*SIN(PHASE1)
      TERM12=TERM1*WT*COS(PHASE1)
      DO 101    LL=1,NKVAL
      KSTOR1=NSTAR(LL)
        WT1=KSTOR1
         WT1=SQRT(WT1)
       WT1=EIGVEC(LL)/WT1
      DO 101    MM=1,KSTOR1
      PHASE2=(LATPR1*KSTARX(LL,MM)/1.732052+LATPR2*KSTARZ(LL,MM)/4.0)
      QX2=PX-KSTARX(LL,MM)
      QY2=PY-KSTARY(LL,MM)
      QZ2=PZ-KSTARZ(LL,MM)
      Q2=SQRT(QX2*QX2+QY2*QY2+QZ2*QZ2)
  125 IF(Q2-QQ(1))2,126,126
  126 DO 127    I=1,60
      J=I
      IF(Q2-QQ(I))129,128,127
  127 CONTINUE
  130 TERM2=A(N,L,60)
      GO TO 131
  128 TERM2=A(N,L,J)
      GO TO 131
  129 TERM2=A(N,L,J-1)+((Q2-QQ(J-1))/(QQ(J)-QQ(J-1)))*(A(N,L,J)-A(N,L,J-
     11))
  131 TERM21=TERM2*WT1*SIN(PHASE2)
      TERM22=TERM2*WT1*COS(PHASE2)
      IF(Q1*Q2.NE.0.0) GO TO 132
      U=1.0
      GO TO 133
  132 U=(QX1*QX2+QY1*QY2+QZ1*QZ2)/(Q1*Q2)
  133 SUM1=SUM1+TERM11*TERM21*U
      SUM2=SUM2+TERM12*TERM22*U
  101 CONTINUE
      RHO=RHO+3.0*(SUM1+SUM2)
      GO TO 11
   54 SUM1=0.0
      SUM2=0.0
```

```
C
C
C
C
      DO 201    JJ=1,NKVAL
      KSTOR=NSTAR(JJ)
      WT=KSTOR
      WT=SQRT(WT)
      WT=EIGVEC(JJ)/WT
      DO 201    KK=1,KSTOR
      PHASE1=(LATPR1*KSTARX(JJ,KK)/1.732052+LATPR2*KSTARZ(JJ,KK)/4.0)
      QX1=PX-KSTARX(JJ,KK)
      QY1=PY-KSTARY(JJ,KK)
      QZ1=PZ-KSTARZ(JJ,KK)
      Q1=SQRT(QX1*QX1+QY1*QY1+QZ1*QZ1)
  207 IF(Q1-QQ(1))2,204,204
  204 DO 221    I=1,60
      J=I
      IF(Q1-QQ(I))223,222,221
  221 CONTINUE
  203 TERM1=A(N,L,60)
      GO TO 224
  222 TERM1=A(N,L,J)
      GO TO 224
  223 TERM1=A(N,L,J-1)+((Q1-QQ(J-1))/(QQ(J)-QQ(J-1)))*(A(N,L,J)-A(N,L,J-
     11))
  224 TERM11= TERM1*WT*SIN(PHASE1)
      TERM12=TERM1*WT*COS(PHASE1)
      DO 201    LL=1,NKVAL
      KSTOR1=NSTAR(LL)
         WT1=KSTOR1
        WT1=SQRT(WT1)
          WT1=EIGVEC(LL)/WT1
      DO 201    MM=1,KSTOR1
      PHASE2=(LATPR1*KSTARX(LL,MM)/1.732052+LATPR2*KSTARZ(LL,MM)/4.0)
      QX2=PX-KSTARX(LL,MM)
      QY2=PY-KSTARY(LL,MM)
      QZ2=PZ-KSTARZ(LL,MM)
      Q2=SQRT(QX2*QX2+QY2*QY2+QZ2*QZ2)
  225 IF(Q2-QQ(1))2,226,226
  226 DO 227    I=1,60
      J=I
      IF(Q2-QQ(I))229,228,227
  227 CONTINUE
  230 TERM2=A(N,L,60)
      GO TO 231
  228 TERM2=A(N,L,J)
      GO TO 231
  229 TERM2=A(N,L,J-1)+((Q2-QQ(J-1))/(QQ(J)-QQ(J-1)))*(A(N,L,J)-A(N,L,J-
     11))
  231 TERM21=TERM2*WT1*SIN(PHASE2)
      TERM22=TERM2*WT1*COS(PHASE2)
      IF(Q1*Q2.NE.0.0) GO TO 232
      U=1.0
      GO TO 233
  232 U=(QX1*QX2+QY1*QY2+QZ1*QZ2)/(Q1*Q2)
  233 SUM1=SUM1+TERM11*TERM21*(1.5*U*U-.5)
      SUM2=SUM2+TERM12*TERM22*(1.5*U*U-.5)
```

```
C
C
C
C
  201 CONTINUE
      RHO=RHO+5.0*(SUM1+SUM2)
      GO TO 11
   55 SUM1=0.0
      SUM2=0.0
      DO 301    JJ=1,NKVAL
      KSTOR=NSTAR(JJ)
      WT=KSTOR
      WT=SQRT(WT)
      WT=EIGVEC(JJ)/WT
      DO 301    KK=1,KSTOR
      PHASE1=(LATPR1*KSTARX(JJ,KK)/1.732052+LATPR2*KSTARZ(JJ,KK)/4.0)
      QX1=PX-KSTARX(JJ,KK)
      QY1=PY-KSTARY(JJ,KK)
      QZ1=PZ-KSTARZ(JJ,KK)
      Q1=SQRT(QX1*QX1+QY1*QY1+QZ1*QZ1)
  307 IF(Q1-QQ(1))2,304,304
  304 DO 321    I=1,60
      J=I
      IF(Q1-QQ(I))323,322,321
  321 CONTINUE
  303 TERM1=A(N,L,60)
      GO TO 324
  322 TERM1=A(N,L,J)
      GO TO 324
  323 TERM1=A(N,L,J-1)+((Q1-QQ(J-1))/(QQ(J)-QQ(J-1)))*(A(N,L,J)-A(N,L,J-
     11))
  324 TERM11= TERM1*WT*SIN(PHASE1)
      TERM12=TERM1*WT*COS(PHASE1)
      DO 301    LL=1,NKVAL
      KSTOR1=NSTAR(LL)
           WT1=KSTOR1
         WT1=SQRT(WT1)
          WT1=EIGVEC(LL)/WT1
      DO 301    MM=1,KSTOR1
      PHASE2=(LATPR1*KSTARX(LL,MM)/1.732052+LATPR2*KSTARZ(LL,MM)/4.0)
      QX2=PX-KSTARX(LL,MM)
      QY2=PY-KSTARY(LL,MM)
      QZ2=PZ-KSTARZ(LL,MM)
      Q2=SQRT(QX2*QX2+QY2*QY2+QZ2*QZ2)
  325 IF(Q2-QQ(1))2,326,326
  326 DO 327    I=1,60
      J=I
      IF(Q2-QQ(I))329,328,327
  327 CONTINUE
  330 TERM2=A(N,L,60)
      GO TO 331
  328 TERM2=A(N,L,J)
      GO TO 331
  329 TERM2=A(N,L,J-1)+((Q2-QQ(J-1))/(QQ(J)-QQ(J-1)))*(A(N,L,J)-A(N,L,J-
     11))
  331 TERM21=TERM2*WT1*SIN(PHASE2)
      TERM22=TERM2*WT1*COS(PHASE2)
      IF(Q1*Q2.NE.0.0) GO TO 332
```

```
C
C
C
C
      U=1.0
      GO TO 333
  332 U=(QX1*QX2+QY1*QY2+QZ1*QZ2)/(Q1*Q2)
  333 SUM1=SUM1+TERM11*TERM21*(2.5*U*U*U-1.5*U)
      SUM2=SUM2+TERM12*TERM22*(2.5*U*U*U-1.5*U)
  301 CONTINUE
      RHO=RHO+7.0*(SUM1+SUM2)
   11 CONTINUE
      RETURN
    2 WRITE(6,10)
   10 FORMAT('0','ERROR IN INPUT TO SUBROUTINE CALC, Q < 0')
   55 WRITE(6,12)
   12 FORMAT('0','ERROR IN INPUT TO SUBROUTINE CALC, L>4')
      RHO=0.0
      RETURN
      END
```

APPENDIX V

Subprograms

```
C
C
C
C
      SUBROUTINE VINTEC
C     THIS SUBROUTINE INTEGRATES SIGMA(R) TO OBTAIN U(R)
      REAL R(100), SIGMA(100),INNER(100),OUTER(100),SMALVR(100), Z(100),
     1RSHIFT(100)
      REAL X(100),Y(100)
      COMMON R,SIGMA,SMALVR,NRVAL,ATNO,Z
      INNER(1)=0.0
      OUTER(1)=0.0
      RSHIFT(1)=0.0
      NRVALM=NRVAL-1
      NRVALP=NRVAL+1
      DO 23    LL=2,NRVALP
      LLM1=LL-1
   23 RSHIFT(LL)=R(LLM1)
      DO 12     I=1,NRVALM
      IP1=I+1
      IP2=I+2
      DO  8     JJ=2,IP1
      JJM1=JJ-1
    8 INNER(JJ)=SIGMA(JJM1)
      DO 9     JJ=IP2,NRVALP
    9 INNER(JJ)=0.0
      DO 10     KK=1,I
   10 OUTER(KK)=0.0
      DO 11    KK=IP1,NRVALP
      KKM1=KK-1
      IF(R(KKM1))21,21,22
   21 OUTER(KK)=0.0
      GO TO 11
   22 OUTER(KK)=SIGMA(KKM1)/R(KKM1)
   11 CONTINUE
      TERM1=2.0*ATNO
   25 CALL REARR(NRVALP,RSHIFT,INNER,N,X,Y)
   26 CALL QTFG(X,Y,Z,N)
   27 TERM2=2.0*Z(N)
   28 CALL REARR(NRVALP,RSHIFT,OUTER,N,X,Y)
   29 CALL QTFG(X,Y,Z,N)
   30 TERM3=(2.0*R(I))*Z(N)
   12 SMALVR(I)=TERM1+TERM2+TERM3
      DO 13    JJ=1,NRVAL
   13 INNER(JJ)=SIGMA(JJ)
      CALL QTFG(R,INNER,Z,NRVAL)
      TERM2=2.0*Z(NRVAL)
      SMALVR(NRVAL)=TERM1+TERM2
      RETURN
      END
```

```
C
C
C
C
      SUBROUTINE REARR(N,X,Y,NDIM,XARR,YARR)
C
C     THIS SUBROUTINE REARRANGES THE STORAGE OF THE INTEGRANDS
C     IN THE EVALUATION OF U(R) SO AS TO AVOID INTEGRATION ERRORS
C     CAUSED BY DISCONTINUITIES IN THE INTEGRAND.
C
      DIMENSION X(1),Y(1),XARR(1),YARR(1)
      DO 2     I=1,N
      IF (Y(I))1,2,1
    1 JINIT=I
      GO TO 3
    2 CONTINUE
      NDIM=1
      GO TO 8
    3 DO 5     I=JINIT,N
      IF (Y(I))5,4,5
    4 JFIN=I-1
      GO TO 6
    5 CONTINUE
      JFIN=N
    6 NDIM=JFIN-JINIT+1
      DO 7   J=JINIT,JFIN
      JJ=J-JINIT+1
      XARR(JJ)=X(J)
    7 YARR(JJ)=Y(J)
    8 RETURN
      END
```

```
C
C
C
C
      SUBROUTINE FVAL(X,INTEG)
C
C     THIS SUBROUTINE FOLDS U(R) WITH THE ZERO ORDER SPHERICAL
C     BESSEL FUNCTION
C
      DOUBLE PRECISION X,Y
      REAL R(100),SIGMA(100),INTEG(100),SMALVR(100)
      COMMON R,SIGMA,SMALVR,NRVAL,ATNO
      BSFCN0(X)=DSIN(X)/X
      INTEG(1)=0.0
      DO 12    I=2,NRVAL
      Y=X*R(I)
      IF(Y)1,1,2
    1 FJZERO=1.0
      GO TO 12
    2 FJZERO=BSFCN0(Y)
   12 INTEG(I)=12.566371*SMALVR(I)*FJZERO*R(I)
      RETURN
      END
```

```
C
C
C
C
      SUBROUTINE OUT(MATRIX,EIGVEC,N)
C
C     THIS SUBROUTINE  CALLS THE DIAGONALIZING SUBROUTINE EIGEN
C     AND PRINTS OUT THE DIAGONALIZED MATRIX AND THE EIGENVECTORS
C
      DIMENSION MATRIX(1),EIGVEC(N,N),ORIG(325)
      CALL EIGEN(MATRIX,EIGVEC,N     ,0)
      WRITE(6,1)
    1 FORMAT('1','MATRIX OF EIGENVALUES')
      I1=N-10
      DO 3    I=I1,N
      IJN=(I*I+I)/2
      IJ1=IJN+I1-I
      WRITE(6,2) (MATRIX(IJ),    IJ=IJ1,IJN)
    2 FORMAT('0',11(F10.5,2X))
    3 CONTINUE
      WRITE(6,4)
    4 FORMAT('1','MATRIX OF EIGENVECTORS')
      DO 6    I=1,N
      WRITE(6,5) (EIGVEC(I,J),   J=I1,N)
    5 FORMAT('0',11(F10.5,2X))
    6 CONTINUE
      DO 10     I=1,N
      DO 10     J=I,N
      IJ=I+(J*J-J)/2
      ORIG(IJ)=0.0
      DO 10     K=1,N
      KK=(K*K+K)/2
   10 ORIG(IJ)=ORIG(IJ)+EIGVEC(I,K)*EIGVEC(J,K)*MATRIX(KK)
      WRITE(6,11)
   11 FORMAT('1','MATRIX AFTER INVERSE TRANSFORMATION')
      DO 13     I=I1,N
      IJN=(I*I+I)/2
      IJ1=IJN+I1-I
      WRITE(6,12) (ORIG(IJ),IJ=IJ1,IJN)
   12 FORMAT('0',11(F10.5,2X))
   13 CONTINUE
      RETURN
      END
```

```
C
C
C
C
      SUBROUTINE FOLD(N,L,NRVAL,Q,INTEG)
C     THIS SUBROUTINE FOLDS THE RADIAL ELECTRON WAVEFUNCTION WITH
C     THE APPROPRIATE SPHERICAL BESSEL FUNCTION
C
       DOUBLE PRECISION X
      REAL R(100),RWFCN(4,4,100),INTEG(100)
      COMMON R
      COMMON/C/RWFCN
      BSFCN0(X)=DSIN(X)/X
      BSFCN1(X)=DSIN(X)/(X*X)-DCOS(X)/X
      BSFCN2(X)=(3.0/(X*X*X)-1.0/X)*DSIN(X)-(3.0/(X*X))*DCOS(X)
      INTEG(1)=0.0
      IF(L-2)1,5,9
    1 DO 4     I=2,NRVAL
      X=Q*R(I)
      IF(X)2,2,3
    2 FJ=1.0
      GO TO 4
    3 FJ=BSFCN0(X)
    4 INTEG(I)=RWFCN(N,L,I)*FJ*R(I)
      RETURN
    5 DO 8     I=2,NRVAL
      X=Q*R(I)
      IF (X)6,6,7
    6 FJ=0.0
      GO TO 8
    7 FJ=BSFCN1(X)
    8 INTEG(I)=RWFCN(N,L,I)*FJ*R(I)
      RETURN
    9 DO 12      I=2,NRVAL
       X=Q*R(I)
      IF(X)10,10,11
   10 FJ=0.0
      GO TO 12
   11 FJ=BSFCN2(X)
   12 INTEG(I)=RWFCN(N,L,I)*FJ*R(I)
      RETURN
      END
```

```
C
C
C
C
      SUBROUTINE QUADR(Z,N,H,S,IER)
C
C     THIS SUBROUTINE GIVES THE INTEGRAL OF A GIVEN TABLE OF
C     FUNCTION VALUES FOR A CONSTANT MESH. EVALUATION IS BY
C     SIMPSON'S RULE
C
      DIMENSION Z(N)
      S=0.0
      IF(N-1)32,32,33
   32 IER=1
      RETURN
   33 IF(H)34,35,34
   35 IER=2
      RETURN
   34 IF(N-5)40,39,38
   38 DO 39 I=5,N,4
   39 S=S+7.*Z(I-4)+32.*Z(I-3)+12.*Z(I-2)+32.*Z(I-1)+7.*Z(I)
      S=S*2./45.
   40 J=N-(N/4)*4+1
      GO TO (45,50,47,48),J
   45 S=S+0.375*(Z(N-3)+3.*Z(N-2)+3.*Z(N-1)+Z(N))
      GO TO 50
   47 S=S+(Z(N-1)+Z(N))/2.
      GO TO 50
   48 S=S+(Z(N-2)+4.*Z(N-1)+Z(N))/3.
   50 S=S*H
      IER=0
      RETURN
      END
```

```
C
C
C
C
      SUBROUTINE QTFG(X,Y,Z,NDIM)
C
C     THIS SUBROUTINE CALCULATES THE INTEGRAL FOR A GIVEN SET OF
C     FUNCTION VALUES AND ARGUMENTS.  EVALUATION IS BY A QUADRATIC
C     FORMULA.
C
      DIMENSION X(1),Y(1),Z(1)
    1 SUM2=0.0
    2 IF(NDIM-2)30,30,4
    4 NINIT=2
    5 NTEST=((NDIM-1)/2)*2+1
    6 N=NTEST-1
   11 DO 24    I=NINIT,N,2
   12 SUM1=SUM2
   13 IF(X(I)-X(I+1))14,23,14
   14 IF(X(I)-X(I-1))15,23,15
   15 IF(X(I-1)-X(I+1))16,32,16
   16 A1=(X(I+1)*X(I+1)*X(I+1)-X(I-1)*X(I-1)*X(I-1))/3.0
   17 A2=(X(I+1)*X(I+1)-X(I-1)*X(I-1))/2.0
   18 A3=X(I+1)-X(I-1)
   19 C1=(A1-A2*(X(I)+X(I+1))+A3*X(I)*X(I+1))/((X(I-1)-X(I))*(X(I-1)-X(I
     1+1)))
   20 C2=(A1-A2*(X(I-1)+X(I+1))+A3*X(I-1)*X(I+1))/((X(I)-X(I-1))*(X(I)-
     1X(I+1)))
   21 C3=(A1-A2*(X(I)+X(I-1))+A3*X(I)*X(I-1))/((X(I+1)-X(I))*(X(I+1)-X(I
     1-1)))
   22 SUM2=SUM2+C1*Y(I-1)+C2*Y(I)+C3*Y(I+1)
   23 Z(I-1)=SUM1
   24 Z(I)=SUM1
   26 IF(NTEST-NDIM)27,30,32
   27 SUM2=SUM2+.5*(X(NDIM)-X(NTEST))*(Y(NDIM)+Y(NTEST))
   30 Z(NDIM)=SUM2
   31 RETURN
   32 WRITE(6,33)
   33 FORMAT('0','ERROR IN  INPUT TO SUBROUTINE QTFG , EXECUTION CONTINU
     1ING')
      Z(NDIM)=0.0
      RETURN
      END
```

Leaf blank to correct numbering.

Leaf blank to correct numbering.

REFERENCES

Akahane, T., Moringa, H., Sueoka, O. and Fujiwara, K. 1971. Proceedings of the Second International Conference on Positron Annihilation, Queen's University, Kingston, Ontario, unpublished.

Arias-Limonta, J. A. and Varlashkin, P. G. 1970. Phys. Rev. B, 1, 142

Arponen, J. and Jauho, P. 1968. Phys. Rev. 167, 239.

Arponen, J. 1970. J. Phys. C, 3, 107.

Barrett, C. S. and Massalski, T. B. 1966. Structure of Metals (McGraw-Hill, New York).

Becker, E. H., Petijevich, P. and Williams, D. L. 1971. J. Phys. F, 1, 806.

Bergersen, B. 1969. Phys. Rev. 181, 499.

Bergersen, B. and Pajanne, E. 1969. Phys. Rev. 186, 375.

Beringer, R. and Montgomery, C. G. 1942. Phys. Rev. 61, 222.

Berko, S., Kelley, R. E. and Plaskett, J. S.,1957. Phys. Rev. 106, 824.

Berko, S. and Plaskett, J. S. 1958. Phys. Rev. 112, 1877.

Berko, S. 1962. Phys. Rev. 128, 2166.

Bethe, H. A. 1935, Proc. Roy. Soc. (London) A150, 129.

Bethe, H. A. and Goldstone, J. 1957. Proc. Roy. Soc. (London) A239, 551.

Bloch, F. 1928. Z. Physik, 52, 555.

Bohm, D. and Pines, D. 1953. Phys. Rev. 92, 609.

Bouckaert, K., Smoluchowski, R. and Wigner, E. 1936. Phys. Rev. 50, 58.

Carbotte, J. P. and Kahana, S. 1965. Phys. Rev. 139, A213.

Carbotte, J. P. 1965. Phys. Rev. 144, 309.

Carbotte, J. P. and Arora, H. L. 1967. Can. J. Phys. 45, 387.

Carbotte, J. P. and Salvadori, A. 1967. Phys. Rev. 162, 290.

Colombino, P., Fiscella, B. and Trossi, L. 1963. Nuovo Cimento, 27, 589.

Colombino, P., Fiscella, B. and Trossi, L. 1964. Nuovo Cimento, 31, 950.

Connors, D. C., Crisp, V. C. and West, R. N. 1971. J. Phys. F, 1, 355.

Crowell, J., Andersen, V. E. and Ritchie, R. H. 1966. Phys. Rev. 150, 243.

Cushner, S., Erskine, J. C. and Berko, S. 1970. Phys. Rev. B, 1, 2852.

Daniel, E. 1957. J. Phys. Radium, 18, 691.

Dave, N. K., McKee, B. T. A., Stewart, A. T., Stott, M. J. and Triftshauser, W. 1971. Second International Positron Conference, Queen's University, Kingston, Ontario, unpublished.

DeBenedetti, S., Cowan, C. E., Konneker, W. R. and Primakoff, H. 1950. Phys. Rev. 77, 205.

Dirac, P. A. M. 1930. Proc. Cambridge Phil. Soc. 26, 361.

Donovan, B. and March, N. H. 1958. Phys. Rev. 110, 582.

Erskine, J. C. and McGervey, J. D. 1966. Phys. Rev. 151, 615.

Ferrell, R. A. 1956. Rev. Mod. Phys. 28, 308.

Friedel, J. 1967. in The Physics of Metals, Vol. 1, edited by J. M. Ziman (Cambridge University Press, London) pp. 340-352.

Fujiwara, K. and Sueoka, O. 1966, J. Phys. Soc. Japan, 21, 1947.

Fujiwara, K. 1970. J. Phys. Soc. Japan, 29, 1479.

Garwin, R. L. 1953. Phys. Rev. 91, 1571.

Green, R. E. and Stewart, A. T. 1955. Phys. Rev. 98, 486.

Hamman, D. R. 1966. Phys. Rev. 146, 277.

Hartree, D. R. 1933. Proc. Roy. Soc. (London) A141, 282.

Hartree, D. R., and Hartree, W. 1936. Proc. Roy. Soc. (London) A157, 490.

Hartree, D. R. 1952. Numerical Analysis (Clarendon, Oxford) Ch. 7.

Hautojarvi, P., Tamminen, A., and Jauho, P. 1970. Phys. Rev. Lett. 24, 459.

Heine, V. 1967. in The Physics of Metals, Vol. 1, edited by J. Ziman (Cambridge University Press, London) pp. 25-27.

Herman, F. and Skillman, S. 1963. Atomic Structure Calculations (Prentice Hall, Englewood Cliffs, N.J.)

Kahana, S. 1960. Phys. Rev. 117, 123.

Kahana, S. 1963. Phys. Rev. 129, 1622.

Kanazawa, H., Ohtsuki, Y. and Yanagawa, S. 1965. Progr. Theoret. Phys. (Kyoto) 33, 1010.

Kittel. 1963. Quantum Theory of Solids (John Wiley and Sons, New York) p.270.

Lang, G. and DeBenedetti, S. 1957. Phys. Rev. 108, 914.

Lee, C. 1958. Soviet Phys. JETP 6, 281.

Lee-Whiting, G. E. 1955. Phys. Rev. 97, 1557.

Lewis, P. A. W. 1969. IBM Systems J. 8, 136.

Lonsdale, K. 1962. International Tables for X-Ray Crystallography, Vol. III (Kynoch Press, Birmingham) p.125

Loucks, T. L. 1966. Phys. Rev. 144, 504.

Mackenzie, I. K., Khoo, T. L., MacDonald, A. B. and McKee, B. T. A. 1967, Phys. Rev. Lett. 19, 946.

Majumdar, C. K. 1965. Phys. Rev. 140, A227.

Mathews, J. and Walker, R. L. 1965. Mathematical Methods of Physics (Benjamin, New York) p.14

Melngailis, J. 1970. Phys. Rev. B, 2, 563.

Melngailis, J. and DeBenedetti, S. 1966. Phys. Rev. 145, 400.

Mikeska, H. J. 1970. Z. Physik, 232, 159.

Mogensen, O. E. and Trumpy, G. 1969. Phys. Rev. 188, 639.

Ore, A. and Powell, J. L. 1949. Phys. Rev. 75, 1696.

Peierls, R. E. 1955. Quantum Theory of Solids (Oxford University Press, London) Sec. 4.2.

Ralston, A. and Wilf, H. S. 1962. Mathematical Methods for Digital Computers (John Wiley and Sons, New York) Ch. 7.

Rockmore, D. M. and Stewart, A. T. 1967. in Positron Annihilation edited by A. T. Stewart and L. O. Roellig (Academic Press, New York) p. 259.

Rose, K. L. and DeBenedetti, S. 1965. Phys. Rev. 138, A927.

Schrader, D. M. 1970. Phys. Rev. A, 1, 1070.

Senicki, E. M. D. 1972. Ph.D. Thesis, University of Manitoba, Winnipeg.

Slater, J. C. 1965. Quantum Theory of Molecules and Solids, Vol. 2 (McGraw-Hill, New York).

Stewart, A. T. 1955. Phys. Rev. 99, 594.

Stewart, A. T. 1957. Can. J. Phys. 35, 168.

Stroud, D. and Ehrenreich, H. 1968. Phys. Rev. 171, 399.

Thompson, A., Murray, B. and Berko, S. 1971. Proceedings of the Second International Conference on Positron Annihilation, Queen's University, Kingston, Ontario, unpublished.

Vlassov, N. A. and Tsirelson, E. A. 1948. Dokl. Akad. Nauk S.S.S.R. 59, 879.

Wallace, P. R. 1960. Solid State Physics 10, 1.

Weisberg, H. and Berko, S. 1967. Phys. Rev. 154, 249.

Weiss, R. J. 1966. X-Ray Determination of Electron Distributions (North Holland, Amsterdam)

West, R. N., Borland, R. E., Cooper, J. R. and Cusack, N. E. 1967. Proc. Phys. Soc. 92, 195.

West, R. N. 1971. Solid State Comm. 9, 1417.

Williams, D. L., Becker, E. H., Petijevich, P. and Jones, G. 1968. Phys. Rev. Lett. 20, 448.

Williams, R. W., Loucks, T. L. and Mackintosh, A. R. 1966. Phys. Rev. Lett. 16, 168.

Woll, E. J. and Carbotte, J. P. 1967. Phys. Rev. 164, 985.

Yang, C. N. 1950. Phys. Rev. 77, 242.

Ziman, J. M. 1964. Principles of the Theory of Solids (Cambridge University Press, London)

Zuchelli, A. J. and Hickman, T. G. 1964. Phys. Rev. 136, A1728.